Thermodynamics and Structure of Plate-Like Particle Dispersions

Maxime Delhorme

Division of Theoretical Chemistry
Lund University, Sweden
and
ICB-UMR 6303 CNRS
Université de Bourgogne, Dijon, France

LUND UNIVERSITY

UNIVERSITÉ DE BOURGOGNE

Doctoral Thesis

The thesis will be publicly defended on Thursday 24th of May 2012, 10.30 in lecture hall B, Center for Chemistry and Chemical Engineering, Lund

The faculty opponents are Emanuela Del Gado,ETH Zurich, Switzerland and Roland Kjellander, University of Goteborg, Sweden

Front cover: Snapshot of a simulation representing a smectic B phase at a volume fraction of 3.6% and salt concentration of 1mM, see Paper II.

Doctoral Thesis

Theoretical Chemistry
Center for Chemistry and Chemical Engineering
Lund University
P.O. Box 124
SE-221 00 Lund
Sweden
and
Laboratoire Interdisciplinaire Carnot de Bourgogne,
UMR 6303 CNRS-Université de Bourgogne,
9 Av. A. Savary, BP 47870
F-21078 DIJON Cedex,
France

ISBN 978-91-7422-301-9
Printed by Media-Tryck, Lund University, Lund

DOKUMENTDATABLAD enl SIS 61 41 21

Organization LUND UNIVERSITY	Document name DOCTORAL DISSERTATION
	Date of issue April 18, 2012
	Sponsoring organization
Author(s) Maxime Delhorme	

Title and subtitle

Thermodynamics and Structure of Plate-Like Particle Dispersions

Abstract

A considerable amount of mineral particles are found to have a plate-like shape. The work in this thesis concerns theoretical investigations, using a Monte Carlo method, of the properties of such particles in aqueous solutions. The objectives were first to create a model that could capture the essential physics of clay suspensions and also to understand the role of thermodynamics in certain chemical processes. For all investigations, the results are related to experimental studies.

The acid-base behavior of clays have been studied, using the primitive model, and an excellent agreement between simulated and experimental results was found.

The formation of gel phases as a function of the charge anisotropy have also been investigated. Liquid-gel and sol-gel transitions are found to occur for high and moderate charge anisotropy, respectively. These transitions were also found to be size and salt dependent. In absence of charge anisotropy, a liquid-glass transition is reported.
The formation of smectic and columnar liquid crystals phases with plate-like particles has been found to be favored by a strong charge anisotropy, in opposition to what was observed for nematic phases. New liquid-crystal phases were also reported.

The stability and growth of nanoplatelets is discussed. It was found that the internal Coulombic repulsion could be the cause of the limited growth of C-S-H platelets. The influence of thermodynamics on the aggregation mode of such platelets was also investigated.

Key words: Statistical mechanics, Simulations, Plate-like particles, Liquid crystal phases, Model clay system, Gel phase, Glass phase, Charge anisotropy

Classification system and/or index termes (if any):

Supplementary bibliographical information:	Language English
ISSN and key title:	ISBN 978-91-7422-301-9

Recipient's notes	Number of pages 138	Price
	Security classification	

Signature Maxime Delhorme Date April 18, 2012

List of Papers

This thesis is based on the following papers, which will be referred to in the text by their Roman numerals. The papers are appended at the end of the thesis.

I **Paper I: Acid-Base Properties of 2:1 Clays. I. Modeling the Role of Electrostatics**
Maxime Delhorme, Christophe Labbez, Céline Caillet and Fabien Thomas
Langmuir, **26**, 9240-9249 (2010)

II **Paper II: Monte Carlo simulation of a Clay Inspired Model Suspension : The Role of Charge Anisotropy.**
Maxime Delhorme, Bo Jönsson and Christophe Labbez
submitted to *Soft Matter* (2012)

III **Paper III: Liquid Crystal Phases in Suspensions of Charged Plate-like Particles.**
Maxime Delhorme, Christophe Labbez and Bo Jönsson
accepted in *Phys. Chem. Lett.* (2012)

IV **Paper IV: Gel and Nematic Phases of Plate-like Particle Suspensions: Charge Anisotropy and Size Effects**
Maxime Delhorme, Bo Jönsson and Christophe Labbez
Manuscript (2012)

V **Paper V: The Growth and Stability of Nanoplatelets**
Maxime Delhorme, Christophe Labbez, André Nonat, Cliff Woodward and Bo Jönsson
Manuscript (2012)

List of Contributions

All papers employed own in-house computer codes/programs. These were developed together with the help and support from Bo Jönsson and Christophe Labbez.

I I conducted the MC simulations and took part in writing the article. MF calculation were conducted by C.L.

II I conducted all the simulations and participated in writing the article.

III I performed all the simulations and took part in writing the article.

IV I performed all calculations and had the main responsibility for writing the manuscript.

V All the MC simulations in 3D were conducted by me. Other simulations were done by B.J. I took part in the writing process of the manuscript.

Contents

Populärvetenskaplig sammanfattning på svenska

De flesta ser nog kemi som ett abstrakt och komplicerat ämne mestadels för att det behandlar byggstenar så små att de inte kan ses med blotta ögat. Men om man tänker på det så finns kemi överallt! Kemiska processer sker runtom och inuti oss oavbrutet: i våra kroppar där proteiners kemi spelar en stor roll, i produkter som schampo och tandkräm, i cement som används för att bygga våra hus etc. Det borde därför inte komma som någon stor överraskning att enormt mycket resurser läggs på att förstå olika kemiska processer.

Så vad är då dessa osynliga beståndsdelar som kemi handlar om? Jag tror mig våga påstå att alla någon gång hört talas om atomer och molekyler (varav de senare utgörs av en grupp sammanlänkade atomer). Atomer och molekyler är inte alltid neutrala, d.v.s., dom kan bära en elektrisk laddning. Övergången från en neutral till en elektriskt laddad enhet kan exempelvis ske när atomer eller molekyler kommer i kontakt med ett lösningsmedel, vilket är fallet när ett salt löses upp i vatten och blir till fria joner. Fler exempel på molekyler som blir laddade i vatten är proteiner, virus, polyelektrolyter etc. Liksom magneters positiva och negativa poler attraherar varandra, kommer den erhållna elektriska laddningen i molekyler spela en viktig roll för hur dessa interagerar. Bland många andra faktorer såsom tex partikelgeometrin, spelar laddningen en primär roll i kemiska processer. Fysikalisk kemi fokuserar på att förstå de processer som äger rum när så kallade kolloidala partiklar interagerar i en lösning under olika förhållanden. Att utföra experiment med partiklar i storleksordningen 1-1000 nanometer är inte trivialt. Här kommer beräkningskemin in som en kraftfullt komplement. Genom att använda matematiska och fysikaliska modeller, så eftersträvar man att simulera de experimentellt erhållna resultaten och samtidigt förstå de underliggande mekanismerna och drivkrafterna på en nivå som ej är möjlig på något annat sätt.

Den här avhandlingen behandlar Monte Carlo-simuleringar av diskformade mineralpartiklar. I första projektet undersöktes hur antalet laddningar på en

diskformad mineralpartikel varierar som funktion av pH i en saltlösning av olika koncentrationer. Därefter studerades hur denna laddningsfördelning påverkar bildandet av geler och flytande kristallina faser. Genom denna studie upptäcktes nya termodynamiskt stabila faser vilket kan leda till utvecklandet av nya material. Slutligen så studerades tillväxten av diskformade nanopartiklar och deras interaktioner under förhållande jämförbara med de förekommande i en cementblandning.

Popular science summary in English

Most people see chemistry as an abstract and complicated subject because it deals with species that can not be seen with bare eyes. But if one thinks about it, chemistry is everywhere! Chemical processes happen all around you and inside you everyday : there is chemistry in the human body where proteins play a great role, in shampoo bottles, the toothpaste, in the cement that is used to build houses. Then it should not come as a surprise that so much effort are put into understanding chemical processes.

So what are those invisible species that chemistry is dealing with ? I can say with few doubts that everyone have heard about atoms and molecules (the latter being an assembly of atoms). Atoms and molecules are not always neutral species, i.e, they can carry an electrical charge (in this case atoms turn into ions). This transition from a neutral to a charged species can occur when the species are put into a solvent (like water). This is the case for example with salt that dissolves in water and form ions. Examples of molecules that becomes charged in an solvent are numerous : proteins, virus, polyeletrolytes ... But why is this electrical charge so important ? Like for magnets, where a positive pole will attract a negative one, the species will start to interact according to their charge. Among other factors like the shape of the particles, the role played by the charges in chemical processes is fundamental.
Physical chemistry focuses on the understanding of the behavior of such small particles (called colloïdal particles) in solution. Nevertheless, down to this scale, the experimental study of colloïdal dispersions is not trivial. In this context computational chemistry happens to be very useful. By the use of mathematical and physical models, one tries to simulate the results obtained by experiments and this way one can access properties that are not obtainable by other means. Hence, it is a complementary technique to experiments.

This thesis deals with simulations, using Metropolis Monte Carlo method, of mineral particles. In a first project I investigate how the number of charges on mineral particles varies when emerged into a salt solution. In a second

project the influence of the charge carried by the particles in the formation of the gels and liquid-crystals is studied. One of the striking result is the discovery of new liquid crystal phases which could lead to the development of new materials. Finally I studied the growth of nanoplatelets and their interaction in conditions comparable to the one encountered in cement paste.

Résumé simplifié en français

Beaucoup de personnes voient la chimie comme un sujet abstrait et difficile parce qu'elle concerne l'étude d'éléments invisibles à l'oeil nu. Mais, en y réfléchissant, la chimie est partout! Des processus chimiques se déroulent tout autour de nous et aussi en nous tous les jours : dans le corps humain oú les protéines jouent un grand rôle, dans les bouteilles de shampoing, dans le dentifrice, dans le ciment utilisé pour bâtir les maisons... Cela ne devrait donc être une surprise pour personne qu'autant d'efforts soient employés dans l'étude des processus chimiques.

Qu'elles sont ces epèces invisibles avec lesquelles la chimie fonctionne ? Je pense pouvoir affirmer avec peu de doutes que vous avez tous entendu parlé des atomes et des molécules (qui sont un assemblage d'atomes). Atomes et molécules ne sont pas toujours des espèces neutres, c'est-à-dire, elles peuvent porter une charge électrique (dans ce cas, les atomes sont appelés des ions). Cette transformation d'une espèce chargé à une espèce neutre peut se dérouler lorsque la particule est plongée dans un solvant (comme l'eau). C'est le cas par exemple lorsque l'on met du sel dans l'eau et que des ions sont formés. Les exemples de particules qui deviennent chargées dans un solvant sont nombreux: protéines, virus, polyélectrolytes ... Mais pourquoi cette charge électrique est elle si importante ? Comme pour les aimants, où le pôle positif attire le négatif, les espèces vont commencer à interagir selon leur charge. Parmi d'autres facteurs, tel que la forme de la particule, le rôle joué par les charges dans les processus chimiques est primordial.
La physico-chimie se concentre sur la compréhension du comportement de telles petites particules (appelés particules colloïdales) lorsqu'elles sont immergées dans une solution. Néanmoins, à cette échelle, l'étude expérimentale des dispersions colloïdales n'est pas triviale. Dans ce contexte, les simulations informatiques se trouvent être très utile. Elles ont pour but, par l'emploi de modèles physiques et mathématiques, d'essayer de reproduire les résultats obtenus expérimentalement et d'accéder à des valeurs qu'aucunes autres techniques ne peuvent procurer. Elles sont donc complémentaires aux expériences.

Cette thèse traite de simulations moléculaires, réalisées à l'aide de l'algorithme de Metropolis, de particules minérales en forme de disques. Dans un premier projet, l'évolution du nombre de charges sur une particule en fonction de la concentration en sel est étudiée. Dans un second temps, l'influence de la charge portée par les particules sur la formation des phases de gels et de cristaux liquides est examinée. Un des résultats les plus marquant est la découverte de nouvelles phases de cristaux liquides qui pourraient permettre le développement de nouveaux matériaux. Enfin, la croissance de nano particules et leurs interactions sont étudiées dans des conditions similaires à celles rencontrées dans les pâtes de ciment.

Chapter 1

Introduction

Nano-particles with a plate-like geometry are common in nature and synthetic materials, or at least can well be approximated as such. The most common examples are minerals like clays, gibbsite and calcium silicate hydrate (C-S-H) the main hydrate found in hydrated cement paste. Plate-like particles are also found in organic chemistry, where bonding molecules into a discotic macromolecule is possible. Clays and C-S-H dispersions in aqueous solutions is the main focus of this work. Their geometry combined, in some cases, with a charge heterogeneity, e.g. clays, give rise to complex and nonisotropic inter-particle potentials. The sign and the magnitude of the overall interparticle potential depends strongly on the anisotropy, concentration, and charge heterogeneity of the particles as well as on pH of the aqueous solution, salt nature and concentration. This results in a vast zoo of atypical macroscopic states and behaviors when dispersed in aqueous solution. As an example, clays are known to form gels at low particle volume fractions (ϕ) and liquid crystals when concentrated. Many industrial applications take advantage of these properties e.g. drilling, plastics [1], construction materials, papers, softeners, photonics and photovoltaic cells. However, the understanding of those systems is still in its infancy.

Clays and C-S-H particles belong to the domain of colloids as at least one of their dimensions is in the nanometer range. Since the forties, the stability of colloidal dispersions in aqueous solution has been rationalized with the help of the DLVO theory [2,3], that combines a short range attractive (van der Waals) potential with a long range electrostatic repulsion. Indeed, a strong attraction

[1] S. Laschat, A. Baro, N. Steinke, F. Giesselmann, C. Hägele, G. Scalia, R. Judele, E. Kapatsina, S. Sauer, A. Schreivogel, and M. Tosoni, Angew. Chem. Int. Ed. **46**, 4832 (2007).

[2] B. V. Derjaguin and L. Landau, Acta Phys. Chim. URSS **14**, 633 (1941).

[3] E. J. W. Verwey and J. T. G. Overbeek, *Theory of the Stability of Lyophobic Colloids* (Elsevier Publishing Company Inc., Amsterdam, 1948).

can force particles to coagulate and lead to a phase separation, whereas a dispersion under strong repulsion can remain stabilized for years [4]. Unfortunately, the DLVO theory is valid only for a limited range of conditions. In particular, it is valid in the thermodynamic limit of infinite particle dilution and for weakly coupled systems, i.e. where ion-ion correlations are not predominant. What is more, the DLVO theory focus on the simplest case: dispersions of charged isotropic particles. The lack of a generalized DLVO like effective potential, on one hand, and of extensive computer simulations on dispersion of anisotropic particles, on the other hand, best explains our poor understanding of these complex systems and the motivations of this work.

Here, computer simulations are used to identify, at the microscopic scale, the different chemical and physical processes when plate-like particles are immersed into a salt solution in an attempt to rationalize macroscopic observables. In Paper I a detailed investigation of the charging process of the titrable edges of natural clay particles is performed in comparison with potentiometric titration experiments. In papers II - IV, the modeling of dispersions of plate-like particles in 1-1 salt solutions in various conditions is considered. Paper II deals with the formation of gels in the low ϕ range and discusses in some details the similarities and differences of the model results with experimental observations on laponite and montmorillonite. Paper III prospects the high ϕ range where several liquid crystal phases are found. In Paper IV a detailed investigation of the geometry and charge anisotropy effects on the formation of gel and nematic phases is performed and discussed in light of recent experimental findings on dispersions of various mineral plate-like particles. Finally, paper V describes the growth and interaction between homogeneously charged disc particles in presence of multivalent counterions in relation to observations on C-S-H nano-hydrates.

The book is organized as follow. First the theoretical background and simulation techniques are described and then in section VII conclusions on this work are drawn. For those who do not want to dwell on a full length article, a brief summary of the important results is also presented. The papers are presented in the appendix at the end of the book.

[4] D. F. Evans and H. Wennerström, *The Colloid Domain where Physics, Chemistry, Technology and Biology meet* (VCH Publishers Inc., New York, 1994).

Chapter 2

System

An interesting point when one works with physical chemistry is the necessity to connect the different scales. As a matter of fact, the connection between a macroscopic system in a gel state (as obtained in an experiment) with the organization of particles and the interparticle forces at a nanometer scale (as obtained by computer simulation) is not trivial. One thing I would like to point out in this book is the route one has to follow to be able to work this way up through the different scales and to link a real experimental system constituted of billions of particles moving around a solution to the hundreds of platelets that are included in a computer simulation.

2.1 Structure

This thesis deals with the simulation of plate-like particles and the results are compared, when possible, to experimental systems of mineral disk-like particles from diverse origin (clays[5], gibbsite [6], cement [7]...). Montmorillonite and laponite clays and C-S-H particles (found in cement paste) are classified as phyllosilicates. It means that their crystalline structure is constituted of an octahedral layer sandwiched by two tetrahedral layers of silicate. In the case of clays, the layers are made of covalently bonded silicate atoms that organize in tetrahedral or octahedral sites. The tetrahedral sites share three of their apex while the last one is linked to the octahedral site. Exchangeable metal ions are present in both type of sites, and can be substituted by ions

[5] G. W. Brindley and J. J. Comer, *THE STRUCTURE AND MORPHOLOGY OF A KAOLIN CLAY FROM LES EYZIES (FRANCE).*

[6] H. Saalfeld and M. Wedde, Zeitschrift fur Kristallographie **139**, 129 (1974).

[7] J. J. Chen, J. J. Thomas, H. F. W. Taylor, and H. M. Jennings, Cement and Concrete Research **34**, 1499 (2004).

of lower valency. This produces a negative structural charge. The cleavage of the crystalline structure gives rise to titratable sites on the edges, which sign and magnitude depend on pH, electrolyte nature and concentration. Natural clays e.g. montmorillonite have a thickness of 1 nm but a diameter that can vary between 100 and 1000 nm. Laponite, a synthetic clay, has a smaller diameter than montmorillonite, typically 20-50 nm, for the same thickness. The crystalline structure of gibbsite contains stacks of sheets formed by aluminum hydroxide octahedral sites. The aluminum ions can be exchanged with anions of lower valency introducing this way a structural charge. Titratable sites are also present on the rims as a consequence of the cleavage of the crystalline structure. Gibbsite particles are often of a hexagonal shape of thickness 10-15 nm and diameter between 100-400 nm. The C-S-H particles are formed through the conjugated reactions of dissolution of tricalcium silicate grains (C_3S) and of precipitation. These particles are in the form of nanoplatelets with dimensions 60 x 30 x 5 nm^3. The C-S-H particles carry titratable silanol sites both on the edges and on the basal surface. At high pH and in presence of calcium salt solutions they are found to be highly negatively charged [8].

2.2 Gels

A gel is a non-ergodic disordered state that displays no long-ranged order. Macroscopically, it is reached when the solution does not flow any longer. The gel phase originates from attractive interactions between particles and thus are formed by percolated particles that form an infinite elastic network. The characteristic length of the network between two adjacent junctions, is much larger than the size of the particle. Moreover, if E is the depth of the attractive potential between two junctions: $E/k_BT \gg 1$ [9]. Experimentally gel phases can be characterized by the static structure factor S(q) obtained from scattering experiments. As a matter of fact, the S(q) curve presents two peaks, the first at large q reflects the short interparticle distance between aggregated particles and the second at low q, followed by a power law tail, reflects the characteristic size and fractal nature of the growing network. Gel and glass present different dynamic properties due to their different characteristic lengths. This can be investigated with the help of dynamic light scattering (DLS) [10,11]. Note that, from simulations, the static structure factor, and dynamic properties (through

[8] C. Labbez, B. Jönsson, I. Pochard, A. Nonat, and B. Cabane, J. Phys. Chem. B **110**, 9219 (2006).

[9] H. Tanaka, J. Meunier, and D. Bonn, Phys. Rev. E **69**, 031404 (2004).

[10] S. Jabbari-Farouji, G. Wegdam, and D. Bonn, Phys. Rev. Lett. **99**, 021402 (2007).

[11] S. Jabbari-Farouji, H. Tanaka, G. Wegdam, and D. Bonn, Phys. Rev. E **78**, 061405 (2008).

time autocorrelation functions) are also reachable [12].

2.3 Attractive glass

Glasses are non-ergodic disordered states but unlike the gel, their elasticity originates from caging effects. The formation of an attractive glass is then possible when attractive interactions are at play in the colloidal system. Typically such a phase would form if the volume fraction ϕ is high enough and if the depth of the attractive well E is of the order of k_BT [9]. Nevertheless, even if attractive interactions are active, the repulsive interactions still play the main role, contrarily to the gel phase. As experimental evidence of the formation of a glass phase, the static structure factor presents only one peak at a distance characteristic of the interparticle distance and shows only a small change when the system ages. According to Jabbari-Farouji et al. [11], attractive glass displays features of both glass and gel when experimentally characterized. Their detection in computer simulations is not trivial.

2.4 Wigner glass

A glass phase can also be found at very low volume fraction and in the absence of attractive interactions. In this case the caging effect originates from the double layer repulsion between the particles. Thus, the particles do not form a network and are spatially disconnected. The formation of the repulsive glass is favored by low ionic strengths as the double layer repulsion is known to decrease when increasing salt. All experimental evidences discussed in the previous section stay true for a Wigner glass. But, unlike the gel phase, a Wigner glass should melt when a dilution is performed on it. Recently Ruzicka et al[13] and Jabbari-Farouji et al [11] reported the formation of a Wigner glass for high volume fractions for a system of laponite platelets. This controversial result is discussed in paper II.

2.5 Liquid crystals

Due to their geometry, plate-like particles have the ability to form liquid crystals at high volume fractions. In these phases, particles present a long-ranged positional and/or orientational order but the phase preserves the properties

[12] E. Del Gado and W. Kob, Soft Matter **6**, 1547 (2010).

[13] B. Ruzicka, L. Zulian, E. Zaccarelli, M. Sztucki, A. Moussaid, and G. Ruocco, Phys. Rev. Lett. **104**, 085701 (2010).

of liquids. Onsager rationalized the formation of liquid crystal phases for uncharged platelets [14,15] and explained, counter-intuitively, that their formation had an entropic origin. Indeed the origin of these phase comes from the competition between the orientational entropy, that tends to favor isotropic phase, with the translational entropy that favors liquid crystals. The main classes of liquid crystals encountered with plate-like particles are the nematic phase, the smectic phase and the columnar phase, presented in figure 2.1.

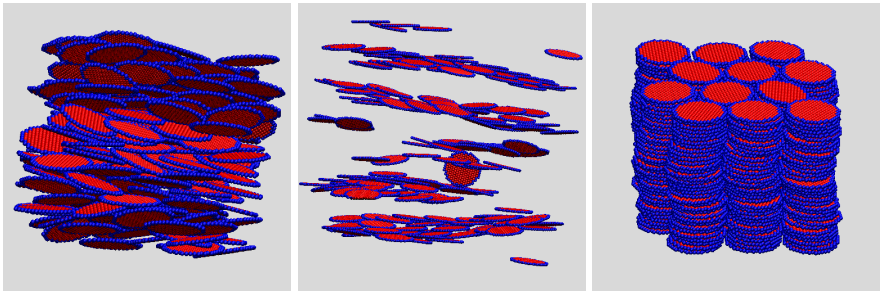

Figure 2.1: Representation of the liquid crystal phases encountered with platelets. a) Nematic phase, b) Smectic phase and c) Columnar phase.

While all of these phases present an orientational order they differ by the positional correlation between the platelets. The nematic phase present no positional order whereas the smectic phase, that is constituted of platelets gathered in parallel sheets, has a one dimensional positional order. Finally, the columnar phase, where the particles are organized in stacks including a large number of platelets, have a two-dimensional positional order. While the formation of such phases with uncharged platelets is now well understood [16], the influence on the liquid crystal formation of charged platelets remains unclear. This is investigated in papers II - IV.

2.6 Coarse graining

Ideally one would try to describe a system as accurately as possible. Unfortunately, as described above, a mineral platelet has a minimum diameter of ~ 50 nm which represents about 30000 atoms. With todays processors, computer simulations can only be done with a limited number of species (around 10^6 species for Monte Carlo as an example). It becomes then mandatory to find

[14] L. Onsager, Phys. Rev. **62**, 558 (1942).
[15] L. Onsager, Ann. N.Y. Acad. Sci. **51**, 627 (1949).
[16] J. A. C. Veerman and D. Frenkel, Phys. Rev. A **45**, 5632 (1992).

a way to reduce the number of species in the simulations. The first way is to consider smaller particles than the actual studied system. This is actually not a big issue if one is interested in a qualitative description of the physical phenomenon that happens in a system. A second way would be to vulgarize the description of some species. That is where coarse graining comes into play. It consists of gathering several units of any constituent of the system into a single grain. The coarse graining has to be done with some care. While decreasing the level of description of the model or the degrees of freedom of the particles, one has to make sure to preserve the principal physical properties. For instance, the detailed description of a charge distribution can be lost when merging several point charges into a single one. In all papers, several different coarse grain models have been used : in paper I, the detailed description of the structure is replaced by hard grains to account for the finite size of the particle. In papers II - IV, the description of the particles evolves with the separation between themselves and in the last article, one platelet is represented as a collection of charged grains. This method has been shown to reduce the computing time up to several orders of magnitude and will be further discussed in chapter 6.1.

Chapter 3

Statistical Mechanics and Thermodynamics

At a microscopic scale, a solution can be seen as an infernal mixture of species in constant motion. How can one link this chaotic states to a macroscopic thermodynamic property as obtained from experiments (pressure, temperature, ...) ? Statistical thermodynamics is the Rosetta stone that provides the connection between the two scales. Originally from the 19th century, statistical thermodynamics is based on two postulates. The postulate about equal a priori probability states that [17] "an isolated system in equilibrium is equally likely to be in any of its accessible microscopic quantum states", and links macroscopic properties of an isolated system to probability theories. Indeed, many of the macroscopic properties are time-averaged properties, which makes them difficult to access. Instead, the ergodic hypothesis allows to access this properties by considering ensemble average. It states : " the time average of any mechanical variable is equal to the ensemble average of the same variable". An ensemble here is defined as an important number of replica of the system.

3.1 Statistical mechanical ensembles

It is common to start looking into statistical thermodynamics [18,19] considering an isolated system with constant energy U, volume V, and number of

[17] R. Kjellander, *The basis of statistical thermodynamics or My favorite path to thermodynamics and beyond* (University of Göteborg, Göteborg, Sweden, 1991).

[18] T. L. Hill, *An Introduction to Statistical Thermododynamics* (Dover Publications Inc., New York, 1986).

[19] D. A. McQuarrie, *Statistical Mechanics* (Harper Collins, New York, 1976).

particles N. In this ensemble, defined as the microcanonical ensemble, the entropy S is given by :

$$S = k_{\mathrm{B}} \ln \Omega_{U,V,N} \tag{3.1}$$

where k_{B} is the Boltzmann constant, and $\Omega_{U,V,N}$ is the microcanonical partition function. It refers to the number of accessible quantum states of the system. In an isolated system this function is sufficient to determine a large amount of thermodynamic properties (P, T, μ, ...). Partition functions are accessible from other ensemble. In the canonical ensemble, where the number of particles N, the volume V and the temperature T are kept constant, it is defined from the microcanonical partition function as :

$$Q_{N,V,T} = \sum_{U} \Omega_{U,V,N} \; e^{-\beta U} \tag{3.2}$$

where β = $1/k_B$T. $Q_{N,V,T}$ is referred as the canonical partition function. Finally, in the grand canonical ensemble, where exchange in particles between the system and a reservoir is allowed, the grand potential, takes the form :

$$\Xi_{\mu,V,T} = \sum_{N} Q_{N,V,T} \; e^{\beta \mu N} \tag{3.3}$$

where μ is the chemical potential of a particle in the system. As for the microcanonical ensemble, thermodynamic properties are derivable from these two last ensemble. This way, the Helmholtz' free energy is defined in the canonical ensemble as :

$$A_{N,V,T} = -k_{\mathrm{B}} T \ln Q_{N,V,T} \tag{3.4}$$

While the product of the pressure and the volume can be related to the grand potential:

$$PV = k_{\mathrm{B}} T \ln \Xi_{\mu,V,T} \tag{3.5}$$

3.2 Classical statistical mechanics

When considering a continuum approach rather than a quantum mechanical one, one has to integrate over all the classical "states" of a system. The canonical partition function becomes :

$$Q_{N,V,T} = \frac{1}{N! h^{3N}} \iint e^{-\beta H(p^N, q^N)} dp^N dq^N \tag{3.6}$$

where h is the Planck's constant, $H(p^N, q^N)$ the Hamiltonian of an N components system of coordinates q and momenta p. As the particles are indistinguishable the factor $N!$ comes into play in the denominator. The Hamiltonian

of the system is indeed the total energy of the system and can be written as the sum of kinetic energy $K(p^N)$ and a potential energy $U(q^N)$, which gives :

$$H(p^N, q^N) = U(q^N) + K(p^N) \tag{3.7}$$

Then, if one integrates over the kinetic part, equation (3.6) can be simplified as follow :

$$Q_{N,V,T} = \frac{1}{N!\Lambda^{3N}} \int e^{-\beta U(q^N)} dq^N \tag{3.8}$$

where $\Lambda = h/\sqrt{2\pi m k_B T}$ and m is the mass of one particle.

3.3 Protonation state

As stated in chapter 2, the studied minerals carry titrable groups, clays on the edges and C-S-H on all surfaces. Several types of groups exist and are formed by a metal atom (Me) linked to a hydroxyl group. The total charge carried by those groups may vary and can be integer or fractional. A typical protonation/deprotonation reaction can be written as:

$$-Me - OH \longleftrightarrow -Me - O^- + H^+ \tag{3.9}$$

The intrinsic dissociation constant of above reaction is defined by :

$$K_{Me-O} = \frac{a_{H^+} a_{Me-O}}{a_{Me-OH}} = \frac{\gamma_{H^+}\gamma_{Me-O}}{\gamma_{Me-OH}} \cdot \frac{c_{H^+} c_{Me-O}}{c_{Me-OH}} \tag{3.10}$$

where a_i are the activities, c_i the concentrations and γ_i activity coefficients of the species i. One can then express the pKa in terms:

$$pKa = -log\frac{\gamma_{H^+}\gamma_{Me-O}}{\gamma_{Me-OH}} - log\frac{c_{H^+} c_{Me-O}}{c_{Me-OH}} \tag{3.11}$$

Let's denote $\Gamma = \gamma_{H^+}\gamma_{Me-O}/\gamma_{Me-OH}$ and pH the negative logarithm of the proton concentration, we obtain:

$$pKa = -log\Gamma - log\frac{c_{Me-O}}{c_{Me-OH}} + pH \Longleftrightarrow -log\frac{c_{Me-O}}{c_{Me-OH}} = log\Gamma - (pH - pKa) \tag{3.12}$$

where $\frac{c_{Me-O}}{c_{Me-OH}}$ is the probability of deprotonation of the group, and can be written as a free energy difference:

$$\beta\Delta A_{MeOH\to MeO} = -ln\frac{c_{Me-O}}{c_{Me-OH}} = ln\Gamma - ln10 \cdot (pH - pKa) \tag{3.13}$$

$ln\Gamma$ is defined as the sum of excess chemical potentials of all the species. This can be used [20,21] to derive an MC move as explain in section 5.3.4 .

[20] M. Ullner, B. Jönsson, and P.-O. Widmark, J. Chem. Phys. **100**, 3365 (1994).
[21] M. Lund and B. Jönsson, Biochemistry **44**, 5722 (2005).

Chapter 4

Intermolecular Interactions

The most accurate way to calculate the total interaction between two particles would be to solve the Hamiltonian of this system. This quantum mechanical calculation is at least very expensive and at worst impossible to carry out. It is then necessary to use interactions like electrostatic interactions, exchange repulsion or van der Waals interactions [22] to describe the behavior between particles [23]. The aim of this chapter is not to give a full descriptions of all the existing interactions but rather to give a brief description of those used in papers I - V.

4.1 Coulombic interactions

Two charged species i and j sitting at a fixed distance r_{ij} from one another will experience the field emitted by the other molecule. This strong and long-ranged interaction is known as the Coulombic interaction [24] and reads :

$$u(r_{ij}) = \frac{q_i q_j}{4\pi\epsilon_0 r_{ij}} \tag{4.1}$$

where q are the charges of the species and ϵ_0 is the permittivity of vacuum (ϵ_0 = $8.854.10^{12}$ $C^2 J^{-1} m^{-1}$). This description of the interplay between two charged species does not take into account any influence of a surrounding medium and remains only correct in vacuum. When the charged molecules are immersed into a solvent, the solvent molecule rearrange according to the total emitted field. The effect is particularly important in a highly polar solvent like water. It can be derived that for purely dipolar solvent the electro-

[22] V. A. Parsegian, *van der Waals Forces* (Cambridge University Press, New York, 2006).
[23] J. Israelachvili, *Intermolecular and Surface Forces* (Academic Press, London, 1991), 2nd edn.
[24] J. D. Jackson, *Classical Electrodynamis* (John Wiley & Sons, Inc., New York, 1999).

static interactions scale with a factor of ϵ_r^{-1}, where ϵ_r is the dielectric constant, changing the Coulomb interaction to its solvent average form :

$$w(r_{ij}) = \frac{q_i q_j}{4\pi\epsilon_0\epsilon_r r_{ij}} \tag{4.2}$$

The most commonly used solvent is water and its dielectric constant is equal to 80 at room temperature. Indeed, dielectric constant is known to be temperature dependent as well as salt concentration dependent [25,26]. The averaged Coulomb interaction is then a free energy. When salt is introduced in the solution, it will influence the interactions the same way the solvent does. It becomes possible to derive the expression of the Coulomb interaction when a simple 1:1 salt is taken into account. This is known as the Debye-Hückel potential [4] , derived from the linearized Debye-Hückel theory [27] :

$$u(r_{ij}) = \frac{q_i q_j}{4\pi\epsilon_0\epsilon_r}\frac{e^{-\kappa r_{ij}}}{r_{ij}} \tag{4.3}$$

where κ is the inverse Debye screening length and is defined as :

$$\kappa^2 = \frac{\sum_i (z_i e)^2 c_i}{\epsilon_0\epsilon_r k_B T} \tag{4.4}$$

where c_i and z_i are the concentration and the valency of the ionic species i, respectively. Scaling the Coulomb interaction with $e^{-\kappa r_{ij}}$ simply represents the decay of the electrostatic interactions due to the salt screening.
Note that in all papers included in the thesis, ϵ_r is considered constant throughout space. This approximation is often used in simulation of colloïds and is known to give a good agreement between simulations and experiments for several types of processes [28], like the charging process for instance.

4.2 Short ranged interactions

Due to Pauli's exclusion principle, it is known that two particles repel one an other at short separation. The simplest way to account for the finite size of the particles in a simulation is to consider them as impenetrable hard spheres. This is denoted as the hard sphere model :

$$u(r_{ij}) = \begin{cases} 0 & r_{ij} > \sigma_{ij} \\ +\infty & r_{ij} < \sigma_{ij} \end{cases} \tag{4.5}$$

[25] J. Hubbard and L. Onsager, J. Chem. Phys. **67**, 4850 (1977).
[26] J. M. Cailol, D. Levesque, and J. J. Weis, J. Chem. Phys. **85**, 6645 (1986).
[27] P. Debye and E. Huckel, Z. Physik **24**, 185 (1923).
[28] M. Lund, B. Jönsson, and C. E. Woodward, J. Chem. Phys. **126**, 225103 (2007).

where σ_{ij} is the minimum separation between species i and j, $\sigma_{ij} = (d_i + d_j)/2$, and d is the diameter. This potential presents inconvenience in the fact that it is not a continuous function and causes problems when one want to derive properties at contact, see e.g. force calculation in chapter 6.3. One way to circumvent this problem is to use a soft repulsive interaction. One of them is the 6-12 Lennard-Jones (LJ) potential expressed by :

$$u(r) = 4\epsilon((\frac{\sigma_{ij}}{r_{ij}})^{12} - (\frac{\sigma_{ij}}{r_{ij}})^{6}) \tag{4.6}$$

where ϵ describes the strength of the interaction. This potential combines the short range attractive part in r^{-6} from the van der Waals attraction with a soft repulsion that decays as r^{-12}. In fact, it is one of the most widely used potentials in the literature. One way to get rid of the attractive part and to preserve soft repulsion is to shift and truncate this potential. This gives rise to the shifted and truncated LJ potential :

$$u(r_{ij}) = \begin{cases} 4\epsilon((\frac{\sigma_{ij}}{r_{ij}})^{12} - (\frac{\sigma_{ij}}{r_{ij}})^{6}) + \epsilon & r_{ij} < \sqrt[6]{2}\sigma_{ij} \\ 0 & r_{ij} > \sqrt[6]{2}\sigma_{ij} \end{cases} \tag{4.7}$$

It has the advantage of being less long-ranged than a pure r^{-12} soft repulsive potential.
Note that the combination of the Coulombic interaction and the hard sphere model is called the primitive model [18] and is often used in simulations of colloïdal systems.

4.2.1 Effective pair potentials

The use of *effective* pair potentials is an attractive and efficient way to model / simulate complex systems [29] like the ones of interest in this work. Indeed, in such systems a brute force calculation that would involve, in addition to the many atoms constituting the particles, a molecular description of the *dense* solvent, i.e. water concentration is roughly 55 mol/l, and all the ions is extremely challenging if not stupid. The philosophy behind the term *effective*, instead, consists in *averaging* over all the configurations of some of the components. An effective pair potential has by its very nature, the characteristics of a free energy. As an example, equation 4.2, introduced in preceding section, is an effective pair Coulombs potential where the solvent molecules has been averaged out and reduced to one single quantity that is the dielectric constant ϵ_r. Similarly, equation 4.3 for the screened Coulombs interaction is a

[29] M. Turesson, B. Jönsson, and C. Labbez, Langmuir **28**, 4926 (2012).

effective potential between two point charges where the degrees of freedom of the solvent molecules and ions have been averaged over.

On a more general ground, the effective pair potential, or the potential of mean force between two macro-particles ($w^{(2)}(R)$), defines the average work needed to bring particles i and j from infinite separation to R,

$$w^{(2)}(R) = -\int_{\infty}^{R} F_{ij}(r)\mathrm{d}r \tag{4.8}$$

where $F_{ij}(r)$ is the average force acting on the macro-particles i and j when separated a distance r. $w^{(2)}(R)$ is also related to the probability P(R) of finding two macro-particles a distance r,

$$P(R) \propto exp(-w^{(2)}(R)/k_B T) \tag{4.9}$$

Chapter 5

Monte Carlo Simulations

Many different simulation techniques from diverse origin exist. Many of them are based on statistical mechanics, like Molecular Dynamic (MD), Brownian Dynamic (BD) or Monte Carlo (MC) [30,31,32]. The one of interest here is the MC simulation technique. While MD and BD are dynamic simulations and calculated properties are time-averaged properties, MC is a stochastic technique and works with ensemble average. From MC, it is possible to evaluate definite multidimensional integrals, like eq. 3.8, which are intractable with analytic techniques. It also provides several advantages inherent to this technique: i) the equilibrium is quickly reached, ii) it allows the use of a large number of ensembles and iii) it allows unphysical displacements of the particles.

5.1 Thermal averages and importance sampling

Actually, MC simulations can not be used to evaluate directly integrals of the form $\int e^{-\beta U(q^N)} dq^N$ but indeed they make reachable thermal average of any observable ξ which expression is given by:

$$< \xi >= \frac{\int \xi(q^N) e^{-\beta U(q^N)} dq^N}{\int e^{-\beta U(q^N)} dq^N} \tag{5.1}$$

Technically, this can be done by averaging over a high number of reproduc-

[30] D. Frenkel and B. Smit, *Understanding Molecular Simulation* (Academic Press, San Diego, 1996).

[31] M. P. Allen and D. J. Tildesley, *Computer Simulation of Liquids* (Oxford University Press, Oxford, 1989).

[32] Landau and Binder, *A Guide to Monte Carlo Simulations in Statistical Physics* (Cambridge University Press, Cambridge, 2000).

tions of the system which are representative of an ensemble. Those are generated stochastically with the help of random numbers. Obviously, the more configurations of the system are generated and averaged over, the more accurate the evaluation of the observable. Note that, it is important to use a good random number generator if one wants to avoid bias in the sampling. This will not be developed in this book, for more detailed information see reference [32]. However, at this point, one problem emerges. Most of the generated configurations of the system will not give any informations about the observable of interest. Then an important number of reproductions would be needed to evaluate correctly $< \xi >$ and it would turn MC simulations into a slow and useless technique. Indeed only configurations which gives informations of interest should be sampled. This problem is solved with the method of the Metropolis Importance Sampling [33]. The idea is to sample configurations with a probability proportional to their Boltzmann weight :

$$P(q_i^N) = \frac{e^{-\beta U_i(q_i^N)}}{\int e^{-\beta U(q_i^N)} dq_i^N} \tag{5.2}$$

where i, refers to the i:th configuration of the system. Then it follows that the probability of going from the configuration i to j is defined as :

$$\frac{P(q_i^N)}{P(q_j^N)} = e^{-\beta(U(q_i^N) - U(q_j^N))} \tag{5.3}$$

Equation 5.3 is actually very useful as it defines the Metropolis acceptance test in a MC simulation in the canonical ensemble, that is : the probability of acceptance to go from configuration i to j is :

$$\alpha_{acc}(i \to j) = min(1, e^{-\beta(U(q_j^N) - U(q_i^N))}) \tag{5.4}$$

The use of this criteria will be detailed in the next section.

5.2 The procedure

In this section, the procedure for a typical MC simulation is described. The first step is to choose a box of any form (cubic, cylindrical, ...), where the model particles are placed (randomly or not). Unfortunately the number of sites (including particles, or other species) that a MC simulation can handle is relatively limited, i.e about 10^6. Hopefully the thermodynamic limit is reached for really small systems, and few particles are needed to get a proper

[33] N. A. Metropolis, A. W. Rosenbluth, M. N. Rosenbluth, A. Teller, and E. Teller, J. Chem. Phys. **21**, 1087 (1953).

statistical average. At this point a problem that may arise, depending on the type simulation box used, is that the surface of the box will have a strong influence on the particles. Or, when interested in bulk properties, one wants to avoid this effect. One way to circumvent it, is to apply periodic boundary conditions to the box. It consists of reproducing the main simulation box in all directions. This creates an artificial periodicity that mimics the bulk conditions. The next step is to run the Markov chain that consists of several operations :

- Choose a particle at random in the simulation box.
- Apply a random move to the particle. Different kind of moves are developed in the next section.
- Calculate the energy difference (using the chosen potential(s)) between the new and the old configuration. $\Delta U = U_{new} - U_{old}$.
- Apply the Metropolis acceptance criteria. For that, one needs to generate a random number, denoted $Rand \in [0, 1]$. The move is accepted if $Rand < \alpha_{acc}$ (Eq. 5.4), else rejected.
- If the move is accepted, sample the desired properties.
- Start again from first step.

Usually a first run is done without any sampling. This is called the equilibration run. The aim of this operation is to make sure that the system has reached equilibrium before one starts sampling equilibrium properties. It is actually in the second run, called the production run, that all properties are sampled. On the paper, running MC simulations seems like an easy task. But sometimes it is a bit more intricate. Highly concentrated systems or systems in (semi-)crystalline phases might reveal themselves tricky to equilibrate due to their slow "natural" dynamics. As an example figure 5.1 shows the evolution of the total energy of a system constituted of 200 platelike particles build of 199 sites at a high volume fraction of 21 % and at a salt concentration of 1 mM. The system needs between 2 and 2.5 10^6 cycles (= moves per particles) to be equilibrated, which corresponds to 8 days of calculation time on 8 processors. This is a typical behavior when one deals with simulations of liquid crystal phases (papers II - IV). At higher volume fraction up to 4 months were necessary to equilibrate the systems.
A way to help the simulations to converge faster is to implement in the Markov chain the use of cluster moves, see after 5.3.2.

5.3 Monte Carlo moves

When a particle is moved in the simulation box, the detailed balance criteria has to be fulfilled, i.e. in equilibrium the probability of accepting a move from

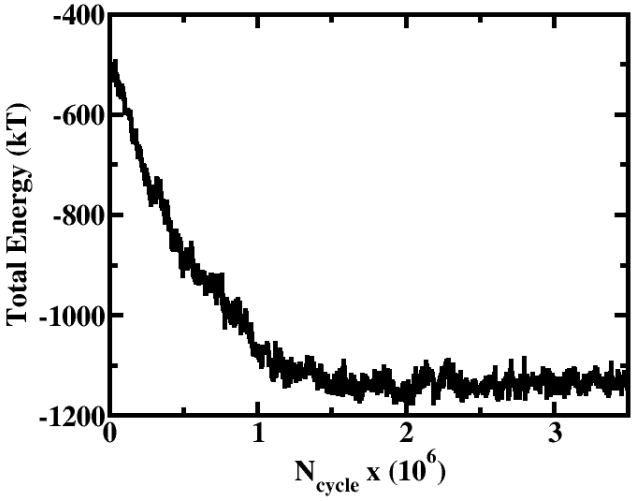

Figure 5.1: Evolution of the total energy as a function of the number of cycles for a system of 200 platelets constituted of 199 sites for a volume fraction of 21 % and a salt concentration of 1mM.

configuration 1 to 2 has to be the same as the reverse move (from 2 to 1). This implies :

$$P(1)\pi(1 \to 2) = P(2)\pi(2 \to 1) \tag{5.5}$$

where *P(x)* is the probability to be in state x and $\pi(a \to b)$ is the transition probability to go from configuration *a to b*. Eq. 5.5 can be rewritten :

$$\frac{\pi(1 \to 2)}{\pi(2 \to 1)} = \frac{P(2)}{P(1)} = e^{-\beta(U(2)-U(1))} \tag{5.6}$$

5.3.1 Single particle displacements

Single particle displacements are the simplest move that exists in a MC simulation. They consist in choosing one particle at random and translate or rotate it a certain distance or angle. The amplitude of the moves are usually set as input parameters of the MC runs. As a rule of thumbs, displacement parameters are usually set so that the acceptance ratio is between 20 and 40%.

5.3.2 Cluster moves

Sometimes moving the particles and sampling the configurational space might be difficult. A trick to help the sampling is to create a "bias" in the MC simulation by using unphysical moves that are more likely to be accepted. A cluster move [30,34]consists in gathering several particles into a cluster and to make a collective displacement (translation or rotation) of all particles that belong to the cluster. The acceptance criteria of such a move is :

$$\alpha_{acc}^{cluster} = min(1, e^{-\beta\Delta U} \prod_{kl} \frac{1 - p^{new}(k,l)}{1 - p^{old}(k,l)}) \tag{5.7}$$

where p(k,l) is the probability for particle k (inside the cluster) and l (outside the cluster) to be in the cluster. The simplest way to use this criteria is to make sure that the total number of particles in the cluster is the same before and after the move. The criteria of affiliation of one particle to the cluster remains of the choice of the user as the results do not depend on the cluster form. This is actually satisfactory since it allows to adapt the cluster shape according to the structure and geometry of the studied system. In papers II -IV, instead of using the common spherical cluster, where all particles included in a sphere of radius R from a random particle belong to the cluster, infinite thin slit and sphero-cylindrical clusters have been developed. A 2D sketch of the cluster moves with a sphero-cylinder is drawn in figure 5.2.

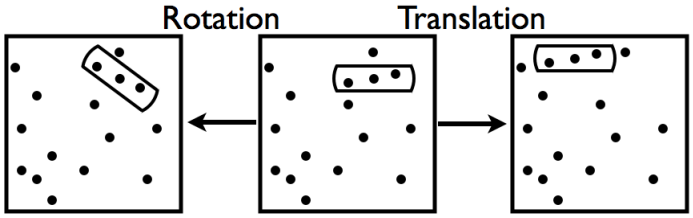

Figure 5.2: Schematic representation of a cluster move. The cluster described is the sphero-cylindrical cluster and the figure on the left hand side describes the result of a rotation while on the right hand side, the result of a translation.

The infinite slit cluster has a fixed thickness (defined in the input parameters).

[34] H. L. Gordon and J. P. Valleau, Mol. Simul. **14**, 361 (1995).

It allows the common displacement of aligned particles. This has been shown to be efficient when dealing with layered liquid crystal phases, e.g. Smectic B and columnar phases. The sphero-cylinder cluster has also a fixed thickness but a variable radius taken at random and allows the displacement of close proximity particles like aggregated particles. It has been shown to be efficient for gel phases. Rotation moves of the slit cluster is, however, limited to small angles, typically $\sim 5 - 6^{\circ}$, since artefacts in the cluster configuration can occur due to the periodic boundary conditions, as illustrated in figure 5.3.

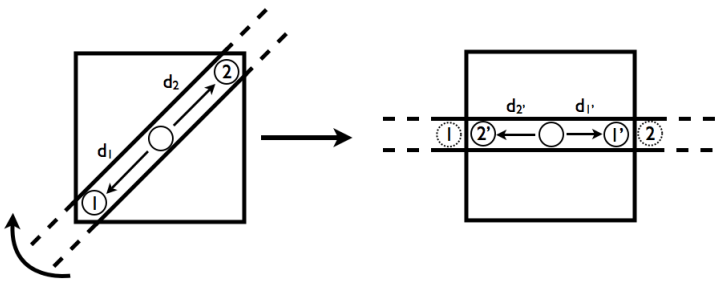

Figure 5.3: Schematic representation of the rejection of a rotation move of an infinite cluster. In this case the periodic boundary conditions lead to the creation of an artefact in the cluster.

In this particular example, particles 1 and 2 are moved out of the simulation box after rotation of the cluster. Once the periodic boundary conditions applied, the particles are found in the new positions 1' and 2' with the new interparticle distances inside the cluster different from the original ones, i.e. $d_1 \neq d_{1'}$ and $d_2 \neq d_{2'}$. In this case the detailed balance is not respected and the MC move is rejected.

5.3.3 Addition or deletion of species

When simulating in the grand canonical ensemble, the simulation box is connected to a reservoir of particles of appropriate species (salt, macroions ...). This implies that besides of the normal moves, the species have to be allowed to enter and leave the simulation box. This is done by trying random additions or deletions of the species in the box [35]. The acceptance criteria for insertion is defined as :

[35] J. P. Valleau and K. Cohen, J. Chem. Phys. **72**, 5935 (1980).

$$\alpha_{acc}^{insertion} = min(1, \frac{V}{\Lambda^3(N+1)} e^{(\beta(\mu-\Delta U))}) \tag{5.8}$$

and for deletion as:

$$\alpha_{acc}^{deletion} = min(1, \frac{N\Lambda^3}{V} e^{(-\beta(\mu+\Delta U))}) \tag{5.9}$$

where ΔU is the energy difference between the new configuration where the species are added or removed and the old configuration, V is the volume of the box, and N the number of species. When changing the number of charged species, one has to be careful to keep electroneutrality in the box. This is done by adding a number of molecules whose total charge is zero.

5.3.4 Grand canonical titration method

From the thermodynamic derivation in section 3.3 we extracted the free energy difference upon deprotonation of a titrable site. This can been used to develop a MC titration move at the level of the primitive model where the protons are treated implicitly and for which the energy difference can be written as:

$$\Delta U = \Delta U^{el} \pm kT \ln 10(\mathrm{pH} - \mathrm{p}K_0) \tag{5.10}$$

where ΔU^{el} is the electrostatic part and the second term on the right hand side accounts for the chemical effects through the log decimal of the intrinsic dissociation constant ($\mathrm{p}K_0$) evaluated in the appropriate thermodynamic reference state (ideality). Note that the minus sign is for deprotonation and the plus sign for protonation.
In practice, the method consists in (i) changing the charge status of the site taken at random and (ii) moving an arbitrary salt ion in or out from the simulation box to maintain the electroneutrality of the system. Steps (ii) makes eq. 5.10 incorrect by an energetic term associated with the move of the simple salt ion. A grand canonical titration method has been proposed [36] to remedy this problem. It relies on the idea that the titration can be decomposed in several steps. As an example the (de)protonation can be decomposed in two successive steps that involve i) the (de)protonation of the surface and ii) the exchange of the ion couple (H^+, B^-) with the bulk. For deprotonation, the acceptance rule thus reads:

$$\alpha^{deprotonation} = min(1, \frac{N_B}{V} e^{-\beta\mu_B} e^{-\beta\Delta U^{el}} e^{+\ln 10(\mathrm{pH}-\mathrm{p}K_0)}) \tag{5.11}$$

[36] C. Labbez and B. Jönsson, Lect. Notes Comp. Sci. **66**, 4699 (2007).

and for protonation :

$$\alpha^{protonation} = min(1, \frac{V}{N_B + 1} e^{+\beta\mu_B} e^{-\beta\Delta U^{el}} e^{-\ln 10(\mathrm{pH}-\mathrm{p}K_0)}) \tag{5.12}$$

where μ_B is the chemical potential of the simple salt anion B^-.
This method was used in paper I.

Chapter 6

Simulations Techniques

An important number of simulation programs (open source and commercial codes) are available, e.g. Gromacs [37](MD), Faunus [38] (MC), Molcas [39] (QM). These codes can, in principle, be handled by a large community of expert and non-expert users. All the codes used during my PhD are in-house written. It is relevant to mention here that a lot of effort were devoted into code development and optimization to obtain the results presented in this work. The purpose of this section is to highlight some of the techniques I used to improve the efficiency of Monte Carlo simulations and to analyze the results.

6.1 Distance dependent coarse graining

As stated in chapter 2, one of the most efficient way to decrease the computing time is to coarse grain the system. For this purpose, a distance dependent coarse graining was developed and used in the simulations presented in papers II-IV. Its principle relies on the idea that at large inter-particle separation the use of the same level of particle description as at short separation is not necessary when calculating the inter-particle interactions. Indeed, a detailed description at short separation and a point-like net charge at large separation give almost the same degree of accuracy. Figure 6.1 illustrates the particle description employed on the fly during simulations as a function of their separation for calculating the interactions.
In practice, three levels of description were used, as described in Fig. 6.1, delimited by two cut-off distances, f_1 and f_2. These conveniently allow to

[37] http://www.gromacs.org/.
[38] http://faunus.sourceforge.net.
[39] http://www.molcas.org/.

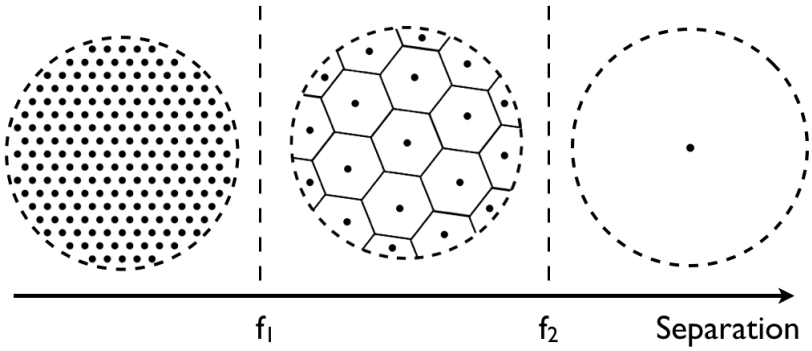

Figure 6.1: Description of a particle as a function of its separation with respect to the others when calculating the interactions. At short separations, the full description is used; at intermediate separations, the sites are gathered into a collection of hexagonal patches and at large separations the particle is reduced to a punctual net charge. f_1 and f_2 are user defined cut-off distances, see the text for more details.

switch from one level of description to another during a simulation. f_1 and f_2 were determined by comparing the energy of interaction between two rings of appropriate charge and size with those obtained with the level of description described above for a large range of screening length. At a given κ, the cut-off distance was defined as the distance that gives an energy difference of $\sim 10^{-6}$ kT. The obtained points were interpolated with a simple exponential function as exemplified in Figure 6.2. Note that the procedure has to be repeated for all particle sizes and net charges considered.

6.2 Phase characterization

6.2.1 Nematic order parameter

A convenient way to characterize a nematic phase in a simulation is to calculate the nematic order parameter (S) which is a measurable quantity in an experiment. S is bound between zero and unity and measures the long range orientational order characteristic of a nematic phase. It takes the value of unity in a sample where all the platelets are perfectly orthogonal to the sample director, $\mathbf{n}$, defined as the spatial and ensemble average of the particle normal vectors, $\mathbf{u}$. $S = 0$ when they are randomly oriented. As a matter of fact, $S^2 = P_2(r \to \infty)$ where $P_2(r)$ is the second Legendre polynomial of the azimuthal angle between the normal vectors of two platelets. $P_2 = 1$ when the normals are parallel and $P_2 = -1/2$ when perpendicular. Typically, $S \sim 0.4$

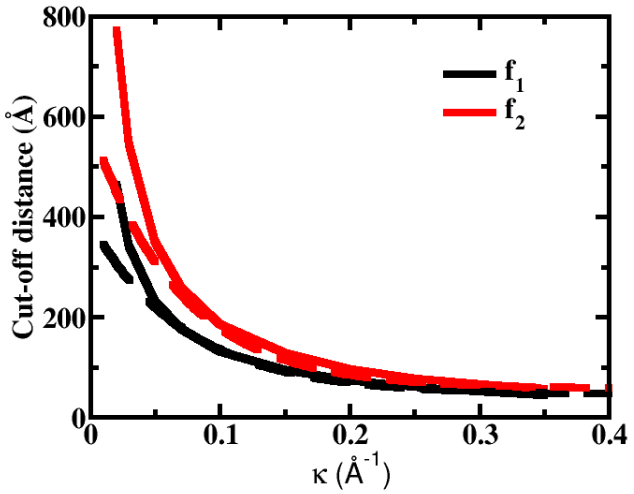

Figure 6.2: Cut-off distances, f_1 and f_2, as a function of the inverse screening length κ for particles having a diameter of 150 Å, a net charge of -103 e and patches with a net charge of -19e. The dashed lines show the result of the exponential fits.

at the isotropic/nematic phase transition. In addition, S is found to increase rapidly with ϕ at the isotropic/nematic phase transition which allows to define quite accurately its position, as exemplified in figure 6.3.
Although S can in principle be calculated from P_2 extrapolated at large r it is in most of the cases computationally cumbersome since this presupposes that simulations are run on large systems. More conveniently, S may be obtained from the evaluation of the director [40]. Indeed, S can be written as the following ensemble average,

$$S = \frac{1}{2N}\langle\sum_{i}^{N} 3\mathbf{u}_i \cdot \mathbf{n} - 1\rangle \tag{6.1}$$

where N is the total number of particles. The length scale of director fluctuations is large compared to a typical simulation box size, and, consequently, a single director apply to the simulated sample at any instant. That is, the typical length scale of a liquid crystal without defect is considerably larger

[40] M. Allen, G. T. Evans, and D. Frenkel, *Hard Convex body fluids* (John Wiley & Sons, Inc., New York, 1993).

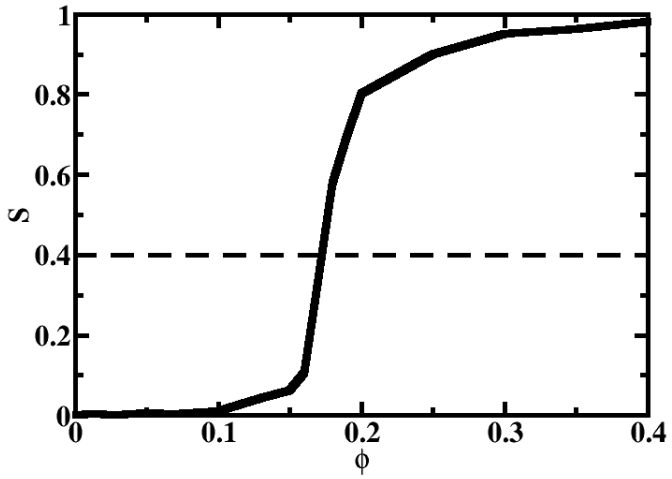

Figure 6.3: Nematic order parameter as a function of ϕ calculated for a system of 200 uncharged platelets constituted of 199 sites and of diameter 150 Å. S is found to increase rapidly at the isotropic/nematic transition.

than what is so far possible to simulate. During the course of a simulation the director, however, slowly fluctuates, i.e. change direction. The difficulty to determine the nematic order parameter is, thus, to determine the director. For this purpose two routes were followed. The first consists in calculating the director for each configuration, since $\mathbf{u}_i = -\mathbf{u}_i$ (no polarity), $\mathbf{n}$ can be calculated like $\mathbf{n} = \sum \pm \mathbf{u}_i$, and S from equation 6.1. The second is based on the maximization of S with respect to rotation of $\mathbf{n}$. It can be shown [40] that writing $S = \mathbf{n} \cdot \mathbf{Q} \cdot \mathbf{n}$, where $\mathbf{Q}$ is the order parameter tensor, reduces the problem to diagonalizing $\mathbf{Q} \cdot \mathbf{Q}$, and may be written as,

$$< Q >= \frac{1}{N} \langle \sum_{i=1}^{N} \frac{3}{2} \mathbf{u}_i \cdot \mathbf{u}_i - \frac{1}{2} \mathbf{I} \rangle \tag{6.2}$$

where $\mathbf{I}$ is the identity matrix. The eigenvalues of this tensor are λ_+, λ_0 and λ_- in order of decreasing size. They are directly related to the order nematic parameter as :

$$\begin{cases} \lambda_+ = S \\ \lambda_0 = -S/2 \\ \lambda_- = -S/2 \end{cases} \tag{6.3}$$

The eigenvector corresponding to λ_+ gives the director.

Figure 6.4 shows the behavior of the calculated nematic order parameter as a function of the number of MC cycles at two different volume fractions using the two methods described above. At low particle concentrations, i.e in the isotropic phase (Fig. 6.4 left), S values obtained from equation 6.3 are converged after $\sim$ 500 cycles. From the direct evaluation of the director, equation 6.1, the results converge more slowly. Equation 6.3 is more accurate at low volume fraction but both techniques are equivalent at high volume fraction, see Fig. 6.4 right). In this example, S obtained from λ_+ and equation 6.1 are indistinguishable and after a few cycles, converge to $\sim$ 0.9. From this comparison and further tests, not presented here, it was found that S determined from λ_+ was the more stable one. All the calculations of S presented in the papers were thus determined from λ_+.

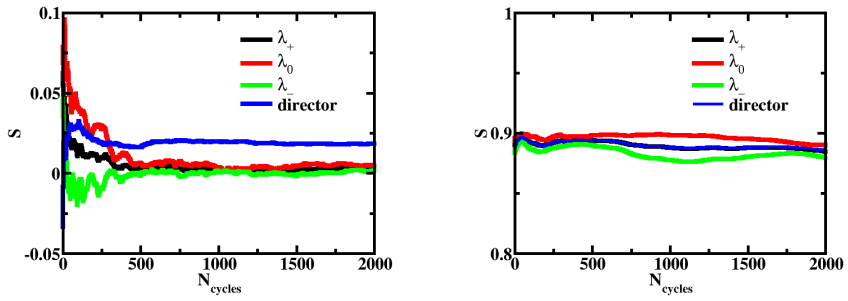

Figure 6.4: Nematic order parameter obtained from equations 6.3 and 6.1, see the text for more details. Simulations are performed for a system of 200 platelets constituted of 199 sites, of diameter 150 Å and net charge Z_{net}=-151e. The salt concentration is 10 mM and the particle volume fractions are chosen such as ϕ=7% (left), and 18% (right).

6.2.2 Columnar phases

In paper III formations of columnar phases are described. In addition to the usual radial distributions, several characteristic structural parameters were determined to characterize them. These are the average inter-columnar distance, the average intra-columnar distance and the average angle of the particles with the columnar phase director as depicted in Figure 6.5
To do so, the following procedure is used and repeated for all particles of a considered configuration. A "columnar" cylinder (dotted) and "planar" sphero-cylinder (dashed lines) centered on a chosen particle are created ori-

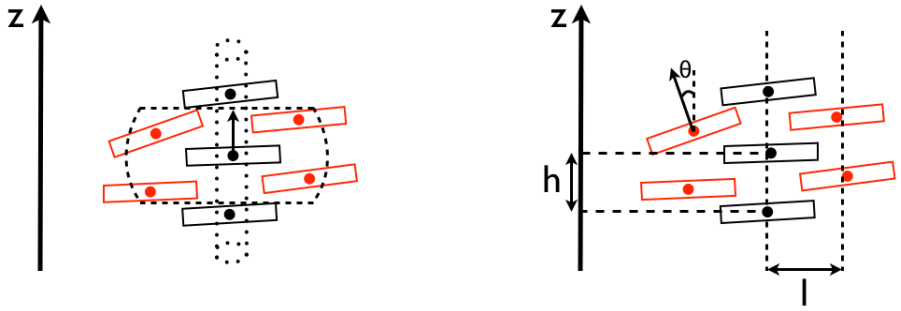

Figure 6.5: Schematic representation of the columnar structural parameters; h: intra-columnar distance; l: inter-columnar distance, θ average particle angle.

ented according to its normal vector. The columnar cylinder is used to determine the nearest neighbors in the same column called *intra-columnar* (black particles). The planar sphero cylinder (dashed line) is used to find the neighbors in the adjacent columns belonging to the same or nearest planes designated as *inter-columnar* (red particles). The geometrical parameters are then recorded as a function of the number of nearest intra- and inter-columnar neighbors. The analysis is included in the Markov chain and takes place typically every 4000 cycles. At the end of the MC simulations the distribution of the different structural parameters are determined. Note that the dimensions of the two geometrical probes have to be adapted according to the columnar phase studied.

6.2.3 Gels

As explained in chapter 5, MC simulations do not provide access to dynamic quantities. Then to capture the gel formation from the simulations, two parameters are considered: the percolation and the elasticity of the system. The percolation is studied through the connectivity of the particles in the simulation box. Two platelets are considered to be "connected" neighbors if the separation between a site in one platelet is within 15Å of a site in the other. Several connected platelets are said to form a cluster. From these definitions several quantities are calculated like:

- The average number of neighbors for a platelet in a cluster ($\langle N_{nei} \rangle$).
- The average number of platelets in a cluster ($\langle N_{cl} \rangle$).
- The probability to find a particle in a cluster of size X ($\langle P_X^{cl} \rangle$).

- The average fraction of particles in a cluster = $\int_2^N P_X^{cl} dX$ ($\langle f^{cl} \rangle$).

The elasticity of the suspension is evaluated calculating the average squared force acting on a particle. For that, the squared force is calculated for the three Cartesian components: $\langle F_x^2 \rangle$, $\langle F_y^2 \rangle$ and $\langle F_z^2 \rangle$ where:

$$\langle F_x^2 \rangle = - \left\langle \left(\frac{\partial w(R)}{\partial x} \right)^2 \right\rangle \tag{6.4}$$

The total average squared force is then considered to be the arithmetic average of the three Cartesian components.

6.3 Potential of mean force between two platelets

In paper V the potential of mean force, pmf, between two charged platelets is studied at the level of the primitive model. The pmf is calculated within a closed cylindrical cell where the particles are allowed to move along the axis of revolution of the cell z.
The pmf calculation of two platelets quickly becomes computer demanding as their size grow. This is related to the difficulty to move the platelets due to their geometrical anisotropy, the number of species involved and the magnitude of the interactions in play. For this reason the calculation of the pmf from the platelet radial distribution function, c.f. equation 4.9, turns out to be rather inefficient although cluster moves were employed and the sampling was split into several windows. Alternatively, the pmf can be extracted from the inter-particle force calculated at fixed positions R. The force can either be calculated at contact with the colloids or at the cylinder mid-plane, see below. The latter was found to be the more efficient mainly because the ion density at the mid-plane is much lower than at contact with the colloids.
Figure 6.6 compares the calculated pmf between two platelets with 19 sites (50 Å in diameter) immersed in a 10 mM 2:1 salt solution at $\phi = 0.013$ using the different approaches described above. In paper V the two last techniques have been used to sample the free energy since they are either easier to use or more accurate.

In the following we will assume two colloids decorated with n_s charged sites, immersed in a salt solution containing N_i ions. In addition, the sites and ions are considered as charged Lennard-Jones (LJ) particles.

6.3.1 Contact force approach

The mean force between two platelets for a fixed colloid center-to-center separation R can be evaluated at contact [30,31]. It can be written as the sum of four distinct terms, see eq. 6.5. The two first terms are the direct Coulombs and LJ

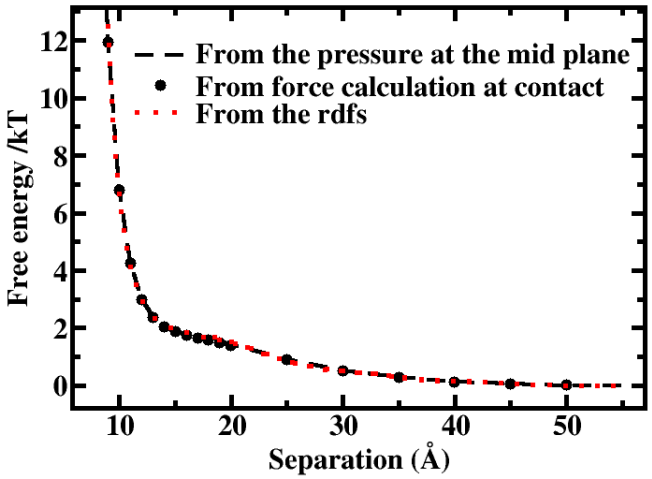

Figure 6.6: Potential of mean force between two platelets with 19 sites (50 Å in diameter) immersed in a 10 mM 2:1 salt solution at $\phi = 0.013$ obtained from three different approaches. Full curve: mid-plane approach; symbols: contact force approach; dotted curve: radial distribution function approach.

forces between the colloids. The two last terms are the ensemble average of the electrostatic and LJ forces exerted on the colloids by the surrounding ions.

$$F(R) = - \left\langle \sum_{i=1}^{n_s} \sum_{j=1}^{n_s} \left(\frac{\partial u^{el}(r_{s_i s_j})}{\partial R} + \frac{\partial u^{LJ}(r_{s_i s_j})}{\partial R} \right) \right\rangle - \left\langle \sum_{i=1}^{N_i} \sum_{j=1}^{n_s} \left(\frac{\partial u^{el}(r_{i s_j})}{\partial R} + \frac{\partial u^{LJ}(r_{i s_j})}{\partial R} \right) \right\rangle \tag{6.5}$$

6.3.2 Mid-plane approach

The mean force can also be evaluated over the mid-plane [41,42] ($z = 0$) for a fixed colloid center-to-center separation R along the main axis, z, of the cylinder cell. By doing so, the total mean force can be divided into three

[41] P. Linse, Adv. Polym. Sci. **185**, 111 (2005).
[42] J. Z. Wu, D. Bratko, H. W. Blanch, and J. Prausnitz, J. Chem. Phys. **111**, 7084 (1999).

terms according to 6.6.

$$F(R) = F^{el}(R) + F^{LJ}(R) + F^{id}(R) \tag{6.6}$$

The terms $F^{el}(R)$ and $F^{LJ}(R)$, are calculated by summing all Coulomb and LJ forces between species residing on different sides of the mid-plane. The last term is the ideal contribution, which can conveniently be defined as

$$\beta F^{id}(R) = [\rho_I(z = 0) - \rho_I(z = \pm L/2)]A \tag{6.7}$$

where $\rho_I(z = 0)$ and $\rho_I(z = \pm L/2)$ are the ion densities at the mid-plane and at the cylinder end walls of cross-sectional area A.

Chapter 7

Summary of Results and Concluding Remarks

7.1 Charging process of 2:1 clays

The role of electrostatic interactions on the acid-base titration of various natural clays is investigated in paper I. With a model that is shown to include the main physics, we demonstrate that the observed pH shift in the titration curves with the ionic strength originates from electrostatic interactions between the titratable edge charges and the permanent basal charge [43,44,45]. An excellent agreement is found between simulations and experimental titrating results. When looking at the titration of clay platelets stacks, like e.g. Illite, the point of zero net proton charge (PZNPC) is found to decrease when increasing the number of sheets in the stacks. These results are used to rationalize the order of apparent PZNPC (or PZSE in the case of pyrophyllite) found in the literature: Pyrophyllite ($4 <$ PZSE < 4.5) $<$ Illite $<$ Montmorillonite. Finally the mean field approach is shown to fail to describe the acid-base behavior of clays for low pH and high salt concentration.

7.2 Gel and glass formations

When attractive interactions are at play in a clay suspension, gels form at low volume fractions. They arise from the strong attraction between positively charged edges and negatively charged basal planes. Their formation is shown

[43] B. Baeyens and M. Bradbury, J. Contam. Hydrol **27**, 199 (1997).
[44] M. Duc, F. Gaboriaud, and F. Thomas, J. Colloid Interface Sci. **289**, 148 (2005).
[45] E. Tombácz and M. Szekeres, Appl. Clay Sci. **27**, 75 (2004).

to be enhanced for large particle sizes, high charge anisotropy and low salt concentration. A detailed study of the gel structure indicates that they are formed by a network of platelets organized in a mixture of "House of Cards" and "Overlapping Coins" configurations as experimentally observed [46].
For large platelets and high charge anisotropy, a phase separation between an equilibrium gel and a isotropic liquid phase is predicted at low volume fractions. The threshold volume fraction value at which the phase separation occurs is further found to increase with salt concentration. The same observations made for aged laponite dispersions, although the phase separated samples were found at lower volume fractions [46,47].
At intermediate charge anisotropy, a gel forms from a sol of clusters of individual particles randomly oriented that progressively grows with volume fraction in qualitative agreement with observations in montmorillonite clay dispersed in low pH and salt concentration aqueous solutions.
For entirely negatively charged platelets, a transition from an isotropic liquid to a glass phase occurs. This transition is favored for small particles in agreement with experimental observations on natural clay dispersions at neutral pH [48]. Reversely, the sol-gel transition and liquid-gel separation are found to be favored for large particles bearing a weak and strong charge anisotropy, respectively.
Finally, in the case of strong charge anisotropy, the liquid-gel separation is predicted to disappear in favor of a sol-gel transition upon decreasing the size of platelets. This is depicted by papers II and III.

7.3 Liquid crystal formation

Several liquid crystal phases were encountered throughout the studies. Their formation is studied as a function of charge anisotropy, ionic strength and size of the platelets in papers II-IV.

- A smectic B phase is found for volume fractions between 1 and 7% and low salt concentration ($<$ 10mM). Its formation is only observed when the particles bear a strong charge anisotropy. This phase dissolves at high salt concentration. Note that, it is the first time that such a phase is predicted for charged plate-like particles dispersed in an aqueous solvent.

[46] P. Mongondry, J. F. Tassin, and T. Nicolai, J. Coll. Interface Sci. **283**, 397 (2005).
[47] B. Ruzicka, E. Zacarelli, L. Zulian, R. Angelini, M. Sztucki, A. Moussaid, T. Narayanan, and F. Sciortino, Nature Mat. **10**, 50 (2011).
[48] L. J. Michot, C. Baravian, I. Bihannic, S. Maddi, C. Moyne, J. F. L. Duval, P. Levitz, and P. Davidson, Langmuir **25**, 125 (2009).

- The formation of the nematic phase has been shown to be favored by low aspect ratio for neutral platelets [16]. This result is also found in our simulations. Its formation is predicted to be further favored for uniformly charged platelets. Reversely, the presence of a charge anisotropy, i.e. positive charges on the edges, hinders the formation of a nematic phase. The latest is shown to disappear when the charge anisotropy is too strong. The isotropic-nematic transition is often close or pre-empted by a liquid-solid transition. We found that a true liquid-nematic transition may occurs when the platelets carry a low charge anisotropy or are entirely negatively charged.
- Finally, columnar phases are encountered for high volume fractions. Their formation is found to be favored by high charge anisotropy and low ionic strength. Depending on the positive charge distribution on the edges and the salt concentration, new columnar phases were discovered as *the zig-zag columnar phase, the interpenetrated rectangular and hexagonal columnar phases*. The latter was also recently predicted by Morales-Andra [49].

7.4 Growth and stability of nanoplatelets

In paper V, the growth of C-S-H nanoplatelets is shown to be limited by their own internal electrostatic repulsions. We also study in some details the stability of such particles in calcium salt solutions and discuss the possible consequences on the kinetic competition between the growth and aggregation of C-S-H platelets. Finally, we investigate the different modes of aggregation of these platelets onto C_3S grain surfaces. In agreement with experimental observations[50,51], it is found that a high calcium concentration and pH enhance the axial "growth" of the platelets, whereas opposite conditions enhance a lateral "growth".

7.5 Concluding remarks

In this book, I present the results I obtained when investigating several scientific problems by the use and development of computer simulations. The goal was not only to create theoretical models but also to bridge experiments and theories in order to give further insights into complicated physico-chemical

[49] L. Morales-Andra, H. H. Wensink, A. Galindo, and A. Gil-Villegas, J. Chem. Phys. **136**, 034901 (2012).
[50] S. Garrault and A. Nonat, Langmuir **17**, 8131 (2001).
[51] S. Garrault, E. Lesniewska, and A. Nonat, Material and Structures **38**, 435 (2005).

systems. The whole range of systems and chemical phenomena considered clearly demonstrate the importance of the study of plate-like particles, more especially as these results are relevant to many other systems.

The development of a model able to reproduce the main behavior and the complete phase diagram of charged plate-like particle suspensions has been an ongoing project for 30 years in physical chemistry. This thesis is a new step in this direction. It shows that the underlying physics of clays and C-S-H in aqueous solution can be partially captured by the use of simple models and theories. Further investigations involving more sophisticated theories or different techniques are of course needed to complete the picture.

An interesting aspect with computational physical chemistry is that computer power increases rapidly with time. There is no doubt that, in few years time, one will be able to approach scientific problems with a much more detailed description of the systems. This is a good thing considering the number of unanswered questions related to the behavior of dispersions of mineral plate-like particles.

Finally, I hope that the reader has found some interest in the work presented in this book and that the results will inspire further experimental and theoretical investigations.

Acknowledgements

I would like first to thank **Christophe** and **Bo** for giving me the opportunity to live this adventure in Sweden, for ALL support, explanations, scientific and personal discussions, encouraging words and interesting projects all along those four and a half years. Thank you for helping me to cross the line from student to researcher, even if it has not always been easy. For sure you have shaped who I am today and I am more than grateful for that. Thanks also to **André** for his advices in the different projects and his jokes in the coffee room.

Thanks to all seniors in France and Sweden and more particularly: **Mikael** for all your help and support and for being an attentive ear to me, **Magnus** for your scientific expertise and for sharing interest in music and drawings, **Jan** for all tips, **Marie** for all interesting seminars, and **Torbjörn** for always taking the time to answer my questions and for all clear explanations.

Martin Trulle, my swedish brother, thank you for making me discover how fun Sweden can be. Thanks also for ALL your help and interesting discussions (scientific or not) during those years.
Martin Ture and **Fabrice**, thanks to both of you for the nice discussions, strong support and all the laughs during the Cappucino and Mac Carthy's evenings.
Marie-Céline and **Mickael**, thanks for all the french evening shared in Sweden and for the moral support!
Björn, thank you for being a good course companion and for the help you provided me.
Segad, for being my office-mate and for the nice discussions.
Anil, for your joy and being the guardian for my bike.
Gleb, thank you for being a good "camping" buddy.
Sofi, thanks a lot for the strong support in the last weeks before printing the thesis.

I also want to thanks all other phD or postdoc that crossed my way during these years. In Sweden: **Jimmy**, **Pär**, **Jonas**, **Asbjörn**, **Samuel**, **Svante**, **Paulius**, **Ryan**, **Marta**, **Axel**, **Fei**, **Joao**, **Olof** in theoretical chemistry, **John**, **Jenny**, **Joakim**, **Nina**, **Luis**, **Salome**, **Agnieszka**, **Sanna**, **Charlotte**, **Patrick**,

Marianna in physical chemistry, and **Stina**, **Johan** and **Eric** in biophysics. In France: **Fafa**, **Stephanie**, **Gilles**, **Jeremy**, **Florent**, **Semra**, **Fousia** and **Guillaume**.

A BIG thank you to all secretaries **Eva**, **Bodil** and **Ingrid** in Sweden and **Agnes** in France for all the help with the paper work. You really made my life a hundred time easier!

Thank you **Paula** for your infinite patience and for all the help with the printing of the thesis.

There is also a couple of friends I would like to thank for being around, for all the joy, fun, laugh and support they brought me. The gang of four: **Laurent**, **Guillaume**, and **Benoit**, you guys are the best buddies ever. Thanks also to those people for being part of my life for so long: **Fanny**, **David**, **Fabo**, **Mathias**, **Mika**, **Fran**, **Lovisa**, **Martin J** and **Daniel J**. Thanks also to **Manu**, **Bertrand**, **Steph** and **Jack Daniel** for all touring with the band. That was hell lot of fun. A stort tack till **Åsa** och **Håkan** for their kindness, all dinner invitations and winter bbq. Merci à ces personnes : **Marie-M**, **Sophie**, **Marjorie**, **Charlotte**, **Alrick**, **Alice F.**, **Pauline**, **Tristen**, **Sam**, **Alice C.**, **JB**, **Frank**, **Terese**, **Coralie** and **Paulina** pour avoir joué un rôle dans ma vie au cours de ces dernières années.

Enfin, je voudrais remercier les membres de ma famille pour leur indéfectible présence à mes côtés, leur soutien en toutes circonstances, leurs conseils avisés et leur amour. Un grand merci à **Papa**, **Maman**, **JB**, **Ludo**, **Alexia**, **Fanny**, **Laeti**, **Fred**, **Tata Joc.**, **Mamie** et **Robert**. Je voudrais finir ce livre en ayant une pensée pour mon grand père **Jean** et ma marraine **Françoise** qui ne me verront malheureusement jamais docteur.

Paper I

Maxime Delhorme, Christophe Labbez, Céline Caillet and
Fabien Thomas
Langmuir, **26**, 9240-9249 (2010)

Paper II

Maxime Delhorme, Bo Jönsson and Christophe Labbez
submitted to *Soft Matter* (2012)

CREATED USING THE RSC LaTeX PCCP ARTICLE TEMPLATE – SEE www.rsc.org/electronicfiles FOR DETAILS

ARTICLE TYPE www. rsc.org/xxxxxx | XXXXXXXX

Monte Carlo Simulations of a Clay Inspired Model Suspension: The Role of Charge Anisotropy†

Maxime Delhorme,[a,b] **Bo Jönsson,**[b] **and Christophe Labbez**[*a]

Received Xth XXXXXXXXXX 20XX, Accepted Xth XXXXXXXXX 20XX
First published on the web Xth XXXXXXXXXX 200X
DOI: 10.1039/b000000x

We present a theoretical investigation of a model clay dispersion in 1-1 salt solutions varying the particle volume fraction, ionic strength as well as the charge distribution on the clay platelets. The platelets are modeled as discs with charged sites distributed on a hexagonal lattice. The edge sites can be positively charged while the remaining sites are negative giving rise to a charge anisotropy. Simulations are carried out using a Monte Carlo method in the canonical ensemble. The interactions between the platelet sites are described with a screened Coulomb potential plus a short range repulsive potential. Simulations show a complex phase behavior. When the charge anisotropy is strong, a repulsive liquid phase is found at low volume fraction and ionic strength. When increasing the latter an attractive liquid phase forms. At these volume fractions the platelets aggregate in an "Overlapping Coins" configuration. With increasing volume fraction the dispersion becomes unstable and the pressure goes through a van der Waals loop. A liquid crystalline phase, Smectic B, forms in the thermodynamically unstable region. On the other side of the van der Waals loop a stable gel phase is found. A phase separation between a liquid and a gel is thus predicted. The threshold value of the volume fraction at which the phase separation occurs is found to increase with the salt concentration. The gel structure is a mixture of "Overlapping Coins" and "House of Cards" configurations. When the charge anisotropy is intermediate, no phase separation occurs. Instead, a gel forms from a sol of clusters of individual particles randomly oriented that progressively growth with the volume fraction. These results are discussed in light of experimental observations on clay suspensions.

1 Introduction

Clay minerals are hydrous aluminium (sometimes magnesium) phyllosilicates with variable amount of other cations. They have an anisotropic structure and form flat hexagonal or discotic sheets (occasionally fibrous) having radii ranging from tens of nanometers to μm and a thickness in the nm range. The sheets are formed from tetrahedral silicate and octahedral aluminate layers. Usually, the basal plane has a negative structural charge (permanent) due to chemical substitution of Al^{III} by Mg^{II} and Si^{IV} by Al^{III} or Fe^{III}, respectively. In contact with water the edges ionize due to the presence of titrable sites, mainly aluminols and silanols[1]. The resulting edge charge is amphoteric, that is, it is positive at acidic or neutral pH and negative in basic solutions[2,3]. Thus, clay platelets dispersed in water have both a *structural* and a *charge* anisotropy. These anisotropies give rise to peculiar structural and dynamic properties, which are exploited in processes and products such as drilling, cements, paints, papers, softeners and composite materials[4–6].

In dilute dispersions, clays with a medium structural charge density (e.g. Montmorillonite, Laponite) swell and form isotropic suspensions of mainly individual clay sheets that exhibit Newtonian flow (the shear rate is proportional to the applied shear stress). Under semi-dilute conditions and beyond, the flow becomes plastic and eventually exhibits a yield stress characteristic of a gel formation[7–11]. In other words, the gel starts to yield only above a critical applied stress. Clay suspensions are anti-thixotropic and have a high viscosity at low shear rate[12] where electrostatic interactions dominate over hydrodynamic forces[13]. At high shear rate, they are thixotropic with a low viscosity which come as a result of the particle alignment along the hydrodynamic forces and of the network restructuration after shear[8,14–18]. Baravian and co-workers[18,19] found that the shear thinning of the flow in dilute and semi-dilute clay dispersions with a volume fraction of $\phi < 0.025$ and at low salt concentrations (< 5 mM) can, to first order, be explained on the basis of excluded volume effects. However, electrostatic interactions still play a significant role, as best illustrated by both the zero and infinite shear limit viscosity[18,19], which are not fully understood. The yield stress has been shown to be highly dependent upon pH with a minimum at a pH value where the edges are neutral[3,12]. In addition, it also exhibits a minimum as a function

† Electronic Supplementary Information (ESI) available: Coarse graining method See DOI: 10.1039/b000000x/

[a]*Laboratoire Interdisciplinaire Carnot Bourgogne, UMR 6303 CNRS, Université de Bourgogne, 21078 Dijon Cedex, France. Fax: +33 (0)380 393819; Tel: +33 (0)380 396176; E-mail: christophe.labbez@u-bourgogne.fr*
[b]*Theoretical Chemistry, Chemical Center, POB 124, S-221 00 Lund, SWEDEN*

of salt concentration [20]. These two examples show the importance of Coulombic interactions and charge anisotropy. It is generally agreed from these experiments that the unusual rheological properties of clay dispersions and other similar particle dispersions [17,21–25] are related to the formation of both *attractive* and *repulsive* networks.

The boundary between the sol-gel transition in ionic strength (I) vs particle volume fraction (ϕ) phase diagrams is in many cases found to have a ">" shape [10,18,26,27]. This shape may be interpreted as follows [28,29]: at low ionic strength, interactions among the particles are dominated by electrostatic repulsion and the dispersion appears as a Wigner glass; when I is increased, the electrostatic interactions are screened and as a result the sol-gel transition moves toward higher ϕ. At high I, electrostatic interactions are completely screened out and the interactions between platelets are then governed by attractive interactions which causes the system to flocculate. Though this picture should be valid for homogeneously charged particles, it is most probably wrong for particles with a charge anisotropy. This is suggested by the relatively small amount of salt needed in order to observe a re-entrant sol-gel transition in some clay systems [18]. A delicate balance between attractive and repulsive Coulomb interactions may significantly contribute to the sol-gel transition and the formation of a gel (or attractive glass) [30].

Several conformations of the clay platelets have been proposed to explain the formation of gels: (i) *House of Cards* (HoC), as first proposed by Hofmann [14,15], in which neighboring particles are in a T configuration, (ii) *Stacked Plates* in which the particles are in a sandwich configuration and (iii) band like structure, proposed by Weiss and Franck [31], where particles are in an *Overlapping Coins* (OC) configuration. The HoC model has often been invoked to explain the gel state and other properties of clay dispersions. A number of neutron and X-ray scattering studies have been made on Laponite [8,17,32,33] and smectite clay [18,26] gels. While these experiments generally confirm that the particles in gels are aggregated and form extensive networks, they do not discriminate between the above configurations [30].

There have been few attempts to simulate the structure and thermodynamic properties in dispersions of charged platelets and even less of platelets having a charge anisotropy. One reason is that such simulations involve particles decorated with explicit charged sites and are thus considerably more computer demanding than a hard core or soft particle system for which the contact function takes a relatively simple closed form. One natural way to handle such a problem is to coarse grain the particle interactions. Dijkstra et al. [34] used a quadrupole moment model. Even though the results of this study point to a reversible sol-gel transition in semi-quantitative agreement with experiments, it has been argued that the quadrupolar disc model is an oversimplification that leads to unrealistic particle configurations. Indeed, at short range, the multipolar expansion is known to break down. Furthermore, at long range, the electrostatic interactions were simply disregarded. Kutter et al. [35] and Leger et al. [36] studied more detailed models by Molecular Dynamics and Monte Carlo simulations, respectively. The main result of these simulations was that clay particles aggregate in the HoC conformation. The coarse graining of the clay platelet is a delicate problem and has to be done with some care. We have earlier argued that the representation of charged sites has to be accurate down to a length scale corresponding to the screening length of the salt or better. Following this prescription it was possible to find two preferential conformations for two platelets, in an infinitely dilute system, depending on the salt concentration : the T-shape HoC conformation and the planar OC conformation [30]. Similarly, Odriozola et al. [37] found both HoC and OC conformations using Brownian Dynamic simulations of many particles with a clay model having a few dozens of charged sites. However, the simulations were restricted to relatively short runs due to the many interactions involved and were restricted to high ionic strengths ($I > 50$ mM).

On the basis of these observations we have developed a multi-level coarse graining of the interactions, which improves the computational time by one to two orders of magnitude, and employed it in Monte Carlo simulations of many platelets using a model where each charged group is treated explicitly [30]. These simulations allow us to calculate the equation of state and to investigate the particle configurations over a wide range of volume fractions. The ionic strength, the magnitude and sign of the edge charge (pH) are varied. We use these results to address the following questions:

- What are the preferential configurations of platelets?
- What is the role played by the edge charges?
- Can the charge anisotropy favor the formation of liquid crystals?
- How does the charge anisotropy affect the sol-gel transition?

2 Model and Simulations

2.1 Model

The model system consists of N platelets dispersed in a cubic box of volume V_{box} filled with a 1-1 salt solution. Periodic boundary conditions are applied using the minimum image convention. The platelets are free to translate and rotate in the available space. A platelet is modeled as a disc of diameter D decorated with n^T soft spheres of diameter 1 nm spread on a compact hexagonal lattice, as illustrated in Fig. 1. There are n_e edge sites, which can be positive, neutral or negative

($n_e < 0$ means that the edge sites are negatively charged). The n_b basal sites located in the center of the disc are always negatively charged, $-e$. The net charge of a platelet is thus given by $Z^{net} = (n_e - n_b)e$.

The solvent, that is water, is treated as a structureless dielectric continuum characterized by its relative permittivity, ε_r, assumed to be constant throughout space. Salt and counterions are represented implicitly via the Debye screening length, κ^{-1}, that depends on both the concentration of salt (c_s) and counterions (c_c),

$$\kappa^2 = \frac{e^2(2c_s + c_c)}{\varepsilon_0 \varepsilon_r kT} \tag{1}$$

where k is Boltzmann's constant, T the absolute temperature and ε_0 is the permittivity of vacuum. From equation 1 it is clear that at high clay concentrations the screening is dominated by the counterions unless the background salt concentration is exceptionally high. Fig. 2 emphasizes this fact and one can notice that it is only at volume fractions of the order of 0.01 and less that there is a significant long range screening effect of the added salt.

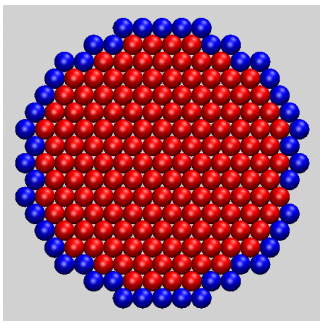

Fig. 1 Schematic picture of a platelet used in simulations. Negative basal sites are colored in red and edge sites (positive, neutral or negative) in blue.

2.2 Interaction potentials

A shifted and truncated Lennard-Jones (LJ) potential is used to account for the finite size of particles. The shift, ε_{LJ}, removes the attractive contribution to the LJ potential. In addition to the shifted LJ potential a screened Coulomb potential is added to describe the electrostatic contribution. The total interaction between two sites, $u^{tot}(r_{ij}) = u^{el}(r_{ij}) + u^{LJ}(r_{ij})$, of charge z separated a distance r_{ij} then reads,

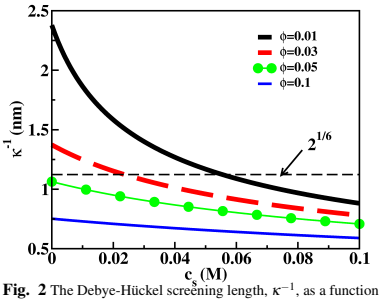

Fig. 2 The Debye-Hückel screening length, κ^{-1}, as a function of added salt for various clay volume fractions (when n_e =-48) and hence counterion concentrations

$$u^{tot}(r_{ij}) = \frac{z_i z_j \exp(-\kappa r_{ij})}{4\pi\varepsilon_r\varepsilon_0 r_{ij}} + 4\varepsilon_{LJ}\left(\left(\frac{\sigma_{LJ}}{r_{ij}}\right)^{12} - \left(\frac{\sigma_{LJ}}{r_{ij}}\right)^{6}\right) + \varepsilon_{LJ} \tag{2}$$

ε_{LJ} and σ_{LJ} are the Lennard-Jones parameters. These were set to $\varepsilon_{LJ} = 0.5kT$ and $\sigma_{LJ} = 1$ nm in all simulations. The full configurational energy of the N platelets system then becomes

$$U = \sum_{i=1}^{N}\sum_{j>i}^{N}\sum_{\alpha=1}^{n^T}\sum_{\beta=1}^{n^T} u^{el}(r_i^\alpha, r_j^\beta) + u^{LJ}(r_i^\alpha, r_j^\beta) \tag{3}$$

where indices i, j refer to platelets and indices α, β to sites on these platelets, respectively. n^T is the number of sites per platelet.

2.3 Model limitations

The model described above has been used in previous simulation studies of dispersion of isotropic and anisotropic particles[35–38] in monovalent salt solutions. However, it suffers from limitations inherent in the Debye-Hückel (DH) theory. The DH theory is known to overestimate electrostatic interactions for highly charged particles where instead, the non-linear Poisson-Boltzmann (PB) theory or exact solution of the PM by Monte Carlo simulation show a saturation of the particle interaction free energy when the particle charge is increased. The fact that the DH theory is easier and computationally more efficient has led to the introduction of the concept of charge *renormalization* or *effective* charge and *effective* Debye screening length. That is, effective parameters within the DH theory that generate the same degree of accuracy as the PB theory for charged colloids, for a review see[39]. This approach has been successfully applied to dispersions of charged *spherical* colloids in monovalent salt solutions. These effective parameters can be obtained from solving the PB equation

or by MC simulations of a single colloid in a Wigner-Seitz cell model or using a Jellium approximation[39,40].

On the other hand, theoretical approaches that describe the phase behavior of charged *disc-like* particles, or generally anisotropic particles, in an electrolyte solution are still in their infancy[41,42]. Rowan et al[41] have developed a screened pair potential between two *homogeneously* charged discs at the DH level from a perturbation expansion in κD. The approach is limited to dilute dispersions, with $\kappa D < 1$ and small charge. Trizac et al. have extended the validity of this pair potential to any charge density by introducing a charge renormalization concept[42] and to any κD using a constant effective potential boundary condition instead of a constant effective surface charge[43]. In this remarkable work, the authors show that their effective potential accounts for the enhanced screening with surface curvature, which in the context of disc like particles with a homogeneous *bare* charge, gives rise to a non-homogeneous radial distribution of *effective* charge neglected in our model. The effective pair potential is limited to particles bearing a homogeneous bare charge and describes well their interaction at large separation, but it becomes less accurate at short separation.

Despite the problems discussed above, we believe that the model used in the present work is able to provide a qualitative insight into the structural and thermodynamic behavior of platelets bearing an homogeneous[38] and heterogeneous charge. Furthermore, if one follows ref[43] and looks at the saturation regime of our particular particle model, it gives a value of κD =12 with $Z^{net} l_b/D$ =7.5 when n_e =0 and κD =7 with $Z^{net} l_b/D$ =4.95 when n_e =+48. That is, given the net charge and diameter of the platelets used in our study, the saturation of the charge is reached for $\kappa^{-1} \geq$1.25 nm when n_e =0 and $\kappa^{-1} \geq$2.4 nm when n_e=+48. This means that except in a very dilute dispersion at low salt concentration, see Fig. 2, the choices of the net charge and diameter of the particle used in this study are reasonable[44].

Finally, it is important to note that eq. 1 for κ naturally arises from a statistical mechanics treatment of electrostatic interactions in colloidal suspensions in the linear formalism[45–47]. This treatment therefore discards the nonlinear effects, unknown for charged platelets, but qualitatively capture the change from the the salt-ion to the counter-ion dominated screening as observed experimentally[48,49] and so far neglected in most of the theoretical work dealing with charged platelets.

To conclude this brief discussion, it is clear that accurate effective potentials for charged anisotropic particles are needed for which promising routes has been recently worked out[43,50]. However, the road for such potential to exist is still long and its lack should not prevent qualitative effective potentials (models) to be used as long as their limitations are well known and controlled.

2.4 Simulations

The model system is solved using Monte Carlo simulations in the canonical ensemble (N,V,T). Collective displacements of platelets were performed in addition to single displacements by the use of the so-called cluster move technique[51]. The clusters employed were cylinders and infinite layers instead of the usual spheres. A multi-level coarse graining approach was developed to reduce the computational cost of the simulations. It relies on the idea that to calculate the electrostatic energy between two particles a detailed charge description is only needed at short separation, see the appendix for more details. The dimensions and the displacement parameters of the different clusters were adapted to each system such as to get between 30 to 50 % of accepted moves. The electrolyte concentration was varied from 1 to 100 mM. The temperature was kept at $T = 298$ K and a fixed solvent dielectric constant of $\varepsilon_r = 78$ was used. If not otherwise stated, simulations were performed with periodic boundary conditions in a cubic box containing 200 platelets with $n^T = 199$ and D = 15 nm, giving a site density of 0.87 sites/nm^2 and n_e = 48, 38, 0 or -48. Simulations with only soft core interactions were also performed. As a test, some simulations were repeated with 100 as well as 1000 particles with the same both qualitative and quantitative results. The particle volume fraction, defined as,

$$\phi = \frac{NV_{part}}{V_{box}} \tag{4}$$

was varied from 0.0007 to 0.14, where the volume of a single platelet, V_{part}, was approximated as $n^T \pi \sigma_{LJ}^3/6$. 5.10^4 to 7.10^7 MC cycles (in a cycle all particles have been moved once) were used to equilibrating the system. A production run typically involved 4.10^5 cycles. Initially at low volume fractions the simulations are well-behaved and convergence of all properties is easily achieved. With increasing concentration the systems become more and more sluggish, related to the formation of various connected structures and the onset of phase transitions. Our canonical simulations do not allow a full description of phase transitions, but they nonetheless describe the formation of gel structures (non-equilibrium), which we believe to be true properties of a clay system.

2.5 Calculated quantities

The characterization of the local structure of a dispersion is provided by several tools. One of them is the radial pair distribution function *g(r)*, which describes the correlation between the center of masses (c.m.) of the platelets. Because of the platelet anisotropy, the local structure needs also to be described by orientation correlation functions. In this study we used two of them. The first is determined from the statistical average of the second Legendre polynomial of the azimuthal angle between the normal vectors of two platelets,

$\cos\theta = \mathbf{u}_i \cdot \mathbf{u}_j$,

$$P_2(r) = \left\langle \frac{1}{2}(3\cos^2\theta(r) - 1) \right\rangle \quad (5)$$

When the platelets are parallel P_2 takes the value 1, while when they are perpendicular $P_2 = -1/2$. The second is obtained from the statistical average of the scalar product between the normal vector, **u**, and the vector separating two particles, $\mathbf{r}_{ij}$, defining the angle $\xi = \mathbf{u}_i \cdot \mathbf{r}_{ij}/r_{ij}$

$$L_2(r) = \left\langle \frac{1}{2}(3\cos^2\xi(r) - 1) \right\rangle \quad (6)$$

$L_2(r)$ takes the value 1 when platelets are face to face and 0 when they are side to side.

These two parameters, P_2 and L_2, give quite a good insight into the clay structure although they do not provide direct evidence for the formation of a gel state or percolated structure. For this reason we have also included an analysis of the "connectivity" of the suspension. Two clay platelets are considered to be "connected" neighbors if the separation between a site in one clay platelet is within 15 Å of a site in the other platelet. Based on this criterion we can calculate,

$$\langle N_{nei} \rangle = \text{average number of neighbors for a platelet in a cluster} \quad (7)$$

which can typically vary between 1 and 7-8. Using the same distance criterion, we can also identify several connected platelets defining a "cluster" with an average cluster size,

$$\langle N_{cl} \rangle = \text{average number of platelets in a cluster} \quad (8)$$

with a maximum value equal to the total number of platelets in the simulation. Furthermore, we can calculate the cluster probability,

$$\langle P_X^{cl} \rangle = \text{probability of finding a particle in a cluster of size X} \quad (9)$$

At low particle concentration P_X^{cl} will have a maximum at $X = 1$, while with increasing concentration it will be bimodal and at really high concentrations it will again have a single maximum for $X = N$. We will also use the integrated quantity,

$$\langle f^{cl} \rangle = \int_2^N P_X^{cl} dX = \text{average fraction of particles in a cluster} \quad (10)$$

Finally, we also use simulation snapshots in order to characterize the structure in the suspension.

The osmotic pressure is evaluated from the virial equation,

$$\Pi = \Pi_{ideal} + \Pi_{ex} = \Pi_{ideal} + \frac{1}{dV} \langle \sum_{\alpha<\beta} \mathbf{F}(r_{\alpha\beta}) \cdot \mathbf{r}_{\alpha\beta} \rangle \quad (11)$$

where $\mathbf{F}(r_{\alpha\beta})$ is the force between two sites in different platelets. If the screening length only depends on the salt concentration, then the excess pressure would look like,

$$\Pi_{ex} \propto \langle \sum_{\alpha,\beta} z_\alpha z_\beta \exp(-\kappa r_{\alpha\beta})(\kappa + \frac{1}{r_{\alpha\beta}}) \rangle \quad (12)$$

However, the counterions will also contribute to the pressure according to eq. 1 and the excess pressure will be,

$$\Pi_{ex} \propto \langle \sum_{\alpha,\beta} z_\alpha z_\beta \exp(-\kappa r_{\alpha\beta})(\kappa + \frac{1}{r_{\alpha\beta}} + \frac{\kappa_c^2}{2\kappa}) \rangle \quad (13)$$

where κ_c is the inverse screening length from the counterions only. Density dependent potentials like the Yukawa potential are tricky to handle when it comes to the evaluation of thermodynamic properties. In an interesting article Louis[52] discusses the possible pitfalls and inconsistencies that could arise. One of his conclusions is that the volume derivative, $\kappa_c^2/2\kappa$, in eq. 13 only makes things worse. In addition to the volume derivative of κ_c one should also include the one-body term coming from the derivation of the Yukawa potential[46]. In the case of a charged spherical particle it is straightforward to calculate this contribution, but for a platelet with a charge anisotropy it becomes rather involved. Considering all the complications we have decided to use eq. 12 when calculating the pressure.

We have tried to quantify the "elasticity" of a clay suspension by calculating the average squared force acting on a particle, which can also be decomposed into its Cartesian components, $< F_x^2 >, < F_y^2 >$ and $< F_z^2 >$,. These should of course be identical and the average force components should be zero, $< F_x >=< F_y >=< F_z >= 0$. Note, that the squared force is directly proportional to the spring constant in a harmonic system.

3 Results

3.1 Isotropic phase

Irrespective of charge anisotropy, at low volume fraction of clay and low salt concentration, $c_s \leq 10$ mM, electrostatic repulsion dominates and a repulsive liquid is found characterized by a broad peak in the pair distribution function at approximately $c_p^{-1/3}$, where c_p is the platelet concentration, see e.g. the 1 mM curve in Fig. 3. The platelets are not in contact, i.e. $c_p^{-1/3} > D$, and no orientation preference is found. At $c_s = 30$ mM and when the charge anisotropy is high, i.e. n_e =+48, the repulsive peak disappears and, instead, a sharp peak around 125 Å appears. This indicates that the overall interaction between the platelets turns from repulsion to attraction and the formation of small aggregates in an Overlapping Coin (OC) configuration. At high salt concentration, $c_s = 100$ mM, the

electrostatic interactions are screened and the particles aggregate in a House of Card (HoC) configuration as indicated by the peak around 75 Å in the pair distribution function (Fig. 3), although a small OC shoulder is still visible.

With lower charge anisotropy, i.e. $n_e = +38$, and $\phi = 0.0007$ (data not shown), we still find the characteristic peak from a repulsive liquid at low salt content, but both the OC and the HoC configurations found with $n_e = +48$ at high salt have disappeared. This gives an indication that the structure can be quite sensitive to the details of the charge anisotropy.

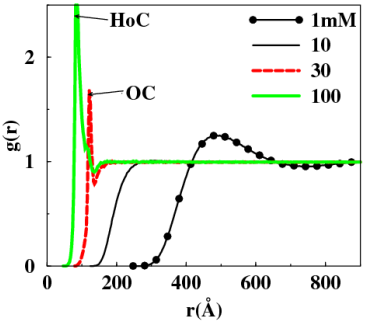

Fig. 3 Influence of the salt concentration on the center of mass radial distribution function with $n_e = +48$. The particle volume fraction is set to $\phi = 0.0007$ and the salt concentrations are given in the legend. The arrows mark the peaks corresponding to the Overlapping Coin and House of Cards configurations.

Fig. 4 shows the effect of charge anisotropy on $g(r)$ at $\phi = 0.07$ and $c_s = 1$ mM. With $n_e = +48$ both OC and HoC configurations are present, while they gradually disappear when n_e decreases. With no positive charges on the edge, $n_e = 0$ and -48, the structure is better described as a collection of "tactoids", with particles arranged in a parallel manner. Further addition of salt has a profound effect on the system with highest charge anisotropy, $n_e = +48$, but has virtually no effect on the other cases (curves are not shown).

Fig. 5 showing the pair orientation correlation, $P_2(r)$ for platelets with $n_e = +48$, confirms the interpretation of the peaks in Fig. 3. The platelets are orientationally uncorrelated at salt concentrations below 30 mM and $P_2(r) \approx 0$ for $r > D$. At $c_s = 30$ mM $P_2(r)$ shows a positive peak at $r \approx D$ indicating a parallel structure like in an OC configuration. Increasing the salt concentration even further destroys the OC structure and a structure with the platelets in HoC configurations takes over. This can be seen from the negative values of $P_2(r)$ at separations around $r \approx D/2$. From the structural analysis we find that the two strong peaks in Fig. 3 correspond to the formation of dimers, that is $\langle N_{nei} \rangle = 1$ - see below. With a salt concentration below 10 mM $\langle N_{nei} \rangle$ is virtually zero.

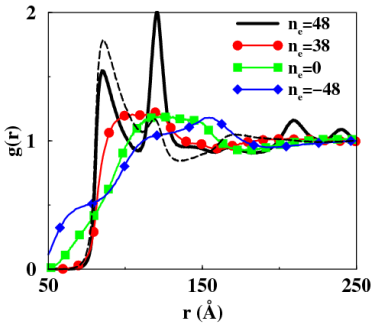

Fig. 4 Influence of charge anisotropy on the center of mass radial distribution function with $\phi = 0.07$ and 1 mM salt. The black dashed curve is for $c_s = 10$ mM salt.

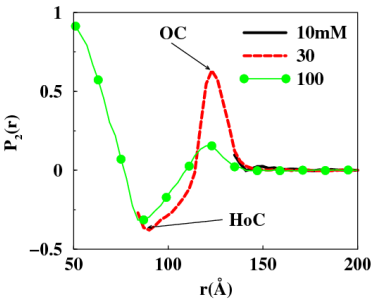

Fig. 5 The second order Legendre polynomial as a function of particle separation. The volume fraction is 0.0007 and $n_e = +48$. The 10 mM curve is virtually zero and hidden under the other curves for $r > 140$ Å.

By increasing the volume fraction at constant salt concentration a more exotic picture emerges - see Fig. 6. At a volume fraction of 0.007 the liquid is dominated by repulsive interactions between the platelets manifested as a single peak in g(r) and $\langle N_{nei} \rangle \approx 0$. However, already at $\phi = 0.02$ a completely different structure can be found and the radial distribution functions show a long range order extending over the length of the simulation box. The number of neighbors now increases to about four and we start to get a two-dimensional percolated structure as indicated by $\langle N_{cl} \rangle$, which increases dramatically - see below. From the position of the first peak in $g(r)$, at $r \sim D$, we can immediately draw the conclusion that the structure is dominated by OC configurations. A further increase of the

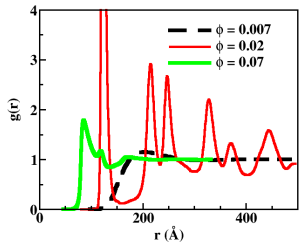

Fig. 6 The radial distribution function at $c_s = 10$ mM and three different volume fractions with $n_e = +48$. Similar curves are found with 1 and 3 mM salt.

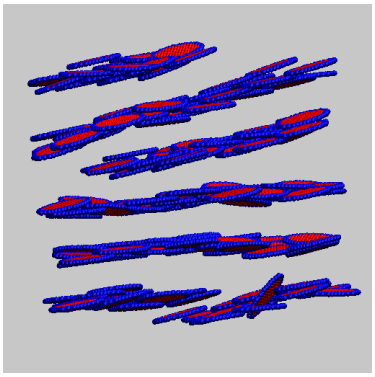

Fig. 7 Simulation snapshot showing a Smectic B phase - $\phi = 0.05$ and $c_s = 1$ mM.

volume fraction to 0.07 destroys the long range structure but maintains a nearly percolated structure. The main peak in $g(r)$ now indicates a local structure characteristic of HoC. Note that Fig. 6 shows the results for a salt concentration of 10 mM, but a similar picture emerges for 1 and 3 mM salt.

Upon decreasing the charge anisotropy at $\phi = 0.02$, that is reducing n_e from 48 to 38, leads to the disappearance of the long range order, while at $\phi = 0.07$ there remains peaks corresponding to HoC and OC configurations. A further decrease of n_e gives rise to stacked configurations without any distinct characteristics as can be seen in Fig. 4.

3.2 Smectic B phase

When the particles exhibit a high charge anisotropy, i.e. $n_e = +48$, a phase transition is found at low salt concentrations, $c_s \leq 10mM$, and between 0.02 to 0.05 in volume fraction. This phase corresponds to the formation of a lamellar liquid crystal where the platelets associate in two dimensions layers in the OC configuration as illustrated in Fig. 7. These two-dimensional layers then form a lamellar structure. The particles show long range order within the layers, while no positional correlation is found between the layers. As an example, the positional order is shown in Fig. 8 with a two-dimensional distribution function of a dispersion of platelets with $\phi = 0.02$ and $c_s = 10$ mM. The radial position of the peaks are related as $a : a\sqrt{3} : a\sqrt{4} : a\sqrt{7} : a\sqrt{9} : a\sqrt{12}$ where a =120 Å. This relation is characteristic of a hexagonal structure of the particles (100, 110, 200, 210, 300, 220 positions) within the layers. The broadness and weakness of the 300 peak demonstrate that the positional order is short ranged, although the hexagonal organization extends over long distances, see Fig. 7. The position of the first correlation peak, a, is also found to be lower than the diameter of the particles at an angle θ close to zero, which is a result of an OC configuration within the Smectic layers.

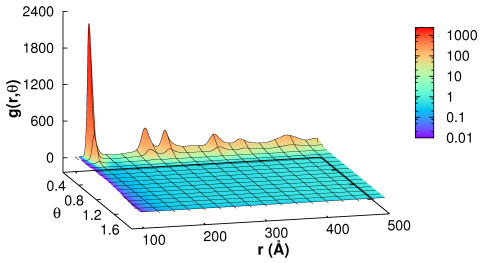

Fig. 8 Pair particle distribution function versus θ and r for $\phi = 0.02$, $n_e = +48$ and c_s =10 mM.

The parallel arrangement of the particles within the layers is also exemplified in Fig. 9 where the angular distribution functions L_2 and P_2 are shown. The former is close to zero as should be expected for a side to side arrangement of platelets. P_2 goes to a non-zero asymptotic value indicating the long range orientation order of the platelets. The most striking ob-

servation is the lack of any correlation peak between the layers which makes a clear distinction between a Smectic B and a hexagonal columnar phase - see also Fig. 7. However, as it will be shown later from the equation of state, the Smectic B phase is probably metastable.

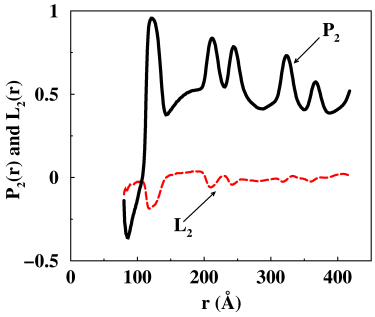

Fig. 9 Angular distribution functions, $L_2(r)$ and $P_2(r)$ for $\phi = 0.035$, $n_e = +48$ and c_s =10mM.

The Smectic B phase can also be traced in $\langle N_{nei} \rangle$ and $\langle N_{cl} \rangle$ - in Fig. 10 and Fig. 12, respectively. The Smectic B phase typically has an average of four neighbors indicative of a two-dimensional structure. When the volume fraction increases beyond about 0.05, the Smectic B phase disappears and $P_2(r)$ goes to zero as seen in Fig. 9 for the $\phi = 0.09$ curve. At the same time $\langle N_{nei} \rangle$ increases slowly to approximately six neighbors. Fig. 11 also contains the curve for a purely repulsive soft core system without electrostatic interactions. For low volume fractions, < 0.02, this curve runs between the 1 and 100 mM curves, demonstrating that in the former case, 1mM, the interactions are predominantly repulsive while in the latter, 100 mM, they are attractive. Consistently with the previous results, above the threshold value $\phi = 0.02$, the attractive interactions between the particles take over at all salt concentrations when a charge anisotropy is present, i.e. all $n_e > 0$ curves lie above that of the soft core system.

3.3 Gel phase

The metastable Smectic B phase is found only at high charge anisotropy and in a limited region of salt concentration and volume fraction; typically below 10 mM in salt and approximately between 0.02 and 0.07 in volume fraction. At higher salt and volume fractions or lower n_e the Smectic B phase dissolves into amorphous aggregates which eventually leads, upon increasing the platelet concentration, to the formation of a fully percolated network characteristic of a gel phase. This transition is depicted in Fig. 12, which gives the average number of platelets in a cluster, see also the snapshots in Fig. 13. The percolation process can also be followed in Fig. 14, which shows how the probabilities for the different aggregate sizes evolve with ϕ. The probability distribution is a monotonic function at low and high volume fraction, while in the intermediate range it becomes bimodal - see for example $\phi = 0.07$ in Fig. 14. Fig. 12 shows that the salt concentration has a rather limited impact on the percolation and hence on the sol-gel transition. This can be explained by the fact that it occurs at $\phi \geq 0.11$ where the screening length is mostly governed by

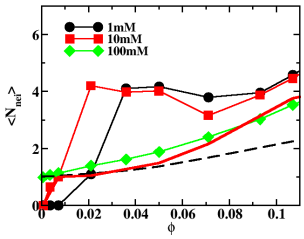

Fig. 10 Lines with symbols show the average number of neighbors as a function of volume fraction of platelets for $n_e = +48$. The 1 mM case is virtually identical to 3 mM and 30 and 100 mM are also very similar. The solid red curve shows the 10 mM case with $n_e = +38$. The dashed black curve shows the result for a system without any electrostatic interactions - only the shifted Lennard-Jones is used.

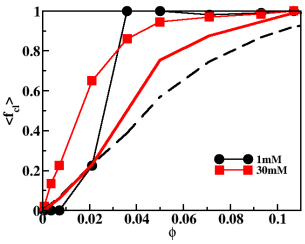

Fig. 11 Lines with symbols show the fraction of particles participating in a cluster (a cluster is defined as a dimer or bigger) as a function of volume fraction for the $n_e = +48$ case. The 3 mM curve has the same qualitative appearance as 1 mM and the 30 mM curve is a good representative for the salt range 10-100 mM. The red solid curve without symbols is a good representative for all salt concentrations for $n_e = +38$. The dashed curve shows the result for a system without any electrostatic interactions - only the shifted Lennard-Jones is used.

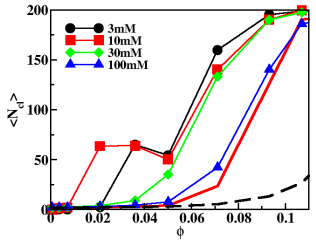

Fig. 12 Lines with symbols show the average number of platelets in a cluster as a function of volume fraction with $n_e = +48$. The solid red curve without symbols shows the 10 mM case with $n_e = +38$. The dashed curve shows the result for a system without any electrostatic interactions - only the shifted Lennard-Jones potential is used. (The actual value of $< N_{cl} >$ should not be taken too serious, since sometimes the simulation box can create one single two-dimensional layer penetrating all space, which is an artifact of the periodic boundary conditions.)

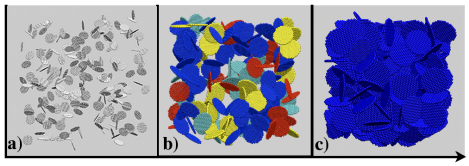

Fig. 13 Snapshot from simulations with increasing volume fraction and fixed salt concentration at 30 mM. a) The volume fraction $\phi = 0.0035$ and all particles are disconnected, b) $\phi = 0.035$ and some particles are connected, which is indicated by a common color and c) $\phi = 0.11$ and all particles are connected.

the counterions, c.f. eq. 2, at least when $c_s \leq 30$ mM. However, the short ranged electrostatic interactions still play a role in the gel phase as best described by the drop in the platelet connectivity, Fig. 10, from ~ 6 to $\sim$ 4-5 when rising c_s from 1 to 100 mM. In this case the particles are mainly found in a HoC configuration.

Upon decreasing the charge anisotropy, the same qualitative picture remains, that is, the particle dispersion progressively aggregates until full percolation with increasing ϕ - see the red curves without symbols in Figs. 10, 11 and 12. However, two differences can be noted: i) the aggregation and sol-gel transition occur at higher ϕ and ii) the curves are more or less salt independent.

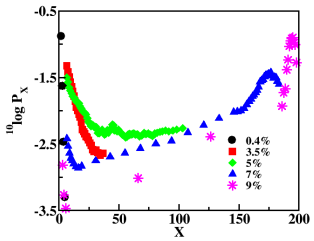

Fig. 14 Logarithm of the probability distribution for different cluster size, X. The salt concentration is 100 mM and $n_e = +48$.

A weakness of the analysis is the lack of a proper definition of what a gel is. One straightforward definition that works very well in a simulation is the percolation measure in terms of $\langle N_{cl} \rangle$. When $\langle N_{cl} \rangle$ exceeds a given threshold value the system is defined as a gel. In an experiment, a gel does neither flow nor melt in its solvent when in contact[53]. Another possibility is to use a threshold value of the force fluctuation, $< F^2 >$, which can be shown to be a reasonable approximation for evaluating the aggregate and gel elasticity, cf. the Lindemann criterion[54].

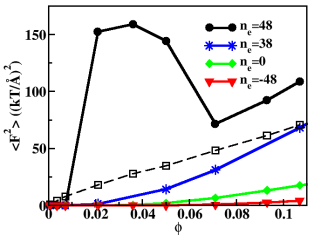

Fig. 15 Force fluctuation as a function volume fraction of platelets at $c_s = 10$ mM. The charge anisotropy is given in the figure. The dashed curve with open symbols is for $c_s = 100$ mM and $n_e = +48$.

Fig. 15 shows how $< F^2 >= (< F_x^2 > + < F_y^2 > + < F_z^2 >)/3$ varies with the volume fraction for different charge anisotropies. The most striking feature is the stiffness of the metastable region around $\phi = 0.035$. From an analysis of the different Cartesian components one finds that it is the direction

normal to the lamellar structure that gives a strong contribution. It turns out that $< F^2 >$ is mainly determined by the number of close contacts, i.e. the platelet connectivity - see Fig. 10, which means that the attractive interactions between the positive edge and negative basal charges in an OC configuration gives a large contribution. Similarly, in the amorphous aggregates and gels, $< F^2 >$ is found to be proportional to the number of close contacts as best illustrated when the $< F^2 >$ curves are compared with those of the particle connectivity, c.f. Fig. 10. Indeed, the same qualitative trend is observed, i.e. both the particle connectivity and aggregate stiffness decrease when n_e decreases and the salt concentration is increased.

3.4 Osmotic pressure

The osmotic pressure (Π) calculated for particles having a strong charge anisotropy ($n_e = +48$) at different ionic strengths are displayed in Fig. 16 and compared with those obtained for platelets having either no charge (Z^{net}=0) or without a charge anisotropy ($n_e = 0, -48$) at c_s=1 mM.
At c_s=100 mM and $n_e = +48$ the osmotic pressure increases monotonically with the particle volume fraction. At $c_s < 100$ mM the Π, ϕ curves are non-monotonic and exhibit the same general trend. That is the osmotic pressure rises up to a particle volume fraction of about 0.035 where after it decreases. At $\phi \simeq 0.11$ it starts to increase again. When c_s = 30 mM the osmotic pressure even becomes negative indicating the existence of a significant overall attraction between the platelets due to their strong charge anisotropy. Such a van der Waals loop is characteristic of a first order phase transition. At a macroscopic level the metastable region that encompasses the maximum and minimum of Π is never observed but instead a plateau in Π is to be found with the coexistence of an isotropic liquid phase and a gel phase. Note that the metastable region observed in the equation of state corresponds to the Smectic B phase. It is instructive to compare the Π curve with $n_e = +48$ at $c_s = 100$mM with that of uncharged platelets. That is, in most cases the pressure for charged platelets lies well below that of uncharged platelets, which is a signature of attractive interactions and the formation of small aggregates/clusters.

When the platelet edge charge is decreased, i.e. $n_e < 48$, the osmotic pressure increases monotonically with ϕ for all salt concentrations, as illustrated in Fig. 16b. The osmotic pressure curves are found in the order $\Pi_{n_e=+38} < \Pi_{n_e=0} < \Pi_{n_e=-48}$, which shows the important role played by the platelet edge charges.

A quantitative comparison with experimental pressures is not straightforward due to simplifications in our model, as discussed above. Nonetheless, magnitudes of the simulated pressures are in surprisingly good agreement with the experimental data for both Laponite[9,55] and Montmorillonite[26] at low volume fractions. In particular, we note that both clay systems

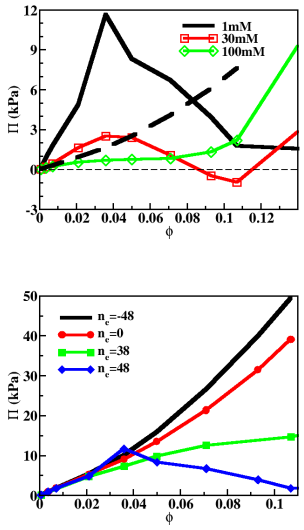

Fig. 16 Equation of state for platelets with various charge anisotropy, n_e, and bulk salt concentrations. a) Platelets with n_e= +48 and varying salt concentration. The dashed curve is obtained for platelets with uncharged sites and repulsive soft core interactions. b) A comparison of different charge anisotropies for $c_s = 1$ mM.

exhibit a plateau at a volume fraction of $\phi \approx 0.007$, which is somewhat lower than the van der Waals loop in our simulations. Martin et al.[55] have measured the pressure for highly compressed Laponite ($\phi \approx 0.3$) in which case they reach MPa values, which is somewhat higher than found in our simulations.

4 Discussion and Conclusion

The existence of both attractive and repulsive interactions in clay systems has been inferred from several experimental sources. The origin of the attractive interactions is, however, still an open question. One possibility would be the always present van der Waals forces with an approximate Hamaker constant[56]. Another possibility is the existence of positively charged sites on the edges of the platelets. Both alternatives suffer from the lack of experimental data, in the former case the value of the Hamaker constant and in the latter the actual

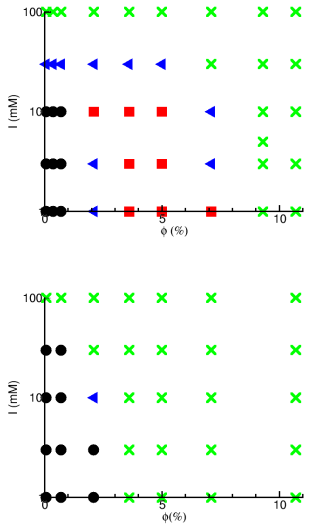

Fig. 17 Tentative phase diagram. Black spheres = repulsive liquid phase; Blue triangles = attractive liquid with particles in an overlapping coin configuration (OC); Green crosses = platelets with house of card configuration in an attractive liquid (cluster fluid) below $\phi \sim 8-10\%$ and a gel above; red squares = Smectic B phase. Left: $n_e = +48$ and right: $n_e = +38$.

number of positively charged edge sites. There is, as mentioned in the introduction, experiments done under varying salt and pH conditions, that would support the importance of the edge charges.

The simulation of highly anisotropic particles is difficult. A typical clay particle, *e.g.* Montmorillonite, has an aspect ratio (diameter/thickness) of around 3-500, while in our simulations we have been forced to settle on a much smaller ratio of approximately 15. The experimental information regarding the quantity and structure of the edge charges is scarce. Thus, we emphasize that the present simulations should be seen as an attempt to create a model clay system with some essential generic features. This precludes any quantitative comparison with experimental data, but hopefully it should give a qualitatively correct picture. Another problem appearing in systems undergoing some sort of phase transition involving an ordered phase is the specific number of particles in the simulation box. For example, choosing the number of particles as N^3 will favor a simple cubic arrangement and similarly for other choices. We have tested the stability of our simulations by a five-fold increase of the system size and the results remain quantitatively the same.

One often overlooked property of clay suspensions is the electrostatic screening due to the clay counterions. For example, in a 1 % Montmorillonite suspension the counterion concentration is approximately 6 mM. That is, addition of salt in the sub-millimolar range should have no effect on the electrostatic interactions. This has also been observed in gibbsite suspensions (weight fraction below 30 %) where the sol-gel transition takes place only at salt concentrations above 100 mM[27]. Another result of the counterion screening is that the phase boundary between the sol and the gel typically appears as a vertical line in an ionic strength vs. volume fraction diagram[23,26]. The osmotic pressure of, for example, Montmorillonite suspensions is insensitive to the addition of salt over a large concentration range[26].

The different structures obtained for a dispersion of platelets with a strong charge anisotropy ($n_e = +48$) are summarized in a tentative phase diagram, Fig. 17. The characterization of the different phases is mainly based on the appearance of $g(r)$. We did not attempt to calculate the coexistence densities at the different phase boundaries.

In the dilute particle regime while increasing the salt concentration the same behavior as in the previously reported simulations between two platelets in a cell is observed[30]. At low salt, below 10 mM, the interactions are repulsive and the dispersion appears as a repulsive liquid (RL). With increasing salt concentration, small clusters of platelets are formed in an OC configuration. A further increase in the ionic strength leads to a change in the clusters from an OC conformation to an HoC conformation. At sufficiently high salinity, electrostatic interactions are completely screened and the introduction of van der Waals forces would cause the precipitation of the platelets and/or the formation of stacks.

The agreement between the two-platelet model[30] and multi-platelet model is limited to low ϕ. Above $\phi > 0.007$ many body interactions play a significant role in the formation of the different structures observed. As an illustration let us take the case where c_s is maintained below 10 mM at increasing ϕ. The disappearance of the RL phase in favor of an attractive liquid can still be rationalized by the increasing electrostatic screening with ϕ. However, the formation of the Smectic B phase as well as a gel phase is clearly a many body effect. Figs. 10 and 12 indicate that the Smectic B phase exists at intermediate volume fractions and salt concentrations. That is, it does not exist at high salt concentration and not at high and low volume fractions either (Fig. 6). We believe that this is a generic result and the actual quantitative boundaries strongly depend on the type of clay as well as solution pH. To our knowledge it is the first time that such a Smectic B phase is observed with

charged platelets. This finding might explain the liquid crystal observed in dispersions of Laponite[57]. However, there is no definite proof from the equation of state that this phase is thermodynamically stable. This would necessitate a full free energy calculation which is out of the scope of this work.

Both counterions and added salt ions contribute to the screening of the electrostatic interactions. This means that the dispersion is rather insensitive to salt addition except at very low volume fractions. The radial distribution functions at constant volume fraction but varying salt concentration in Fig. 18 demonstrates this effect. At $\phi = 0.035$ more than 10 mM of salt is needed before the Smectic B phase disappears. At 100 mM of salt, the Smectic B phase is totally dissolved and, instead, an intense peak at $r \sim D/2 = 75$ Å in $g(r)$ appears, which is characteristic of an HoC configuration.

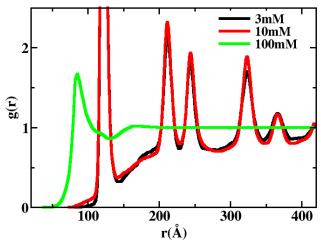

Fig. 18 Influence of the salt concentration on the stability of the Smectic B phase as seen in the radial distribution function; $\phi = 0.035$ and $n_e = 48$

As shown in Fig. 17, however, when the inter-particle interactions are dominated by attraction, the location of the sol-gel transition is found to decrease with the ionic strength. Similarly, the size of the particle clusters grows faster when the salt concentration is low and the charge anisotropy is important. Consequently, the line that delimits the sol-gel transition in the phase diagram c_s versus ϕ should have a positive slope. This result points out that contrary to the general understanding based on the sign of such a slope in systems of isotropic particles[58,59], a positive value does not necessarily mean that the platelets are governed by repulsive interactions and that the solid thus formed is a Wigner glass[60]. Note that the salt dependence of the sol-gel transition for $c_s \leq 10$ mM, is small in agreement with experimental observations on clays and gibbsite[23,26,27].

It is also informative to put these results in perspective with the equation of state plotted in Fig. 16. Indeed when the charge anisotropy is high, Π shows a strong first order transition at low volume fraction ($\phi \sim 0.035$) followed by an increase in the osmotic pressure when entering the gel phase. This tells us that the gel is stable and co-exists with a dilute repulsive liquid in a limited range of ϕ. Following an approximate construction, the liquid-gel transition is found at ϕ as low as 1-2% when c_s =1mM and increases with c_s. As long as one can consider that Laponite possess a strong charge anisotropy, these results are found in good qualitative agreement with the revisited phase diagram of Laponite by Mongondry et al[61,62] who experimentally observed for 100 mM $\geq c_s \geq 0.1$ mM the co-existence of a sol and gel phases at low ϕ that increases with c_s. Such observations were confirmed recently at $c_s \sim 0.1$ mM by Ruzicka et al and were used to validate their concept of empty liquid[63]. They established that Laponite dispersed in solutions closed to salt free conditions forms an empty liquid for particle weight concentration, C_w, below 1% and an equilibrium gel for C_w between 1 and 2%. From small angle X-ray scattering measurements, the particles were inferred to be in a HoC configuration in agreement with our simulation predictions. Ruzicka et al rationalized these results using an attractive patchy disc model. this model neglects the strong electrostatic repulsions that prevail in such systems while we show here that both ingredients, i.e. attractive and repulsive electrostatic interactions, are important to understand the co-existence of a liquid with a gel at low ϕ for particles having strong charge anisotropy. Note, however, that our results largely over-predict the volume fraction of the phase separation. Similarly to our results with n_e =48 and n_e =38 (Fig. 16), it has been shown that the equation of state of both Montmorillonite[26] and Laponite[9,10] exhibit a plateau at small ϕ corresponding to the sol-gel transition. However, in contradiction with the experimental results of Mongondry et al[61,62] and Ruzicka et al[63] as well as our simulations these authors did not observe any phase separation or evidence for a HoC configuration in the gel phase[9,26,32].

On the other hand, at C_w above 2% Ruzicka et al[53] and Jabbari et al[48] observed that Laponite form a solid state which differs from the gel observed at lower C_w, which they attributed, from SAXS and time correlation intensity functions from dynamic light scattering measurements, to a Wigner glass. Without giving a clear explanation, they justified their results arguing that at high C_w ($C_w \geq 2\%$) Laponite dispersions are governed by electrostatic repulsions which lead to the formation of a Wigner glass, while in diluted conditions ($C_w < 2\%$) the dispersions are governed by basal-edge attractions and thus form a gel. Thus, taking the exact opposite model as used for rationalizing gels, they modeled the Laponite particles as discs with 19 discrete sites all negatively charged, neglecting the positive edge charges, and the interaction with a purely repulsive Yukawa potential[53]. The latter allowed them to fit their experimental structure factor extrapolated from SAXS measurements for $2\% \leq C_w \leq 3\%$. In our work where a self-consistent model is used for all particle volume fractions such a transition from a gel to a Wigner glass when concentrating

the dispersion in particles is not observed. On the contrary, our model qualitatively predicts the opposite. That is, the system is found to be governed by electrostatic repulsions at low volume fraction (≡ low ionic strength). When increasing the particle concentration (≡ the ionic strength), the electrostatic repulsions are progressively screened (see Fig. 2) and, eventually, the system is found to be dominated by the short range basal-edge electrostatic attraction at sufficiently high ϕ (≡ high ionic strength). Consequently, within the approximation of our model, a gel cannot dissolve into a Wigner glass when increasing the particle concentration. Interestingly, in an earlier study Mourchid et al[10] reported a state transition for the same C_w as Ruzicka et al and Jabbari et al. In this study, the solid state was ascribed to an isotropic gel. Also, Shahin et al[49] recently suggest the existence of an attractive glass or gel from extensive rheological measurements of Laponite dispersions at C_w =2.8%.

Although more theoretical and experimental studies are clearly needed to clarify these conflicting results, we would like to make four remarks. Firstly, clay suspensions age slowly. For diluted dispersions, i.e. $C_w < 2$ %, the observations by Mongondry et al[61,62] and Ruzicka et al.[63] were made over a significantly longer period of time than previous studies. In particular, at low c_s (< 1mM) and C_w (≤ 1 %), phase separation and the HoC configuration were only observed after aging the Laponite samples for more than one year. Before that, SAXS patterns on solid states only revealed well separated particles in agreement with earlier studies[9,32,64–66].

Secondly, in more concentrated Laponite dispersions, C_w >2%, the aging time in ref[48,53] was never longer than 100 hours[48,63], considerably smaller than the year reported before for diluted dispersions, which might explain partly the striking observation of a Wigner glass at C_w larger than the gel phase. Indeed, Shahin et al[49] who did perform intensive rheological measurements on Laponite dispersions at C_w =2.8% and 0.1mM ≤ c_s ≤ 7 mM as function of time elapsed over a considerably longer period ot time (∼ 1200 hours) demonstrated the importance of the aging time even at this relatively high particle concentration. For the all range of salt concentrations they obtained a self similar trend in the aging behavior. They obtained much higher shear melting viscosity for experiments carried out at greater aging times and evidenced the difficulty to melt the so obtained solid phases. The measured conductivity of 2.8 wt % Laponite suspension having no externally added salt was ∼850μS/cm (≡ κ^{-1} ∼ 3.2nm) and at 7mM less than twice this value. Their results, in qualitative agreement with our simulation results, give a strong support to the facts that i) the screening length is much shorter than the particle diameter even at c_s =0.1mM (see Fig. 2) and ii) the low free energy state (≡ high shear melting viscosity) of the solid phase is associated with the formation of strong attractive interactions among the Laponite particles. These facts contradict the existence of a Wigner glass (governed by repulsive interactions) for $C_w > 2$% Laponite suspensions and suggest, instead, a gel or an attractive glass. As a matter of fact, some of authors supporting the idea of a Wigner glass, in ref[53], recognize that "longtime attraction may also affect the repulsive Wigner glass, through the formation of subsequent additional bonds" after performing one dilution experiment on a high-concentration sample aged one and half week and observing that it does not melt as expected for a Wigner glass. However, they reject the idea of an attractive glass or gel arguing that the pattern of the structure factor obtained from SAXS was not altered significantly (see Fig. 2 in ref[53]) although it closely resemble that of gel samples at $C_w < 2$% at a comparable aging time (see e.g. Fig. 1-g in ref[63]. Whatever it is, we strongly believe that more experimental and theoretical work are needed to clarify the status of the solid state of Laponite suspensions at $C_w > 2$%.

Thirdly, Laponite is known to have a weak stability in aqueous solution below pH 9[67]. When aged over a long period of time, pH of Laponite dispersions in CO_2 free atmosphere environment, initially set to 10, was found to drop below 9[61] which might cause a partial particle dissolution with the release of Mg^{2+} and Li^{+} counterions[67] and partly explain the various behaviors observed.

Finally, smectite clays are considerably larger, by one to two order of magnitude, than Laponite ($D \sim 30$ nm) which is comparable to our model clay. As a consequence, one would expect a larger repulsive contribution to the interaction between smectite clays than in between our small model clay particles. Indeed, the edge charge is linearly proportional to D and the basal charge to $\sim D^2$. Nevertheless, it would be tempting to rationalize how the sol-gel transition varies with particle size in i) Montmorillonite and Beidellite[65] and ii) Nontronite at $c_s < 1$ mM[68] and Mg/Al layered double hydroxides[69] with changes in the edge charge. As a matter of fact, the sol-gel transition of the former, is found to increase with the size of the platelets while the opposite trend is observed for the latter.

It is also informative to compare our simulation results to the case of Montmorillonite at low pH conditions for which the edge charge has been clearly identified to be positively charge while the basal plane remains negative[3]. Note that the comparison can only be qualitative since the aspect ratio of such clays (1:100) is considerably larger than our model plate particle. A careful characterization of the phase diagram of sodium Cloisite (type of Montmorillonite clay) at pH∼ 4, for 0.01mM < c_s < 1 M and 0 wt% < C_w < 4.5 wt% has been performed recently by the group of P. Schurtenberger, see Figure 1 and 7 of ref[33], by mean of SAXS, small-angle neutron scattering and dynamic light scattering. Below c_s =0.02 mM they observed a Wigner glass containing clusters stabilized by electrostatic repulsions. For 0.02 mM < c_s < 10 mM and low C_w the suspension

forms a fluid of clusters with particles randomly oriented, characteristic of a sol, while for high C_w a continuous gel with a random orientation of the individual discs is found. Similarly to Laponite suspensions, the threshold value of C_w for the sol-gel transition is first found to increase with the salt concentration up to $c_s = 3$ mM then to decrease upon further addition of salt. Above $c_s = 10$ mM the samples are phase separated with a weak percolation gel formed by small stacks of particles on the bottom and a few smaller clusters on the top. This state diagram is, on a general ground, found to be in a good qualitative agreement with that shown in Fig. 17-b. In particular, we found a sol at low ϕ and a sol-gel transition that increases with salt concentration up to $c_s \sim 10$ mM and decreases above. The particles in the clusters and gels are also found to be randomly oriented. Note, that we did not observe a Wigner glass since we did not prospect the phase diagram at c_s below 1 mM. On the other hand, gels found at high c_s are qualitatively different. In these conditions, the simulated gels are still formed by individual particles while experimental gels are formed by the percolation of small stacks. Note, however, that the effective pair potential between the model platelets used in the simulations do not include any dispersive interactions. In a recent paper[30] we showed that the inclusion of such interactions can explain the formation of stacks at high salt concentration.

To conclude, using a self consistent model at all volume fractions and salt concentrations we have shown that despite its simplicity we could reproduce the general features of the state diagram of Laponite and Montmorillonite clays when they bear a charge anisotropy. In particular, the simulations successfully predict a phase separation between a liquid and a gel at low particle volume fraction and salt concentration when the charge anisotropy is strong in accord with the experimental observations on Laponite. The threshold ϕ value at which the phase separation is predicted is found to increase with c_s in full agreement with the experimental observations. At higher ϕ a Wigner glass could not be found. On contrary, the effective pair potential between the platelets is found to be mainly driven by repulsion in highly diluted dispersions and, upon increasing the particle concentration, to be mainly attractive. Simulations in the full primitive model and further experimental work would be needed to clarify the status of this solid phase.

5 Acknowledgments

The authors thank B. Cabane and E. Trizac for interesting and stimulating discussions. Financial support from the Région Bourgogne and computational support from CRI, Université de Bourgogne are gratefully acknowledged.

6 Appendix: Coarse graining

A multi-level coarse graining approach was developed to reduce the computational cost. It relies on the idea that for calculating the electrostatic energy between two particles a detailed charge description is only needed at short separation. At sufficiently large distance the electrostatic potential generated by the many charged sites distributed on the surface of a particle can be collapsed to one single charge positioned at the c.m. and taking the value of the net particle charge Z^{net}. Between these two limits, denoted f_1 and f_2, the charged sites can be collapsed locally into domains, see Fig. 19, hereafter called patches, with the requirement that their size is negligible compared to r.

For simplicity reasons we only used one patch size, which leads to the definition of two levels of coarse graining. A hexagonal shape was chosen in order to facilitate the reconstruction of particles from the patches, see Fig. 19. A full patch (red) contains 19 sites and has a net charge $Z^p = -19e$ located at its center of mass (c.m.). The edge patches (green) are generally not full and their net charge depends on n_e. For technical convenience, when the c.m. did not coincide with an existing site, Z^p was positioned on the closest site.

The different levels of coarse graining are delimited by the cut-off distances f_1 and f_2. During simulations, the switch from one level to another is simply based on a distance criterion. At a separation $r_{ij} > f_2$ the electrostatic energy between two platelets i and j reduces to

$$u^{el}(r_{ij}) = \frac{Z_{net}^2 \exp(-\kappa r_{ij})}{4\pi\varepsilon_r\varepsilon_0 r_{ij}} \tag{14}$$

When the center-to-center distance between two platelets, $r_{ij} < f_2$ and the distance between two patches, k and l, is $r_{kl} > f_1$ then the electrostatic interactions between two patches simplifies to,

$$u^{el}(r_{kl}) = \frac{Z_k^p Z_l^p \exp(-\kappa r_{kl})}{4\pi\varepsilon_r\varepsilon_0 r_{kl}} \tag{15}$$

where Z^p is the patch charge. If $r_{kl} < f_1$ the full site description of those patches is used and the interaction becomes

$$u^{el}(r_{kl}) = \sum_{\alpha=1}^{N^p}\sum_{\beta=1}^{N^p} \frac{z_\alpha z_\beta \exp(-\kappa r_{\alpha\beta})}{4\pi\varepsilon_r\varepsilon_0 r_{\alpha\beta}} \tag{16}$$

f_1 and f_2 were determined by comparing the energy of interaction between two rings of appropriate charge and size with those obtained from equations 14 and 15 for a large range of κ. At a given κ, the cut-off distances were defined as the distance that gives an energy difference of $\sim 10^{-6}kT$. The obtained points could be interpolated with a simple exponential function and the expressions for f_1 and f_2 read,

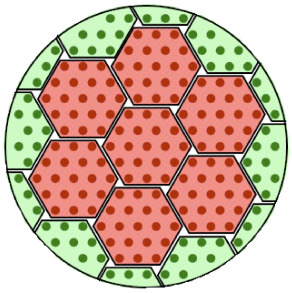

Fig. 19 Representation of a 199 sites particle (D=15 nm) split into 19 patches. The red patches located in the middle of the particle carry a negative charge while the charge of the green patches depend on n_e.

$$f_1(\kappa) = 44.85 + 341.7\exp(-13.4\kappa) \quad (17)$$

$$f_2(\kappa) = 57.0 + 528.3\exp(-14.8\kappa) \text{ for } D\text{=}15 \text{ nm and } n_e = +48: \quad (18)$$

Similar expressions were obtained for other values of D and n_e.

This coarse graining significantly reduces the computing time, i.e. between one to two order of magnitude, without creating a noticeable error in the energy calculation. The code was parallelized and scales linearly up to eight processors.

References

1 H. van Olphen, *J. Coll. Sci.*, 1962, **17**, 660–667.
2 H. Zhao, S. Bhattacharjee, R. Chow, D. Wallace, J. H. Masliyah and Z. Xu, *Langmuir*, 2008, **24**, 12899–12910.
3 M. Delhorme, C. Labbez, C. Caillet and F. Thomas, *Langmuir*, 2010, **26**, 9240–9249.
4 H. van Olphen, *An Introduction to Clay Colloid Chemistry*, John Wiley and Sons Inc., New York, 2nd edn, 1977, p. 176.
5 L. I. Ltd., *Laponite Techn. Bull.*, 1990, **L104/90/A**, 1.
6 K. Faisandier, C. H. Pons, D. Tchoubar and F. Thomas, *Clays and Clay Minerals*, 1998, **46**, 636–648.
7 G. Lagaly, *Appl. Clay Sci.*, 1989, **4**, 105–123.
8 F. Pignon, A. Magnin and J.-M. Piau, *J. Rheol.*, 1996, **40**, 573–587.
9 A. Mourchid, A. Delville, J. Lambard, E. Lecolier and P. Levitz, *Langmuir*, 1995, **11**, 1942.
10 A. Mourchid, E. LeColier, E. van Damme and P. Levitz, *Langmuir*, 1998, **14**, 4718.
11 S. Cocard, J. F. Tassin and T. Nicolai, *J. Rheol.*, 2000, **44**, 585.
12 U. Brandenburg and G. Lagaly, *Appl. Clay Sci.*, 1988, **3**, 273–284.
13 D. Quemada and C. Berli, *Adv. Colloid Interface Sci.*, 2002, **98**, 51.
14 U. Hofmann and A. Hausdorf, *Kolloid Z.*, 1945, **110**, 1–17.
15 U. Hofmann, R. Fahn and A. Weiss, *Kolloid Z.*, 1957, **151**, 97–115.
16 F. Pignon, J.-M. Piau and A. Magnin, *Phys. Rev. Letters*, 1996, **76**, 4857.
17 C. Martin, F. Pignon, J.-M. Piau, A. Magnin, P. Lindner and B. Cabane, *Phys. Rev. E*, 2002, **66**, 021401.
18 L. J. Michot, C. Baravian, I. Bihannic, S. Maddi, C. Moyne, J. F. L. Duval, P. Levitz and P. Davidson, *Langmuir*, 2009, **25**, 125–139.
19 C. Baravian, D. Vantelon and F. Thomas, *Langmuir*, 2003, **19**, 8109–8114.
20 H. van Olphen, *Discuss. Faraday Soc.*, 1951, **11**, 82–84.
21 D. van der Beek and H. N. W. Lekkerkerker, *Europhys. Lett.*, 2003, **61**, 703.
22 B. Ruzicka, L. Zulian and G. Ruocco, *Phys. Rev. Lett.*, 2004, **93**, 258301.
23 D. van der Beek and H. N. W. Lekkerkerker, *Langmuir*, 2004, **20**, 8582–8586.
24 J. E. G. J. Wijnhoven, D. D. van't Zand, D. van der Beek and H. N. W. Lekkerkerker, *Langmuir*, 2005, **21**, 10422–10427.
25 J. Zhang, L. Y. L. andW. X. Zhu, S. Y. Liu and D. Sun, *Langmuir*, 2007, **23**, 5331–5337.
26 L. J. Michot, I. Bihannic, K. Porsch, S. Maddi, C. Baravian, J. Mougel and P. Levitz, *Langmuir*, 2004, **20**, 10829–10837.
27 M. C. D. Mourad, D. V. Byelov, A. V. Petukhov, D. A. M. de Winter, A. J. Verkleij and H. N. W. Lekkerkerker, *J. Phys. Chem. B.*, 2009, **113**, 11604–11613.
28 K. Norrish and J. P. Quirke, *Farraday Soc.¡*, 1954, **18**, 120.
29 R. K. Schofield and H. R. Samson, *Discuss. Faraday Soc.*, 1954, **18**, 135.
30 B. Jönsson, C. Labbez and B. Cabane, *Langmuir*, 2008, **24**, 11406.
31 A. Weiss and R. Franck, *Z. Naturforsh.*, 1961, **16**, 141–142.
32 P. Levitz, E. Lecolier, A. Mourchid, A. Delville and S. Lyonnard, *Europhys. Lett.*, 2000, **49**, 672.
33 A. Shalkevich, A. Stradner, S. K. Bhat, F. Muller and P. Schurtenberger, *Langmuir*, 2007, **23**, 3570–3580.
34 M. Dijkstra, J. P. Hansen and P. A. Madden, *Phys. Rev. Letters*, 1995, **75**, 2236.
35 S. Kutter, J.-P. Hansen, M. Sprik and E. Boek, *J. Chem. Phys.*, 2000, **112**, 311–322.
36 D. Leger and D. Levesque, *J. Chem. Phys.*, 2002, **116**, 2251–2260.
37 G. Odriozola, M. Romero-Bastida and F. de J. Guevara-Rodriguez, *Phys. Rev. E*, 2004, **70**, 021405.
38 L. Morales-Anda, H. H. Wensink and A. Gil-Villegas, *J. Chem. Phys.*, 2012, **136**, 034901.
39 J. Dobnikar, R. Castaneda-Priego, H. von Grünberg and E. Trizac, *New J. Phys.*, 2006, **8**, 277–307.
40 V. Lobaskin and P. Linse, *J. Chem. Phys*, 1999, **11**, 4300–4309.
41 D. Rowan, J.-P. Hansen and E. Trizac, *Mol. Phys.*, 2000, **98**, 1369–1378.
42 E. Trizac, L. Bocquet, R. Agra, J.-J. Weis and M. Aubouy, *J. Phys.: Condens. Matter*, 2002, **14**, 9339–9352.
43 A. Agra, E. Trizac and L. Bocquet, *Eur. Phys. J. E*, 2004, **15**, 345–357.
44 E. Trizac, *Private communication*, 2012.
45 B. Beresford-Smith and D. Y. C. Chan, *Chem. Phys. Lett.*, 1982, **92**, 474–478.
46 B. Beresford-Smith, D. Y. C. Chan and D. J. Mitchell, *J. Colloid Interface Sci*, 1985, **105**, 216.
47 E. Trizac, L. Bocquet, R. Agra, J.-J. Weis and M. Aubouy, *Langmuir*, 2003, **19**, 4027–4033.
48 S. Jabbari-Farouji, H. Tanaka, G. Wegdam and D. Bonn, *Phys. Rev. E.: Stat., Nonlinear, Soft Matter Phys.*, 2008, **78**, 061405.
49 A. Shahin and Y. M. Joshi, *Langmuir*, 2010, **26**, 4219–4225.
50 M. Turesson, C. Labbez and B. Jönsson, *Langmuir*, 2012, in press.
51 R. H. Swendsen and J.-S. Wang, *Phys. Rev. Lett.*, 1987, **58**, 86–88.

52 A. A. Louis, *J. Phys. Condens. Matter*, 2002, **14**, 9187.
53 B. Ruzicka, L. Zulian, E. Zaccarelli, M. Sztucki, A. Moussaid and G. Ruocco, *Phys. Rev. Lett.*, 2010, **104**, 085701.
54 F. Lindemann, *Z. Phys.*, 1910, **11**, 609.
55 C. Martin, F. Pignon, A. Magnin, M. Meireles, V. Lelievre, P. Lindner and B. Cabane, *Langmuir*, 2006, **22**, 4065–4075.
56 J. Israelachvili, *Intermolecular and Surface Forces*, Academic Press, London, 2nd edn, 1991.
57 J. C. P. Gabriel, C. Sanchez and P. Davidson, *J Phys. Chem.*, 1996, **100**, 11139–11143.
58 S. Hachisu, Y. Kobayashi and A. Kose, *J. Coll. Interf. Sci.*, 1973, **42**, 342.
59 M. Wadati and M. Toda, *J. Phys. Soc. Jpn.*, 1972, **32**, 1147.
60 H. Tanaka, J. Meunier and D. Bonn, *Phys. Rev. E*, 2004, **E 69**, 031404.
61 P. Mongondry, *Structure et comportement rhéologique des suspensions aqueuses de Laponite en présence de plusieurs additifs.*, Université du Maine, Le Mans, PhD thesis edn, 2003, p. 224.
62 P. Mongondry, J. F. Tassin and T. Nicolai, *J. Coll. Interface Sci.*, 2005, **283**, 397–405.
63 B. Ruzicka, E. Zacarelli, L. Zulian, R. Angelini, M. Sztucki, A. Moussaid, T. Narayanan and F. Sciortino, *Nature Mat.*, 2011, **10**, 56–60.
64 D. Bonn, H. Kellay, H. Tanaka, G. Wegdam and J. Meunier, *Langmuir*, 1999, **15**, 7534.
65 E. Paineau, I. Bihannic, C. Baravian, A.-M. Philippe, P. Davidson, P. Levitz, S. S. Fa, C. Rochas and L. J. Michot, *Langmuir*, 2011, **27**, 5562–5573.
66 E. Paineau, L. J. Michot, I. Bihannic and C. Baravian, *Langmuir*, 2011, **27**, 7806–7819.
67 D. W. Thompson and J. T. Butterworth, *J. Coll. Interface Sci.*, 1992, **151**, 236.
68 L. J. Michot, I. Bihannic, S. Maddi, C. Baravian, P. Levitz and P. Davidson, *Langmuir*, 2008, **24**, 3127–3139.
69 L. J. Michot, J. Ghanbajaa, V. Tirtaamadja and P. Scales, *Langmuir*, 2001, **17**, 2100.

Paper III

Maxime Delhorme, Christophe Labbez and Bo Jönsson
accepted in *J. Chem. Phys. Lett.* (2012)

Paper IV

Maxime Delhorme, Bo Jönsson and Christophe Labbez
Manuscript (2012)

Gel and nematic phases of plate-like particle suspensions: Charge anisotropy and size effects

E-mail:

M. Delhorme[1,2], Bo Jönsson[1], and C. Labbez[2]

(1) Theoretical Chemistry, Chemical Center, POB 124, S-221 00 Lund, SWEDEN. (2) Laboratoire Interdisciplinaire Carnot de Bourgogne, UMR 6303 CNRS, Université de Bourgogne, 21078 Dijon Cedex, FRANCE.

Abstract

In this paper, the influence of the charge anisotropy and the size of the platelets on the formation of the gel and the nematic phases in suspensions of plate-like particles is investigated using Monte Carlo simulations in the canonical ensemble. The platelets are modeled as discs with charged sites distributed on a hexagonal lattice. The edge sites can carry a positive charge while the remaining sites are negatively charged giving rise to a charge anisotropy. A screened-Coulomb potential plus a short range repulsive potentials are used to describe the interactions between the sites of the platelets. The liquid-gel transition is found to be favored by a high

*To whom correspondence should be addressed

charge anisotropy and by large particles. Oppositely, the liquid-glass transition is favored for small particles without charge anisotropy, i.e, fully negatively charged. Finally, we find that the isotropic/nematic transition is disfavored by the charge anisotropy and for a strong charge anisotropy, the nematic phase does not form anymore. Instead, a gel/columnar transition is found.

Introduction

The transition in suspensions of plate-like particles from an isotropic to an arrested state has been widely studied during the past 60 years due to the important number of industrial applications they are involved in: cosmetics, paint products, drilling fluids ... Tanaka et al.[1] give a good description of all the nonergodic states of charged colloidal suspensions. In brief, a disordered state which is percolated and whose characteristic length of the network between two adjacent junctions is much larger than the particle size is defined as a gel. Therefore, gel phases can only be formed when attractive interactions are at play in a system. Similarly, a disordered state whose elasticity originates from caging effect and whose characteristic length scale between two adjacent junctions is about the distance between two particles is defined as a glassy state. One part of the confusion between gel and glassy states arises from the fact that glass can either be attractive or repulsive while gels are only attractive. Then depending on the charge carried by the edges of the platelet, two different transitions are considered, that is, a transition to a gel phase in presence of charge anisotropy and a transition to a glassy state without charge anisotropy. Unfortunately, the experimental characterization of the charge distribution of minerals is not trivial, and to the best of our knowledge no experimental studies of mineral platelets as a function of their charge anisotropy has been reported. In a recent work on a model clay system[2] we report three different transitions according to the charge anisotropy of the platelets: a liquid-gel transition is found for high charge anisotropy, a sol-gel transition

for a moderate charge anisotropy and a liquid-glass one without charge anisotropy in agreement with experimental observations on laponite.[2] Similarly, studies of the influence of particle size on the transition to an arrested state are scarce. In a general, when sol-gel or sol-glass transitions involve perfectly exfoliated platelets, the transition is shifted to lower volume fractions for smaller platelets, as observed on montmorillonite,[3] nontronite[4,5] and beidellite[6] clays.

Another remarkable property of anisotropic plate-like particles, is their ability to form liquid crystalline phases. Langmuir first reported the self assembly of colloidal particles in suspensions of California hectorites.[7] The transition from an isotropic to a nematic phase was rationalized by Onsager as a competition between orientational and translational entropy.[8,9] This explanation, first developed for hard rods and then extended to the disk-like particles, has been confirmed by Monte Carlo simulations.[10] Since then, efforts have been put into experimental studies in order to understand the isotropic/nematic (I/N) transition of mineral platelets. Gibbsite,[11–13] layered double hydroxides like takovite,[14] Mg/Al,[15] hydrotalcite,[16] copper sulfide[17] and many different sort of clays[4,6,18,19] were found to display a transition to a liquid crystalline phase. However, few of these studies present results about the size dependence of the I/N transition. Michot et al.[4] reported the formation of a nematic phase when the nontronite particle size was increased, but the opposite trend was found experimentally for beideillite clays.[6] According to the authors, this difference in behavior is the result of an incomplete exfoliation of particles in the suspension. Computer simulations of infinitely thin platelets[20,21] and for different aspect ratio[22] are in fairly good agreement with experimental results showing that polydispersity disfavors the formation of the nematic phase, while decreasing the aspect ratio enhances its formation. However, more informations about the influence of the charge anisotropy on the I/N transition is needed. Only recently, Martínez-Haya et al.[23] presented a new tool where the directionality of the interactions between the platelets could be tuned. They show that the nematic stability is favored for homogeneous or weakly directional interactions, i.e without or with a very low charge anisotropy.

The aim of this paper is to investigate further the influence of both the particle size and the charge anisotropy on the I/N transition and the transition from an isotropic to a kinetically arrested state. For this purpose, Monte Carlo simulations with a screened Coulomb potential combined with a soft repulsion are used to simulate dispersions of mineral platelets.

Model and Simulations

Model

In this study we use the same model and simulation techniques as employed in a previous paper[2] and they are only briefly described below. A dispersion of N platelets in a 1-1 salt solution is considered. A single platelet, of diameter D, is decorated with a collection of n^T sites of diameter L =1 nm spread on an compact hexagonal lattice with a density of 0.87 site/nm^2. A platelet is composed of n_e edge sites, chosen to be positive, neutral or negative and n_b basal sites which are always negatively charged. The net charge of a single platelet therefore reads $Z^{net} = (n_e - n_b)e$. The platelets are dispersed in a cubic box of volume V_{box}, where periodic boundary conditions are applied in all directions using the minimum image convention.

The solvent, that is water, is treated as a structureless dielectric continuum and is implicitly represented by its relative dielectric permittivity, ε_r, which is assumed to be constant throughout space. Salt and counterions are also implicitly represented through the Debye screening length κ^{-1}, which is described as :

$$\kappa^2 = \frac{e^2(2c_s + c_c)}{\varepsilon_0 \varepsilon_r kT} \tag{1}$$

where k is the Boltzmann's constant, T the absolute temperature, ε_0 is the permittivity of vacuum, and c_s and c_c the salt and counterions concentration, respectively.

Interaction potentials

A shifted and truncated Lennard-Jones (LJ) potential is used to account for the finite size of particles. In addition to the shifted LJ potential a screened Coulomb potential is employed to describe the electrostatic contribution. The total interaction between two sites, $u^{tot}(r_{ij}) = u^{el}(r_{ij}) + u^{LJ}(r_{ij})$, of charge z separated a distance r_{ij} then reads,

$$u^{tot}(r_{ij}) = \begin{cases} \frac{z_i z_j \exp(-\kappa r_{ij})}{4\pi\varepsilon_r\varepsilon_0 r_{ij}} + 4\varepsilon_{LJ}\left(\left(\frac{\sigma_{LJ}}{r_{ij}}\right)^{12} - \left(\frac{\sigma_{LJ}}{r_{ij}}\right)^{6}\right) + \varepsilon_{LJ} & r_{ij} < \sqrt[6]{2}\sigma_{ij} \\ \frac{z_i z_j \exp(-\kappa r_{ij})}{4\pi\varepsilon_r\varepsilon_0 r_{ij}} & r_{ij} > \sqrt[6]{2}\sigma_{ij} \end{cases}, \quad (2)$$

where ε_{LJ} and σ_{LJ} are the Lennard-Jones parameters. These were set to $\varepsilon_{LJ} = 0.5$ k_BT and $\sigma_{LJ} = 0.5$ nm in all simulations. The full configurational energy of the N platelets system them becomes

$$U = \sum_{i=1}^{N}\sum_{j>i}^{N}\sum_{\alpha=1}^{n^T}\sum_{\beta=1}^{n^T} u^{el}(r_i^\alpha, r_j^\beta) + u^{LJ}(r_i^\alpha, r_j^\beta) \quad (3)$$

where indices i, j refer to platelets and indices α, β to sites on these platelets, respectively.

Systems

Three different platelet sizes are considered with $n^T = 61$, 91 and 199 which correspond to $D =$ 90, 110 and 150 Å, respectively. In addition, four different charge anisotropies are considered, that is:

- *high charge anisotropy* (HiCh) where all edge sites are positively charged;
- *moderate charge anisotropy* (ModCh) where half of the edge sites are positive and the other neutral (organized as an alternation of charged and neutral sites);
- *low charge anisotropy* (LoCh), where only neutral sites on the edges are present;

- *without charge anisotropy* (NoCh), where all sites on the platelet are negatively charged.

Soft core systems, i.e. without electrostatic interactions, for the three sizes of platelets are also considered for comparison. In all calculations, the salt concentration of the equilibrium solution is kept constant at $c_s = 10$ mM. The particle volume fraction, defined as,

$$\phi = \frac{NV_{part}}{V_{box}} \tag{4}$$

is varied from 0.001 to 0.4, where $V_{part} = n^T \pi \sigma_{LJ}^3/6$ is the volume of a single platelet.

Simulations

The calculations are carried out using the same procedure as in a previous paper.[2] In brief, the model is solved using Monte Carlo simulations in the canonical ensemble (N,V,T) and the standard Metropolis algorithm. Collective platelets displacement and multi-level coarse graining are employed. The simulations are performed with 1000/500/200 particles for the small, medium and big platelets, respectively. An equilibrium run is done with $2{\cdot}10^6$ cycles (in one cycle all particles have been moved once), and a typical production run involve $4{\cdot}10^6$ cycles.

Measured quantities

The nematic order parameter, S, is used to characterize the nematic phase. It is evaluated from the tensor[22] :

$$\mathbf{Q} = \frac{1}{2N} \left\langle \sum_{i=1}^{N} 3\mathbf{u}_i \cdot \mathbf{u}_i - \mathbf{I} \right\rangle \tag{5}$$

where N is the number of particles, $\mathbf{u}_i$ is the normal vector to the i^{th} particle and $\mathbf{I}$ the identity matrix. The highest eigenvalue, λ^+, was used to evaluate S, $S = \lambda^+$. S is calculated over an

average of $2{\cdot}10^4$ cycles for the isotropic and $4{\cdot}10^6$ cycles in the nematic phase. ϕ value at which $S = 0.4$ is taken as the position of the I/N transition.[24]

The percolation of the system and the elasticity of the suspension are evaluated using the same procedure as in the previous study.[2] In brief, two clay platelets are considered to be "connected" neighbors if the separation between one site of a particle is located at less than 15 Å from a site of another particle. A cluster is defined as a collection of connected platelets. From these considerations we calculate :

- $\langle N_{nei} \rangle$ = average number of neighbors around one platelet in a cluster
- $\langle N_{cl} \rangle$ = average number of platelets in a cluster
- $\langle N_{pour} \rangle$ = percentage of particles aggregated in the system

The elasticity is approximated by calculating the average force fluctuation per platelet in the three Cartesian directions:

$$\langle f^2 \rangle = \frac{\langle f_x^2 \rangle + \langle f_y^2 \rangle + \langle f_z^2 \rangle}{3}$$

Results

Nematic phase

The I/N transition is investigated in Figure 1, which shows the variation of S as a function of volume fraction for various platelet sizes and charge anisotropies in comparison to the soft platelet case. The estimated I/N transition at $S = 0.4$ for the various cases treated are summarized in Table 1. All curves present the same behavior - at low ϕ, S is close to zero. This is characteristic

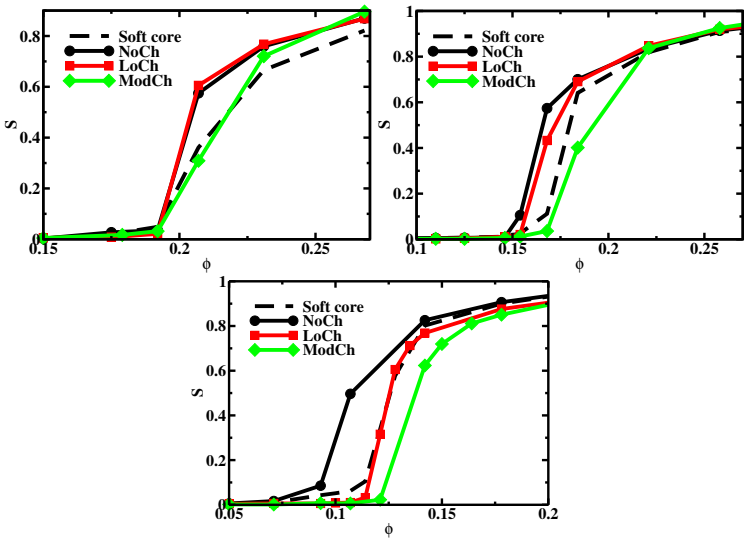

Figure 1: Nematic order parameter as a function of the volume fraction ϕ. The diameter of the particles is a) 90 , b) 110 and c) 150 . The NoCh case is represented in full black lines with circles, LoCh in full red lines with squares and ModCh in full green lines with diamonds. The soft core case is given for comparison (black dashed lines).

Table 1: Volume fractions at which the I/N transition occurs for various platelet sizes, D, and charge anisotropies. The I/N transition is extracted from Figure 1 at $S = 0.4$. The statistical error in the calculation of S is $\pm$ 0.05.

D	Soft core	NoCh	LoCh	ModCh	HiCh
90 Å	0.21	0.20	0.20	0.21	–
110 Å	0.18	0.16	0.16	0.18	–
150 Å	0.12	0.10	0.12	0.13	–

of an isotropic phase (I) where the platelets are randomly oriented. When increasing ϕ, a transition from an isotropic to a nematic phase occurs characterized by the rapid rise of the nematic order parameter. In agreement with Onsager's prediction, the transition is found to be shifted toward lower volume fractions as the platelet size is increased - see Table 1. This is an example of the role of the excluded volume in such phase formation. Interestingly, the I/N transition is also found to be dependent of the charge carried by the edges. When the platelet edges bear the

same charge as the basal plane (NoCh) or when they are neutral (LoCh), the formation of the nematic phase is favored, i.e. compared to the soft core case. This seems to be true for all particle sizes, and illustrates the role of the electrostatic repulsions. When the edges are oppositely charged (ModCh) the transitions are shifted toward high volume fractions. The formation of the nematic phase is then disfavored. This is an important effect since for high charge anisotropy (HiCh), the I/N transition is replaced by a gel/columnar transition, see below and ref.[25] Note as well that, the smaller the platelets, the less important the effect of the charge anisotropy. The obtained results are consistent with the recent findings of Martínez-Haya et al.[23] with the use of anisotropic dispersive potentials.

Gel phase

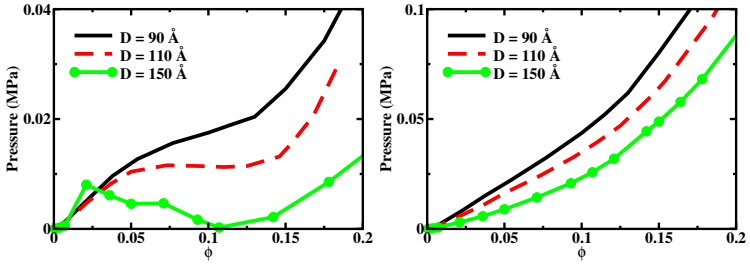

Figure 2: Equation of state for platelets with various charge anisotropies and sizes, D. a) HiCh; b) ModCh.

Figure 2 and Figure 3 display the osmotic pressure and structural parameters for dispersions of platelets with various sizes and moderate to high charge anisotropy. As already shown elsewhere,[2] in the case of strong charge anisotropy, dispersions of platelets with $D = 150$Å experience a first order phase transition as revealed by the van der Waals loop in the equation of state. This corresponds macroscopically to a phase separation between a repulsive liquid and a percolated network, see Figure 3-a and -b, of randomly oriented particles characteristic of a gel phase. The gel forms due to the strong basal-edge attraction between the platelets. The gel

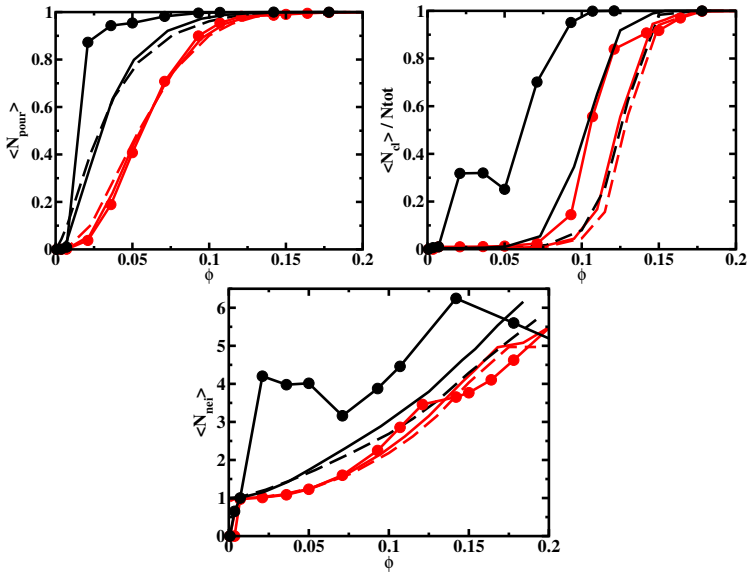

Figure 3: Structural parameters for dispersions of platelets at two charge anisotropies and with various sizes: (ModCh) = red; (HiCh) = black; $D = 90$ (dashed lines); $D = 110$ (full lines); $D = 150$ (full line with circles). a) Percentage of particles in the simulation box that are included in a cluster, $< N_{pour} >$. b) Average number of particles that form a cluster normalized with N_{tot}, $< N_{pour} >$. c) Number of neighbors around a particle inside a cluster, $< N_{nei} >$.

structure is characterized in Figure 3 through the quantities $< N_{cl} >$, $< N_{nei} >$ and $< N_{cl} >$ which all show, a strong increase with volume fraction. In particular, a percolated network is found above $\phi = 10\%$, c.f. Figure 3-b. The steep increase in $< N_{cl} >$ and $< N_{nei} >$ at low ϕ, in Figure 3 has been shown to be associated with the formation of the metastable Smectic B phase.[2] On the other hand, the drop in the number of neighbors, Figure 3-b, at $\phi > 0.15$, is related to the formation of a columnar phase, see ref.[25] When the particle size is decreased, $< N_{cl} >$, $< N_{nei} >$ and $< N_{cl} >$ are, instead, monotonically increasing functions. The percolation point, i.e. ϕ at which the system is fully percolated, is seen to increase as the particle size is reduced, see Figure 3-b, although, due to a weaker Z^{net}, smaller particles start to aggregate

earlier, as best seen in Figure 3-a. The equation of state, Figure 2, shows that the liquid-gel separation is greatly soften when decreasing the platelets size to D=110 Å and, upon a further decrease in D, is replaced by a continuous sol-gel transition. Using an approximate Maxwell construction, the phase transition from a liquid to a gel is thus found to increase from $\phi \sim 3\%$ to $\sim 15\%$ as the platelet size is decreased.

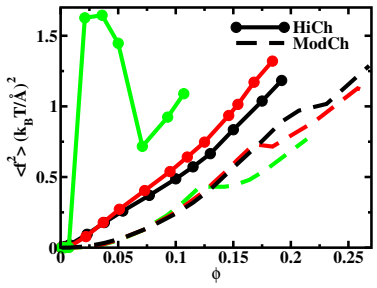

Figure 4: Force fluctuation per particle as a function of the volume fraction ϕ for platelets with various sizes and charge anisotropies. Dashed lines: moderate charge anisotropy; full lines: strong charge anisotropy; black curves: $D = 90$; red curves: $D = 110$; green curves: $D = 150$.

In the case of platelets with moderate charge anisotropy, a continuous sol-gel transition is found for all D, c.f. Figures 2-b and 3, respectively. Note that the osmotic pressure is approximatively two times bigger as a result of the drop of the charge anisotropy and the related rise of Z^{net}. The evolution of $< N_{pour} >$ and $< N_{cl} >$ with the particle size, Figure 3-a and -b, shows that, although less pronounced, the same conclusion as in the case of strong charge anisotropy can be drawn. That is, the bigger the particle size is, the easier the sol-gel transition. Interestingly the same trend has been observed on dispersions of Mg/Al layered double hydroxide[14] and nontronite clay[4] at low salt concentration. Although such a rationalization is appealing, a full characterization of the charge anisotropy of these minerals would be needed in order to conclusively ascertain the dependence of the liquid-gel transition with the size of the platelets. A closer look at Figure 3-c, reveals a step in the increase in the number of neighbors with ϕ for all moderate charge anisotropy curves (ModCh), induced by the spatial reorganization of platelets,

characteristic of the I/N transition, c.f. Figure 1. Note that, however, above this transition a true nematic phase is not observed but, instead, what can be called a nematic gel.

Again the same conclusions can be drawn from the force fluctuation per particle shown in Figure 4 , i.e. a measure of the gel elasticity. Indeed, the gel becomes stiffer with increase in particle size and charge anisotropy. The stiffness goes up with the volume fraction, but slows down at the transition to the nematic gel.

Glass phase

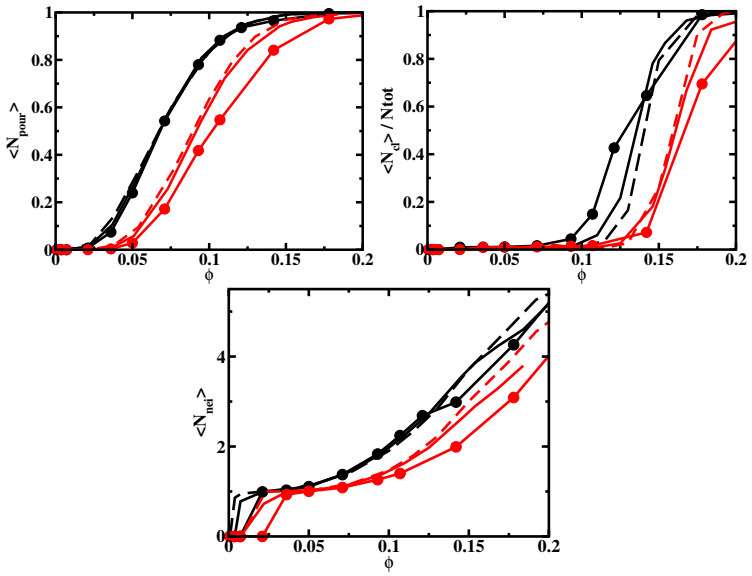

Figure 5: Structural parameters for dispersions of platelets at two charge anisotropies and with various sizes: (LoCh) = black; (NoCh) = red; $D = 90$ (dashed lines); $D = 110$ (full lines); $D = 150$ (full line with circles). a) Percentage of particles in the simulation box that are included in a cluster, $< N_{pour} >$. b) Average number of particles that form a cluster normalized with N_{tot}, $< N_{pour} >$. c) Number of neighbors around a particle inside a cluster, $< N_{nei} >$.

Figure 5 presents the structural parameters versus ϕ of dispersions for fully negatively charged

platelets, i.e. $n_e = 0$. Globally, the same trend is obtained for $< N_{pour} >$, $< N_{cl} >$ and $< N_{nei} >$ as compared to the moderate and strong charge anisotropy case. Indeed, due to the strong repulsive electrostatic interactions that prevail in these systems, the "filled space" by the spatial organization of the platelets is found to be reduced as depicted by the global shift of the curves toward higher volume fractions. This is emphasized when the platelets are large and do not present a charge anisotropy. As an example, the number of close neighbors, stays lower than two up to $\phi \sim 15\%$ for all D when the platelets are fully negatively charged, while at high charge anisotropy and $D = 150$ it drops to $\phi \sim 2\%$ - see Figures 3-c and 5-c.

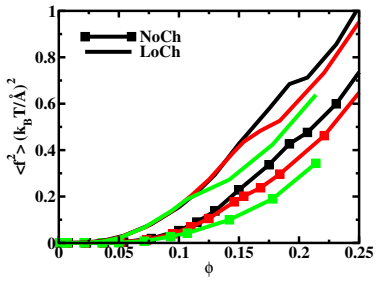

Figure 6: Force fluctuation per particle as a function of the volume fraction ϕ for platelets with various sizes and charge anisotropies. Full lines: low charge anisotropy; full lines with symbols: no charge anisotropy; black curves: $D = 90$; red curves: $D = 110$; green curves: $D = 150$.

A striking feature is the change in stiffness of the repulsive glass (Wigner glass) as the volume fraction and the particle size are increased. The stiffness is found to increase, as expected, with the volume fraction, but contrary to the gel case, it decreases with particle size. This surprising behavior is illustrated in Figure 6. Similarly to a previous finding on gels,[2] $< f^2 >$ is found to be proportional to the number of close neighbors, see Figure 5-c. Indeed, the same qualitative trend is observed, i.e. both the number of close neighbors and glass stiffness decrease when edge sites become negatively charged and particle size is increased. The liquid-glass transition is thus expected to be favored with small platelets. Interestingly, the same behavior has been observed with dispersions of nontronite,[5] bedeillite[6] and montmorillonite.[3]

Conclusion

We have provided new insight into the transition from an isotropic liquid to a nematic and to various solid phases. Our results shed more light on how the different phases depend on the charge heterogeneity of the platelets. In particular, we find that at high charge anisotropy the liquid-gel transition is favored for dispersions of large platelets and reversely when the platelets are fully negatively charged. These two different regimes (i.e. at low and high charge anisotropy) may explain the differences in the liquid-solid transition observed between, on one hand, montmorillonite, beidellite, and, on the other hand, nontronite, Mg/Al layered double hydroxides, with changes in the particle size distribution. However, a full characterization of the charge anisotropy of these minerals would be needed in order to conclusively ascertain the dependence of the liquid-solid transition with the size of the platelets. In addition, we found that the I/N transition is disfavored by the charge anisotropy, and, thus, often found to be pre-empted by a gel phase. Surprisingly, this transition is found to disappear in favor of a gel-columnar transition for strong enough charge anisotropy.

Acknowledgment

The autors acknowledge the support of the CRI of the Université de Bourgogne and Lunarc from Lund University for providing access to the common computer facilities.

References

(1) Tanaka, H.; Meunier, J.; Bonn, D. *Phys. Rev. E* **2004**, *E 69*, 031404.

(2) Delhorme, M.; Jönsson, B.; Labbez, C. *Submitted to Soft Matter* **2012**,

(3) Michot, L. J.; Bihannic, I.; Porsch, K.; Maddi, S.; Baravian, C.; Mougel, J.; Levitz, P. *Langmuir* **2004**, *20*, 10829–10837.

(4) Michot, L. J.; Bihannic, I.; Maddi, S.; Baravian, C.; Levitz, P.; Davidson, P. *Langmuir* **2008**, *24*, 3127–3139.

(5) Michot, L. J.; Baravian, C.; Bihannic, I.; Maddi, S.; Moyne, C.; Duval, J. F. L.; Levitz, P.; Davidson, P. *Langmuir* **2009**, *25*, 125–139.

(6) Paineau, E.; Antonova, K.; Baravian, C.; Bihannic, I.; Davidson, P.; Dozov, I.; Impŕor-Clerc, M.; Madsen, A.; Meneau, F.; Michot, L. J. *Langmuir* **2009**, *25*, 125–139.

(7) Langmuir, I. *J. Chem. Phys.* **1938**, *6*, 873–896.

(8) Onsager, L. *Phys. Rev.* **1942**, *62*, 558.

(9) Onsager, L. *Ann. N. Y. Acad. Sci.* **1949**, *51*, 627–659.

(10) Vieillard-Baron, J. *Mol. Phys.* **1974**, *28*, 809.

(11) van der Kooij, F. M.; Lekkerkerker, H. N. W. *J. Phys. Chem. B* **1998**, *102*, 7829–7832.

(12) van der Kooij, F. M.; Kassapidou, K.; Lekkerkerker, H. N. W. *Nature* **2000**, *406*, 868–871.

(13) van der Beek, D.; Lekkerkerker, H. N. W. *Europhys. Lett.* **2003**, *61*, 703.

(14) Michot, L. J.; Ghanbaja, J.; Tirtaatmadja, V.; Scales, P. J. *Langmuir* **2001**, *17*, 2100–2105.

(15) Liu, S.; Zhang, J.; Wang, N.; Liu, W.; Zhang, C.; Sun, D. *Chem. Mater* **2003**, *15*, 3240.

(16) Mourad, M. C. D.; Devid, E. J.; van Schooneveld, M. M.; Vonk, C.; Lekkerkerker, H. N. W. *J. Phys. Chem. B.* **2008**, *112*, 10142–10152.

(17) Saunders, A. E.; Ghezelbash, A.; Smilgies, D. M.; Sigman, M. B.; Kargel, B. A. *Nano Lett.* **2006**, *6*, 2959–2963.

(18) Mourchid, A.; LeColier, E.; van Damme, E.; Levitz, P. *Langmuir* **1998**, *14*, 4718, Clays.

(19) Gabriel, J. C. P.; Sanchez, C.; Davidson, P. *J Phys. Chem.* **1996**, *100*, 11139–11143.

(20) Frenkel, D.; Eppenga, R. *Phys. Rev. Lett.* **1982**, *49*, 1089.

(21) Bates, M. A.; Frenkel, D. *J. Chem. Phys.* **1999**, *110*, 6553–6559.

(22) Veerman, J. A. C.; Frenkel, D. *Phys. Rev. A* **1992**, *45*, 5632.

(23) Martínez-Haya, B.; Cuetos, A. *Phys. Rev. E* **2010**, *81*, 020701.

(24) Eppenga, R.; Frenkel, D. *Mol. Phys.* **1984**, *52*, 1303.

(25) Delhorme, M.; Labbez, C.; Jönsson, B. *Submitted to Phys. Chem. Lett.* **2012**,

Paper V

Maxime Delhorme, Christophe Labbez, André Nonat, Cliff Woodward and
Bo Jönsson
Manuscript (2012)

1

June 5, 2012

The Growth and Stability of Nanoplatelets

M. Delhorme[1,2], C. Labbez[1] and A. Nonat[1], C. Woodward[3] and Bo Jönsson[2]

(1) Laboratoire Interdisciplinaire Carnot de Bourgogne, UMR 6303 CNRS, Université de Bourgogne, 21078 Dijon Cedex, FRANCE.
(2) Theoretical Chemistry, Chemical Center, POB 124, S-221 00 Lund, SWEDEN.
(3) PEMS, University of New South Wales, Canberra, 260x ACT, AUSTRALIA.

Abstract

In this study, the growth and stability of mineral nanoplatelets are investigated with Monte Carlo simulations (MC) and illustrated for the case of calcium silicate hydrate, C-S-H, the main product of cement hydration. In a first model, 2D MC simulations in the canonical ensemble are used to demonstrate that the growth of a single C-S-H platelet could be limited by its own internal repulsion. In this case short range attractive interactions are modeled with a square well potential and electrostatic interactions with a screened Coulomb potential. Then the interaction between two charged platelets in a 2:1 salt is studied to investigate the competition between the growth and the aggregation of C-S-H particles. The platelets are represented as a collection of sites distributed on a hexagonal lattice. MC simulations in the grand canonical ensemble are used, and interactions are modeled with Lennard-Jones and Coulombic potentials between all species. The attraction between the C-S-H platelets are shown to increase with salt concentration and size of the platelets. The results confirm that the competition between aggregation and growth has a kinetic origin. Finally, the different modes of aggregation of the C-S-H platelets onto C_3S surfaces are investigated. For that purpose, a charged surface is introduced in the simulation box. We report that, similarly to experimental results, a high charge density ($\sim$ pH) and calcium concentration favor the axial aggregation.

Introduction

Cement is a widely used material today and as such it also has a strong impact on the environment - high energy consumption and large CO_2 emission. Thus, there is a considerable interest in making cement use more efficient. One way to achieve this is by obtaining a better understanding of the setting of cement on a microscopic scale. Modern *Portland cement* is made from limestone and clay, which are heated to 1500 ^{o}C, producing a cement clinker, which is a polyphasic material including calcium silicates (Ca_3SiO_5=C_3S and Ca_2SiO_4), calcium aluminate and aluminoferrite. The final cement

product is obtained by grinding the clinker with gypsum ($CaSO_4$). One interesting aspect of this mix of components is the conformity of the final concrete construction. That is, the chemical composition can vary within generous limits, still the final product has the desired strength. This indicates to us that the forces operating on the microscopic scale are generic and largely of direct electrostatic origin.

After mixing cement with water and sand, one obtains a concentrated suspension of 10-100 μm grains with embedded gravels. The suspension, or paste, has a high volume fraction and is best described as a colloidal suspension, although cement paste is very rarely mentioned in colloidal chemical textbooks. When C_3S comes into contact with water a dissolution process begins and the grains start to dissolve. The solution soon contains a variety of anions and cations and the ionic strength is high. After a few minutes the solution becomes supersaturated with respect to calcium silicate hydrate ($CaO\text{-}SiO_2\text{-}H_2O$ = C-S-H) and calcium sulfoaluminate hydrate (ettringite) that precipitate. Among the precipitated hydrates, the former constitutes at least 60 % of the fully hydrated cement paste. The growth of C-S-H particles is both very directional and limited. A typical C-S-H particle is a platelet with approximate dimensions of $50 \cdot 30 \cdot 5$ nm [1, 2, 3]. The platelets are highly charged due to titrating silanol groups and the dissolution of C_3S and precipitation of C-S-H take place at high pH (≈ 12 or higher).

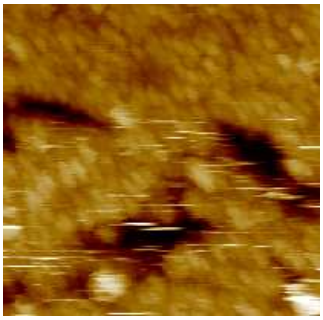

Figure 1: Atomic Force Microscopy image of the growth of C-S-H nano-platelets on the C_3S grains. The size of the image is 1 μm x 1 μm. The size of the platelets is 50 x 30 x 5 nm^3. From [1]

In the case of cement hydration, C-S-H nucleates onto the surface of C_3S [4] and platelets grow until they have reached a certain size. Then new platelets grow next to the previous to form a network of C-S-H platelets which grows out into the solution [1, 5] - see Fig. 1. The limited growth of the single nano-platelet is an intriguing observation. It does not occur only in the case of cement hydration but also in the case of precipitation from solutions of soluble salts, i.e. sodium silicate and calcium nitrate or from a mix of silica and lime (see Fig. 2). In that case, the final arrangement is a more or less random aggregation of these small platelets. The aggregation of the platelets onto a C_3S surface is strongly oriented and depends on the ionic content of the solution. Low pH and low calcium concentration promotes a lateral aggregation of platelets (i.e. next to each other)

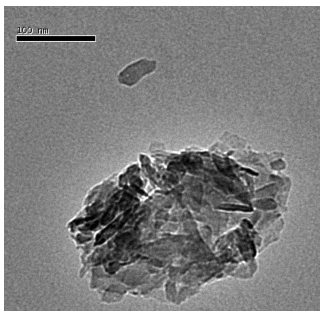

Figure 2: TEM image of C-S-H (x40 000) obtained from lime and silica. Platelets also aggregate. An isolated one shows the same size than in the case of C_3S hydration. (Courtesy J. Haas)

and a high calcium concentration promotes an axial aggregation of the platelets (i.e. on top of each other) [5, 6].

The growth of charged aggregates in colloidal solution is often controlled by electrostatic interactions and limited due to internal electrostatic repulsion. For example, in protein solution it has been observed that the aggregation process halts once a certain aggregate size is reached. This has been explained as a result of internal Coulombic repulsion [7, 8, 9, 10]. In cement paste, however, this could be a less likely mechanism, since the electrostatic screening is significant - in a typical paste, the range of the electrostatic interactions might only be a nanometer or less, although the surface charge density is much greater [11].

Thus, the explanation for the limited growth can be sought after somewhere else. One possible explanation is that the aggregation is the determining factor for the growth. That is, initially when the C-S-H platelet form they have a negative surface charge and according to simple theory they should, repel each other. The interaction with the negatively charged C_3S grains should be also initially repulsive. When the platelets grow and become increasingly negatively charged, the presence of divalent Ca^{2+} will, however, induce an attractive interaction due to ion-ion correlations [12, 13, 14]. This attraction, together with van der Waals forces, will eventually dominate and lead to an aggregation between C-S-H platelets and the dissolving C_3S grains as well as between the C-S-H platelets themselves.

Below we will prospect on the mechanisms of growth inhibition and aggregation of nanoplatelets and discuss the obtained results in light with experimental observations on hydrated cement paste systems. The paper is organized as follows: firstly, we show, based on a simple two-dimensional model, in what range of parameters (charge and ionic strength) the internal electrostatic repulsion is not the growth limiting factor. Thereafter we describe a more sophisticated model used in Monte Carlo simulations of particle aggregation to investigate the interaction between two platelets alone or in presence of a large sur-

face which mimics the C_3S surface. The results of these simulations are described and discussed at some length and we end by some conclusions.

Model Systems

A single platelet

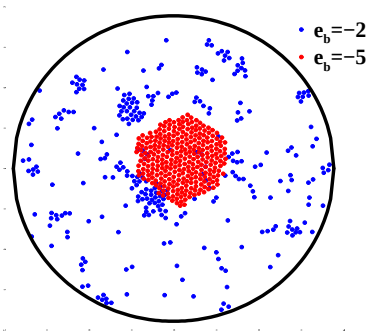

Figure 3: The final structure from two simulations with no electrostatic interactions and varying binding energy. $N = 289$ and $R_c = 378$ Å. A binding energy of 2 k_BT is not enough to maintain a compact cluster but 5 k_BT leads to an aggregated structure.

This model system depicted in Fig.3 is used by us to study the growth of a single platelet in two dimensions. Spherical particles, with radius R are allowed to move on a circular area with radius R_c. The interaction between any two particles i and j, with separation r_{ij} is given by a short-ranged square well potential, with depth e_b and width w,

$$\begin{aligned} \beta u_{sw}(r_{ij}) &= \infty \quad r_{ij} < 2R \\ &= -e_b \quad 2R < r_{ij} < 2R + w \\ &= 0 \quad \text{otherwise} \end{aligned} \tag{1}$$

This potential models a generic attractive interaction that promotes aggregation. We assume that it is largely unaffected by other mobile ions. Actual C-S-H platelets, are likely held together via a combination of short-ranged electrostatic correlations, dispersion forces and covalent bonds. In addition, C-S-H plates are highly charged, thus the particles of charge $-\alpha e$ that comprise the platelets experience strong electrostatic repulsion, that will inhibit aggregation. This effect is modeled with a screened Coulomb potential, which also accounts for the ambient electrolyte concentration,

$$\beta u_{sc}(r_{ij}) = \frac{\alpha^2 l_B \exp(-\kappa r_{ij})}{r_{ij}} \quad r_{ij} > 2R \tag{2}$$

Here, $l_B = e^2/4\pi\epsilon_0\epsilon_r k_B T$ is the Bjerrum length and κ is the inverse Debye-Hückel screening length, determined by the salt concentration. The solvent (water) is treated as a dielectric continuum with a relative dielectric permittivity, $\epsilon_r = 78$. e is the elementary charge and α is the number of charge carried by each particle that comprise the platelets; ϵ_0 is the permittivity of vacuum, T is the absolute temperature and k_B is Boltzmann's constant.

Two platelets

A more elaborate model is used to study the interaction between two C-S-H platelets in a 2:1 salt solution, see Fig.4. Each platelet is modeled as a disc composed of n_p spherical particles (diameter, $d = 1$ nm) arranged on a regular hexagonal lattice. Simulations of these two discs are carried out in a cylindrical box of volume V_{box}. To study the effect of changing platelet size, we use the values, $n_p = 19$, 37, 61, 91 and 127. Similarly to the previous model the particles that make up the platelets are also assigned a charge of, $-\alpha e$, where α is chosen as an input parameter. Hence, the total charge of a C-S-H platelet is,

$$Z_{CSH} = -n_p \alpha e \tag{3}$$

We investigate the role of surface charge by varying α. The following surface charge densities are used in our studies, -0.6, -1.2 and -2.4 e/nm^2.

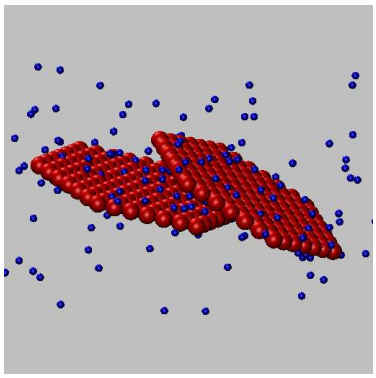

Figure 4: Schematic picture of two platelets in a salt solution and confined to a cylinder (not shown). The center of mass of the platelets are constrained to the cylinder axis. The sites of the platelets are shown as red spheres while the divalent counterions as blue spheres.

As in the single platelet model above, the solvent is treated implicitly using the primitive model. That is, charges are assumed embedded in a structureless dielectric continuum

described by the relative dielectric permittivity. Thus, charged particles, i and j, interact via a Coulomb potential,

$$U^{el}(r_{ij}) = \frac{q_i q_j}{4\pi\epsilon_0\epsilon_r r_{ij}} \tag{4}$$

where q_i is the charge carried by particle i and r_{ij} the particle separation. In this way, all mobile ions are treated explicitly, unlike the implicit treatment of salt used in the previous model. In all cases we considered, we assumed divalent counterions to the surface charges. All particles also interact via a dispersion potential, modeled with the Lennard-Jones function,

$$U^{LJ}(r_{ij}) = 4\epsilon_{LJ}((\frac{\sigma_{LJ}}{r_{ij}})^{12} - (\frac{\sigma_{LJ}}{r_{ij}})^{6}) \tag{5}$$

where, if not otherwise stated, the Lennard-Jones parameters took the values, $\epsilon_{LJ} = 0.1k_BT$ and σ_{LJ} was equal to the sum of the radii of the two interacting species.

Two platelets and infinite surface

On top of the two platelets, a charged surface is introduced in the simulation box and positioned at one end of the cylinder. The same model as for the platelets is used to describe the charged surface, i.e. the surface is decorated with charged sites distributed on a hexagonal lattice with the same density, charge and size as those of the platelets.

The aim of this model is to investigate two different modes of aggregation of the C-S-H platelets onto the C_3S surface, that is the axial and the lateral aggregation see Fig. 5-a and -b, respectively. In the first case, Fig. 5, the center of mass of one platelet is kept fixed in the close vicinity of the surface. Its position is further chosen such as to be at the free energy minimum. The center of mass of the second platelet is moved along the z axis, i.e. the rotation axis of the cylinder. In the second case, the centers of mass of the two platelets are positioned in the free energy minimum with the surface and moved along the x axis, parallel to the surface. Note that in all the simulations the platelets are allowed to rotate.

Two particle sizes are used, $n_p = 19$ and 37, and the surface charge density is chosen to be the same for the surface and the platelets by varying α. Three surface charge densities, -0.5, -1.2 and -1.9 e/nm^2, are studied. As for the two platelets case the primitive model is used and the interactions between all species are described using a Coulomb and a Lennard-Jones potential. The Lennard-Jones parameters are chosen as follow $\epsilon_{LJ} = 0.01k_BT$ between ions and sites and $\epsilon_{LJ} = 0.1k_BT$ otherwise and σ_{LJ} like in the two platelet model.

Monte Carlo simulations

The Monte Carlo simulations for the single platelet system is carried out in two dimensions using the standard Metropolis algorithm in the Canonical Ensemble, i.e., constant

7

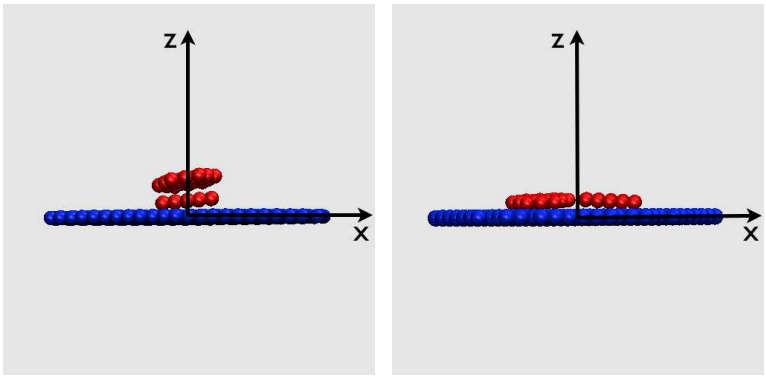

Figure 5: Sketches of the two platelets and one infinite surface model used to study the a) axial aggregation and b) lateral aggregation.

number of particles, constant area and temperature. Most of the simulations for the two platelets and for the two platelets and surface are carried out in the Grand Canonical Ensemble (μ,V,T) when a finite salt concentration is considered. When only counter-ions are present, the Canonical Ensemble (N,V,T) is used. Three different kinds of moves are employed; i) *single ion translations*, ii) *platelet rotation*, where a platelet is rotated around a random axis and iii) *cluster displacements*. Note that the centers of mass (CoM) of the platelets are kept fixed during the simulations. The cluster move involves the rotation of a single platelet together with the surrounding ions. Maximum displacements (displacement parameters) for all moves are set so as to return an acceptance ratio of between 20% and 40%. The temperature was kept constant, equal to $T = 298K$, for all simulations. Three different salt concentrations are considered : 0, 10 and 20 mM. The volume fraction of the platelets is defined as,

$$\phi = \frac{n_p \pi d^3}{3V_{box}} \tag{6}$$

At a given fixed distance between the CoM of the platelets, the force exerted on one platelet is evaluated by summing the forces exerted by each particle that interacts with the platelet. To obtain good precision, the force is sampled every 100th *move*, where the term *move* refers to any of the three different types of displacement of the different species (as described above) or the attempted creation and deletion of mobile ions in the simulation box in (μ,V,T) simulations.

In the case of the simulations of two particles with a surface the volume fraction is kept fixed to $\phi = 0.005$.

8

Results and Discussion

A single platelet

Here we study the factors that control the growth of a single platelet. The free energy of the platelet is a combination of energetic and entropic contributions. The latter will disfavor aggregation, hence the energy term drives the clustering of particles and the formation of the platelets. It also provides a lower bound on the cluster free energy and hence an indication of its relative stability. That is, a stable cluster will always have a negative energy.

We estimate the cluster energy by using the potential model, Eqs.(1) and (2). Assuming n particles in the cluster, the short-ranged binding energy is approximately $-nE_b$, where $E_b \approx me_b/2$ with m being the number of nearest neighbors. Here we assume that the range of the square well potential extends only to nearest neighbors. For the system we investigated, the most stable sphere packing in the plane is hexagonal, hence we choose m=6. The repulsive electrostatic energy can be estimated by integrating the screened Coulomb potential over the cluster area. We assume the latter to be circular, with radius $R_{clus} \approx \sqrt{n}R$.

$$E_{el} = \int_0^{R_{clus}} dr 2\pi r \frac{l_B \alpha^2}{\pi R^2} \frac{\exp(-\kappa r)}{r} = \frac{2l_B\alpha^2}{R^2} \int_0^{R_{clus}} dr \exp(-\kappa r) \tag{7}$$

which gives the following electrostatic energy per particle

$$E_{el} = \frac{2l_B\alpha^2}{\kappa R^2}[1 - \exp(-\kappa R\sqrt{n})] = E_{el}^{\infty}[1 - \exp(-\kappa R\sqrt{n})] \tag{8}$$

where E_{el}^{∞} is the repulsive electrostatic energy (per particle) of the infinite cluster. This expression only approximately accounts for the truncating effects of the cluster boundary on the electrostatic potential. The total energy is thus

$$E_{tot} = n[(E_{el}^{\infty} - E_b) - E_{el}^{\infty} \exp(-\kappa R\sqrt{n})] \tag{9}$$

Minimizing with n, i.e., $\partial E_{tot}/\partial n = 0$, we obtain

$$\frac{(E_{el}^{\infty} - E_b)}{E_{el}^{\infty}} = (1 + \frac{\kappa R\sqrt{n}}{2}) \exp(-\kappa R\sqrt{n}) \tag{10}$$

If $E_{el}^{\infty} > E_b$, then the electrostatic energy per particle in the infinite cluster becomes greater than the square well contribution. One can reduce the electrostatic repulsion per particle by reducing the cluster size. Thus, in this regime, finite clusters can be stabilized by electrostatic repulsions and Eq.(10) has solutions corresponding to finite $n(> 0)$. As $E_b \to E_{el}^{\infty}$ the cluster begins to grow uncontrollably, $n \to \infty$. Figure 6a gives the solution to eq.(10) for three different values of E_b. The dashed vertical lines shows the minimum value of κ/α^2 for which the cluster growth is limited. That is, to the right of the dashed lines the crystal size is no longer electrostatically constrained in size.

Simulations of this system were carried out in the Canonical Ensemble, so the conditions at which electrostatics does not constrain the cluster size is estimated as that where a single cluster forms in the simulation volume. Clearly this estimate becomes more accurate in the thermodynamic limit. In Fig. 6b we show the phase diagram derived from simulations of 222 particles in a spherical simulation cell of radius 200 Å with $\alpha = 1$, together with the predictions based on our simple energy analysis. The theory gives a surprisingly good prediction of the phase boundary between finite and infinite clusters. This indicates that the entropy plays a relatively minor role in determining the cluster free energy, especially at high binding energies. The major discrepancy at small binding energies can be explained by the neglect of the entropy. On the other hand, surface effects are unimportant in determining the position of the bulk phase boundary. Without any electrostatic interactions we observed from simulations that an initial single cluster disintegrates when $E_b \leq 2$. Increasing the binding energy to $E_b = 5$, one obtains a well-condensed single cluster. This cluster does not disintegrate upon introducing short-ranged electrostatic repulsions, $\kappa/\alpha^2 = 0.02$. However, for longer ranged repulsions, $\kappa/\alpha^2 = 0.015$, the single cluster breaks apart into smaller clusters. Figure 7 shows the distribution of cluster sizes in such a simulation. We see that the average cluster consists of approximately 20 particles. Using eq.(10) we get $n \approx 13$. The agreement between simulations and the simple model is surprisingly good, considering the neglect of entropic and surface contributions to the free energy.

E_b is the major stabilizing component for the cluster. It is expected to be in the range 10-100 k_BT. The ionic concentration and pH in pure equilibrium solutions of C-S-H vary a lot without having a significant effect on the size of the particles. The lowest values correspond to an ionic strength of I = 3.6 10^{-3} M and pH = 11 and the highest I = 5.5 10^{-2} M and pH = 12.5. The charge density of the platelets at these pH values are -1.9 and -4.8 e/nm^2 [11], which give $\kappa/\alpha^2 = 0.0072$ Å^{-1} and 0.0044 Å^{-1}, respectively. In a typical cement paste one obtains $\kappa/\alpha^2 = 0.016$ Å^{-1}. Thus, according to our model we would require $E_b > 120$ in the case of C-S-H suspensions for an infinite growth of C-S-H, and 35 in the case of cement hydration. Thus, we are led to conclude that the growth of C-S-H platelets is most likely limited by electrostatic repulsions despite the high ionic strength met in these systems. Both the analytical theory and the simulations are based on a simple description of the electrostatic interactions, that is the screened Coulomb potential. This approximate form is strictly only valid at low electrostatic coupling. However, the screened Coulomb approximation usually underestimates the electrostatic screening and one could expect weaker electrostatic repulsion, and hence stronger growth, in real systems.

While it seems that equilibrium mechanisms could explain the finite size of C-S-H platelets, it has been observed an extensive growth of the platelets in the peculiar condition where the platelets are grown in contact with an atomistically flat surface and in an electrolyte solution close to equilibrium conditions [15]. Here, the competition between aggregation and growth have probably a kinetic origin. This hypothesis shifts the investigation away from the growth of single platelets to the study of interactions between platelets. In particular, our conjecture would be supported if aggregation did not occur until platelets

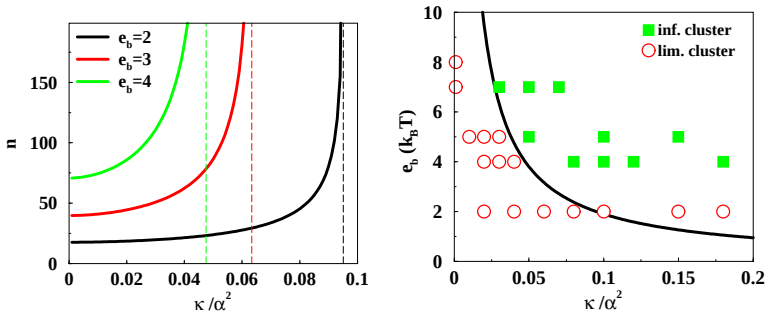

Figure 6: a) Solutions to eq.(10) for different binding energies as a function of electrostatic screening in terms of the Debye-Hückel inverse screening length. The dashed lines show the boundary at which the crystals start to grow infinitely. b) The black solid line shows the function $e_b = 2l_B/3R^2.\alpha^2/\kappa$ describing the boundary between infinite and finite growth, from eq.(10). The symbols show the corresponding Monte Carlo results obtained for a system with $N = 222$ and $R_c = 200$ Å.

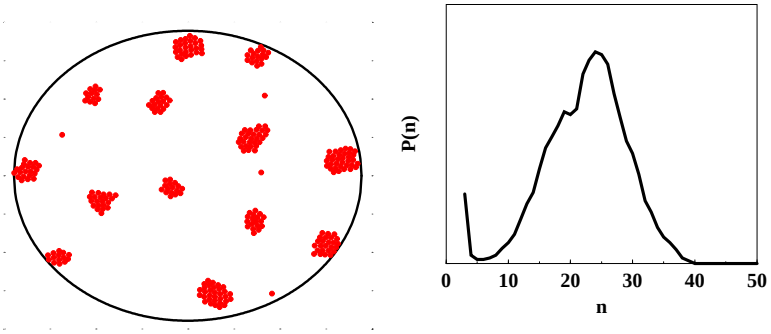

Figure 7: a) The final configuration from a long simulation with $\kappa/\alpha^2 = 0.015$, $N = 289$, $R_c = 378$ Å and $E_b = -5$. b) The corresponding probability distribution for cluster size n.

reached a particular critical size, and that significant growth did not seem to extend much beyond this value. In the next section we explore mechanisms that give rise to attractive interactions *between* platelets and changes in those interactions due to varying platelet sizes.

The interaction of two platelets

Competition between mono- and divalent counterions: Figure 8 illustrates the striking change of behavior between two rotating platelets when the salt is varied from

monovalent to divalent. As known for a long time, a double layer repulsion is observed between the particles when a 1:1 salt is present in the box. Note that, this repulsion increases when increasing the size of the particles. When introducing a 2:1 salt in the simulation box, ion correlations come into play. It results in a net attraction between the particles, as it can be seen in Figure 8. The later also display size dependence interactions. This will be further discussed in the next section.

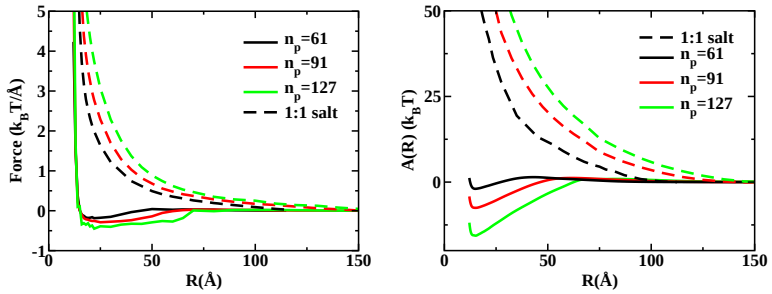

Figure 8: a) The average force between two rotating platelets with σ=-1.2 e/nm^2 in 10mM of a 2:1 salt (full lines) and a 1:1 salt solution (dashed lines) at a volume fraction of 0.023. The number of sites, 61 and 127, corresponds to 90 and 130 nm in diameter; $\epsilon_{LJ} = 0.1k_BT$. b) The corresponding free energy curves.

Size dependent attraction: Recall that for the investigations described in this section, the platelets are constructed from charged spheres arranged in a two-dimensional hexagonal array. Fig. 9 shows the interactions between a pair of platelets that have been constrained to be parallel. We note the attractive interaction, typical of highly charged surface in the presence of divalent counterions. The major contribution to the attraction is due to the correlations between counterions in the space between the surfaces. For the three platelet sizes depicted in the figure, one notes that the magnitude of the attraction increases with platelet size. Normalizing the force with the platelet area shows that the depth at the force/area minimum is similar for all three cases. This indicates that the total force between platelets scales approximately with the surface area. This becomes more precise as the platelet size increases. For very large platelets, the force per unit area of infinite surfaces then becomes the relevant quantity. We will explore this fact below. Integration of the force curves gives the free energy of interaction of two parallel platelets and is strongly negative at short separations.

In reality, platelets will generally only adopt parallel (or near parallel) orientations when they are at close separation. Two freely rotating platelets with their centers of mass at some fixed separation will possess a rotational entropy S_{rot}. As the platelets approach, this entropy decreases, which creates a repulsive force. The *qualitative* behavior of the entropy loss versus platelet separation is the same for platelets of all sizes. Indeed, we expect to obtain identical behavior if the center of mass separation, R, is scaled by the average radius of the platelet, R_p. Thus, the rotational entropy is a function of the reduced

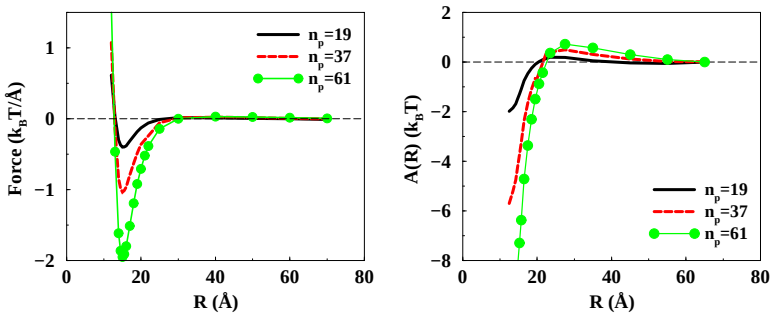

Figure 9: a) The average force between two parallel platelets with σ=-1.2 e/nm^2 in a 10 mM 2:1 salt solution at a volume fraction of 0.023. The number of sites, from 19 to 61, corresponds to 50 to 90 nm in diameter; $\epsilon_{LJ} = 0.1k_BT$. b) The corresponding free energy curves.

separation between platelets, i.e., $S_{rot}(R/R_p)$. Furthermore, we expect that,

$$S_{rot}(R/R_p) \approx S_{rot}(R) - S_{rot}(2R_p) \quad \text{for } R < 2R_p \tag{11}$$

That is, the effect of increasing R_p is to essentially decrease the entropy by a constant amount for all R. This approximation is more accurate for small R/R_p. On the other hand, the electrostatic interaction between the platelets grows as R_p^2. Thus, the distance dependent part of the rotational entropy becomes negligible for large platelets. The platelet sizes, which we are able to simulate in this work are still in the range where the orientational entropy plays a role. In Fig. 10 we consider two freely rotating interacting platelets. Here we see that it is only for the cases, n_p = 37, 61 and 91, that the force becomes net attractive.

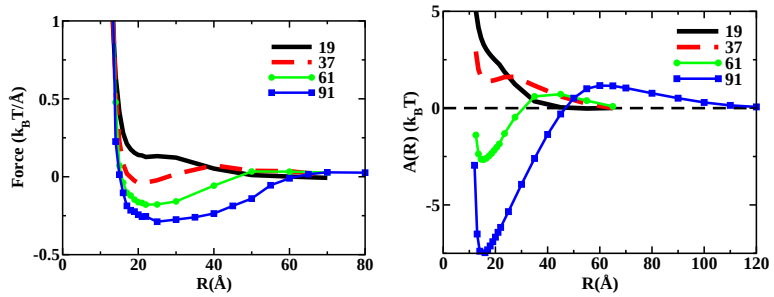

Figure 10: a) The average force between two freely rotating platelets with σ=-1.2 e/nm^2 in a 10 mM 2:1 salt solution at a volume fraction of 0.023. $\epsilon_{LJ} = 0.1k_BT$. b) The corresponding free energy curves.

van der Waals attraction: In addition to the ionic correlation attraction there is also the van der Waals term to take into account. Strictly speaking these two interactions can

not be separated in a rigorous way, but an approximate treatment of them as two independent terms facilitate the understanding of the underlying physics. Both terms will act so as to aggregate the platelets, but we know that with only monovalent counterions, there is no aggregation. The strength of the van der Walls term is not easily chosen. There exists, however, a wealth of experimental data that indirectly addresses this issue and in many cases it is possible to make a reasonable estimate of the interaction strength. The general result for many colloidal systems with monovalent counterions is that the electrostatic repulsion dominates unless the salt concentration is very high. With divalent counterions the situation is qualitatively different, since the ordinary double layer repulsion is weak and the interaction is already determined by the correlation term. The effect of the van der Waals attraction is merely to increase the attraction, but it does not change the qualitative picture. There is of course a transition regime, where the correlation term has not overcome the usual entropic double layer repulsion and in such a case the van der Waals attraction can change the total interaction from repulsion to attraction. Figure 11 shows an example of this, where the attraction is NOT determined by ion-ion correlations, but rather by the van der Waals term.

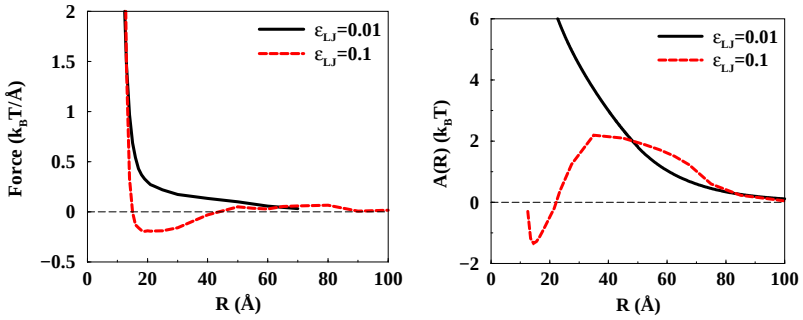

Figure 11: a) The average force between two freely moving platelets constituted of 61 sites with σ=-1.2 e/nm^2 in a 10 mM 2:1 salt solution at a volume fraction of 0.023. The Lennard-Jones parameter ϵ_{LJ} has been varied. b) The corresponding free energy curve.

Surface charge density (pH): The surface charge density of a C-S-H platelet is determined by the titrating silanol groups on its surface (the same is true for the C_3S grains). The titration of the C-S-H surface is strongly affected by the repulsion between the dissociated silanol groups, which means that the titration does not follow the titration behavior of a simple acid, but presents a much more extended titration curve. The presence of large amounts of divalent calcium ions, however, facilitates the dissociation [11]. The number of titratable site is estimated to be around 4-5 sites/nm^2 and a completely ionized surface is reached in presence of calcium ions at pH = 12.5, that is the usual cement conditions. Fig. 12 shows the counter intuitive result, that two equally charged surfaces attract each other more the higher their surface charge density is. This phenomenon has been observed experimentally in many different systems [16, 17, 18, 19] and is well understood from both simulation work [12] and analytical studies [20, 21, 22].

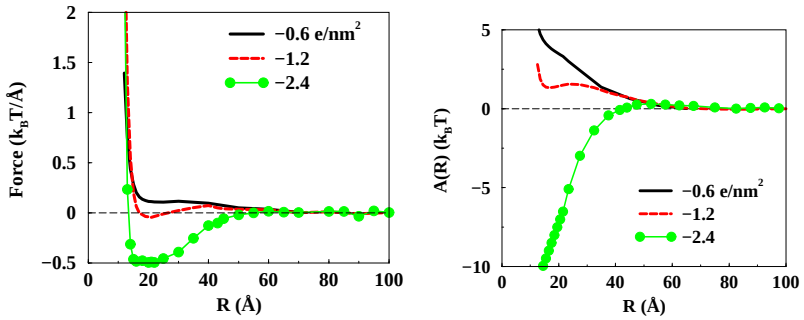

Figure 12: a) The average force between two freely moving platelets constituted of 37 sites in a 10 mM 2:1 salt solution at a volume fraction of 0.023. The surface charge density has been varied and $\epsilon_{LJ} = 0.1k_BT$; b) The corresponding free energy curves.

Additional salt: Standard double layer theory tells us that the addition of inert salt should reduce the double layer repulsion. In the present case with a net attraction, the effect of added salt is still the same - it makes the interaction less repulsive (=more attractive). This is demonstrated in Fig. 13 where the addition of 20 mM 2:1 salt (e.g. $Ca(OH)_2$) makes the interaction significantly less repulsive and creates a local minimum at short separation. For larger particles and/or higher surface charge density, this minimum will become a global one.

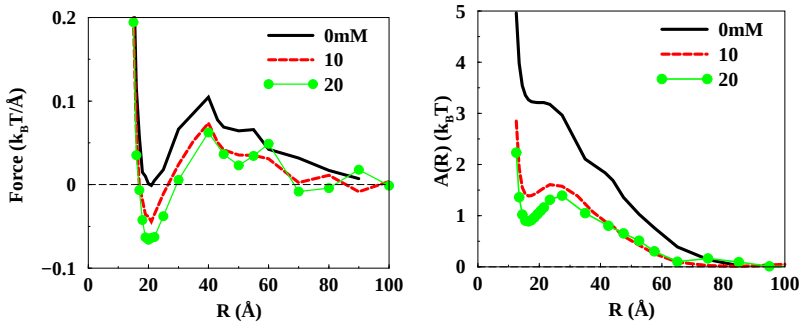

Figure 13: a) The average force between two freely moving platelets constituted of 37 sites with σ=-1.2 e/nm^2 in a 2:1 salt solution at various concentration. and at a volume fraction of 0.023; $\epsilon_{LJ} = 0.1k_BT$ b) The corresponding free energy curves.

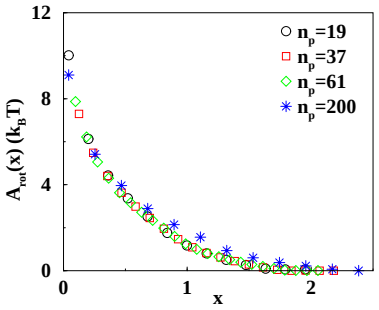

Figure 14: The potential of mean force between two platelets consisting of neutral sites arranged as hexagons. The number of sites is given in graph. The plate-plate separation has been scaled by the average platelet radii - 18.9, 26.3, 33.8 and 61.2 Å.

Alternative treatment of two interacting platelets

The simulations of two rotating platelets with neutralizing counterions and possibly added salt is a time-consuming procedure due to the different length scales involved - the size of the platelet on one hand and the "size" of a counterion on the other. The computation times also scales in a deterrent way with the size of the platelet. In contrast, it is very easy to carry through a simulation of two infinite charged surfaces as well as the interaction between two neutral platelike particles. Combining these two types of simulations, the former giving the attractive term due to ion-ion correlations and the latter providing the repulsive contribution due to the hindered rotation of the platelets, one could more efficiently obtain an approximate potential of two charged platelets of a given size. An additional benefit of this approach is that the rotational entropy term scales in a neat way with particle size. Figure 14 shows the potential of mean force for four different platelet sizes where the interparticle separation has been scaled by the platelet radius. The four curves are virtually on top of each other meaning that one can obtain the potential of mean force for any platelet size from a universal curve - see Eq.(11).

We can now combine the repulsive term from the orientational degrees of freedom with the calculated interaction between two infinite plates. The result is shown in Fig. 15 and one finds the same qualitative behavior as in the simulation of two finite charged platelets. For small platelets the rotational entropy term dominates, while for sufficiently large platelets the attractive ion-ion correlation term takes over and there is always a deep minimum at short separation.

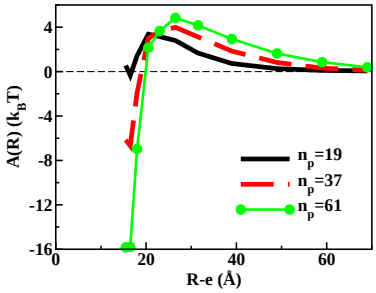

Figure 15: The potential of mean force between two charged platelets based on the sum of an entropic rotational repulsion and an attractive correlation term evaluated for a system consisting of two infinite charged walls with neutralizing counterions in between. e is the estimated closest contact distance of the platelets. The platelet size is indicated in figure and the results should be compared to Fig.10.

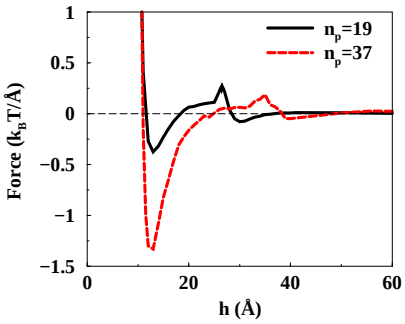

Figure 16: The force between a single platelet with σ=-1.2 e/nm^2 and a surface with the same surface charge density in a 10mM 2:1 salt solution at various platelet sizes.

The interaction of one platelet with a surface

In the initial phase of the hydration of cement, the C-S-H platelets form near the C_3S grain and will be attracted to its surface. In order to mimic this situation we have also simulated a single platelet outside an infinite (large) charged surface, see Fig. 16. Without any detailed knowledge about the surface charge density of neither the C_3S grain nor the C-S-H platelets, it seems reasonably to assume that they have the same charge density. The free energy of interaction is larger in this case than for two equally sized platelets, since the correlation term is stronger - the orientational entropy is the same for the two situations. An interesting feature in Fig. 16 is the initial weak minimum, which appears for a perpendicular arrangement. It will, however, disappear for larger particles, since the rotational entropy term is more long ranged than the attractive interaction. This can already be seen in the comparison of platelets with $n_p = 19$ and $n_p = 37$ sites.

17

The interaction of two platelets with a surface

From the previous results, one can conclude that at a critical size, a C-S-H platelet will aggregate onto the C_3S surface. The aggregation of further platelets onto the C_3S surface and on the first C-S-H particle, will then be dependent on both thermodynamics and kinetics factors. In this section, we investigate the role played by thermodynamics in the different modes of C-S-H aggregation onto C_3S surfaces.

Axial aggregation. We investigate the case of the axial aggregation of charged platelets on a charged surface of the same sign using the model sketched in Fig. 5-a. Figure 17 displays the axial force acting between the particles at different 2:1 salt concentrations. The same qualitative behavior as in the case of one particle and a surface is observed. Indeed, the force displays two minima, the first one at $R = 30$Å corresponds to a *T shape* configuration while the second at $R \sim 15$Å corresponds to a *stack* configuration. Both minima increase with the calcium salt concentration. Again, this is attributable to the increase of the ion-ion correlations when increasing c_s. The interaction free energy, Fig. 17-b, indicates that a net attraction is only reached at high salt concentration, 20mM. The free energy minimum corresponds here to a T shape configuration.

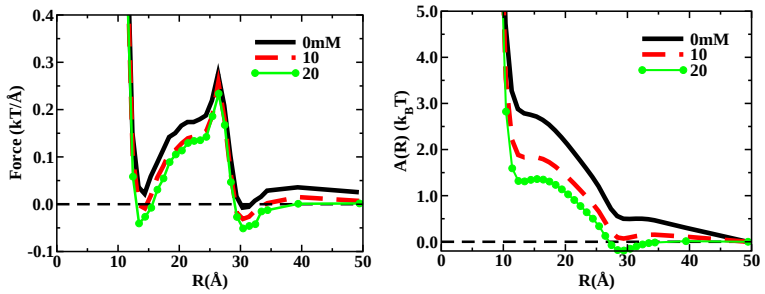

Figure 17: a) Axial force acting between the platelets constituted of 19 sites in a 2:1 salt solution of varying concentration obtained with the model sketched in Fig. 5-a. b) The corresponding free energy curves.

A net attraction in the stack configuration is found when increasing the size of the particles as shown in Fig. 18-b, which gives the axial interaction free energy between two platelets with 37 sites in presence of a charged surface. Under the same conditions but in absence of a charged surface, two platelets of 37 sites do not show any attraction, c.f. Fig. 10. This demonstrates the importance of the charged C_3S surface in the aggregation process of C-S-H during the hydration of cement.

Figure 19 shows the influence of the platelet charge density ($\sim$ pH) on the axial force between the platelets and the corresponding free energy. At low surface charge density (low pH), the platelets repel each others. When increasing the charge density from -0.5

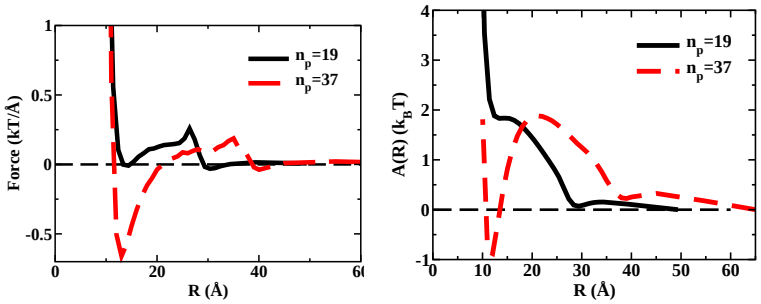

Figure 18: a) Axial force acting between the platelets constituted of 19 sites in a 10 mM 2:1 salt solution at two different platelet sizes, i.e. 50 nm and 70 nm, obtained with the model in Fig. 5-a. b) The corresponding free energy curves.

to -1.2 e/nm^2 the same qualitative result is observed. Upon a further increase in pH, a net attraction is obtained at a separation corresponding to a T-Shape configuration. Note that, in the usual conditions of a cement paste, the surface charge density of C-S-H is twice the highest value used, i.e. -4.8 e/nm^2. For this surface charge density, a net attraction should also be observed in the stack configuration.

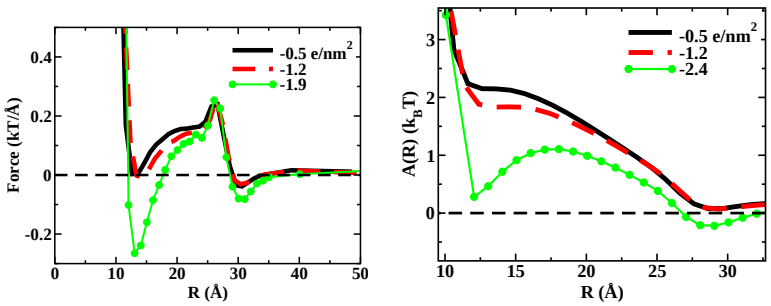

Figure 19: a) Axial force acting between the platelets in a 10 mM 2:1 salt solution at various charge densities obtained with the model in Fig. 5-a; the same value is used for both the surface and platelets. b) The corresponding free energy curves.

Lateral aggregation. The lateral aggregation of charged platelets on a charged surface of the same sign is studied using the model in Fig. 5-b. Figure 20 gives the lateral force (along the x axis) felt by the platelets when they are both lying at the surface. The obtained force curves oscillates around 0 k_BT is a consequence of the geometric

representation of the surface and platelets with explicit sites distributed on a regular lattice. Indeed, the same oscillating curve is obtained when sliding just one particle on the surface (not shown). No attraction or repulsion is found between the particles until the Lennard Jones potential comes into play. Furthermore, varying the salt concentration has virtually no effect on the lateral force. The same conclusion can be drawn when the size of the platelets or the surface charge density are varied. This suggests that there is no preferential lateral position when a C-S-H particle adsorbs or starts to grow from a C_3S surface.

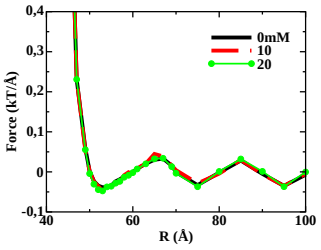

Figure 20: Lateral force acting acting between the platelets in a 2:1 salt solution at different salt concentrations obtained with the model sketched in Fig. 5-b.

Conclusions

We have shown that the limited growth of C-S-H nanoplatelets in solution could be explained by internal Coulomb repulsions - despite the high ionic strength that prevails in a cement paste. We also suggest that the competition between growth and aggregation of the C-S-H platelets arises from a kinetic origin. The fact that charged platelets under "cement like" conditions initially repel each other, but once the particles have reached a certain size attract each other lends support to our suggestion. The properties of this correlation attraction also explains why the initial C-S-H layer formed on the dissolving C_3S grains is denser. Finally, we have shown that the different modes of C-S-H aggregation onto C_3S grain surfaces can be partly explained with some thermodynamic considerations. In agreement with experiments [5, 6], a high pH and calcium concentration is found to favor the axial aggregation of the platelets.

References

[1] S. Garrault, E. Finot, E. Lesniewska, and A. Nonat, C. R. Acad. Sci. Paris **327**, 213 (1998).

[2] D. D. Double, A. Hellawell, and S. J. Perry, Proc. R. Soc. Lond. A **359**, 435 (1978).

[3] A. Nonat, Cement and Concrete Research **34**, 1521 (2004).

[4] S. Garrault-Gauffinet and A. Nonat, J. cryst. growth **200**, 565 (1999).

[5] S. Garrault, E. Lesniewska, and A. Nonat, Material and Structures **38**, 435 (2005).

[6] S. Garrault and A. Nonat, Langmuir **17**, 8131 (2001).

[7] W. C. Pan, O. Galkin, L. Filobelo, R. L. Nagel, and P. G. Vekilov, Biophys. J. **92**, 267 (2007).

[8] P. G. Vekilov, Ann. N. Y. Acad. Sci. **1161**, 377 (2009).

[9] B. Hutchens and Z. G. Wang, J. Chem. Phys. **127**, 084912 (2007).

[10] A. J. Archer, D. Pini, R. Evans, and L. Reatto, J. Chem. Phys. **126**, 014104 (2007).

[11] C. Labbez, B. Jönsson, I. Pochard, A. Nonat, and B. Cabane, J. Phys. Chem. B **110**, 9219 (2006).

[12] L. Guldbrand, B. Jönsson, H. Wennerström, and P. Linse, J. Chem. Phys. **80**, 2221 (1984).

[13] R. Pellenq, J. Caillot, and A. Delville, J. Phys. Chem. B **101**, 8584 (1997).

[14] B. Jönsson, , A. Nonat, C. Labbez, B. Cabane, and H. Wennerström, Langmuir **21**, 9211 (2005).

[15] C. Plassard, E. Lesniewska, I. Pochard, and A. Nonat, Proceedings of the Fifth International Conference on Scanning Probe Microscopy, Sensors and Nanostructures **3-4**, 331 (2004).

[16] B. P. Warkentin, G. H. Bolt, and R. D. Miller, Soil Soc. Proc. **000**, 495 (1957).

[17] J. Marra, Biophys. J. **50**, 815 (1986).

[18] S. M. Mel'nikov, V. G. Sergeyev, and K. Yoshikawa, J. Am. Chem. Soc. **117**, 2401 (1995).

[19] R. Kjellander, S. Marčelja, and J. P. Quirk, J. Coll. Interf. Sci. **126**, 194 (1988).

[20] R. Kjellander and S. Marčelja, Chem. Phys. Letters **112**, 49 (1984).

[21] C. E. Woodward, B. Jönsson, and T. Åkesson, J. Chem. Phys. **89**, 5145 (1988).

[22] Z. Tang, L. E. Scriven, and H. T. Davis, J. Chem. Phys. **97**, 9258 (1992).